Design of a Coreless Hydrokinetic Turbine

A Major Qualifying Project
Submitted to the Faculty of
WORCESTER POLYTECHNIC INSTITUTE
in partial fulfillment of the requirements for the
Degree of Bachelor of Science
in Mechanical Engineering

Submitted by:

_____
Jillian Chu

_____
Alexander Kim

_____
Joseph Pagliuca

Approved by:

_____
Selcuk Guceri

Abstract

This project involves the design of a novel coreless hydrokinetic turbine. The goal was to develop a power plant that could harvest energy from a river or tidal basin to meet the energy needs of remote regions. The hydraulic turbine was designed as a rotating tube with turbine blades extending inwards in contrast with a traditional design in which blades extend radially outwards from the axis of rotation. This turbine is enclosed in an outer casing, similar to that of a jet engine, which contains three generators driven by the turbine. Performance optimization was conducted through simulations using ANSYS Fluent. Blade profiles were refined using blade element momentum theory in MATLAB with airfoil characteristic data calculated in XFOIL. An operational small-scale prototype was built for concept demonstration through physical water tunnel tests. The deliverables include design specifications for a hydroelectric power plant capable of producing electricity to meet energy demands in remote regions.

Table of Contents

List of Figures

List of Tables

Nomenclature

Alphabets

A	Area
a	Axial Induction Factor
a´	Tangential Induction Factor
b	Chord Length
C	Coefficient
c	Absolute Fluid Velocity
F	Force
g	Gravitational Acceleration
I	Moment of Inertia
KE	Kinetic Energy
L	Length
ṁ	Mass Flow Rate
N	Number of Blades
P	Power
p	Pressure
R	Turbine Inner Radius
Re	Reynold's Number
r	Radius
U	Tangential Blade Velocity
V	Volume
W	Relative Fluid Velocity
z	Height

Greek Symbols

α	Angle of Attack
η	Efficiency
θ	Angle
λ	Tip Speed Ratio
μ	Kinematic Viscosity
ξ	Blade Stagger Angle
ρ	Density
τ	Torque
φ	Swept Angle per Blade, Flow Angle
ω	Angular Velocity

Subscripts

1	Upstream of Turbine
2	Downstream of Turbine

A	Axial
act	Actual
bl	Blade
d	Drag
h	Hydraulic
i	Input
l	Lift
max	Maximum
o	Output
P	Power
T	Thrust
z	Axial
θ	Tangential

Abbreviations

1D	One Dimensional
2D	Two Dimensional
3D	Three Dimensional
BSM	Bottom Structure Mounting
CAD	Computer Aided Design
FSM	Floating Structure Mounting
GHG	Greenhouse Gas
IRENA	International Renewable Energy Agency
NACA	National Advisory Committee for Aeronautics
NSM	Near Surface Mounting

1 - Introduction

Electricity is indispensable in modern life, providing necessities such as heat, and luxuries such as entertainment. Over 60% of the world's electricity is generated by burning fossil fuels, such as coal and natural gas. However, burning fossil fuels is the largest contributor to greenhouse gas (GHG) emissions, and concerns over global warming and climate change as a result of GHG emissions has increased over the past half century [5]. One of the most obvious steps towards limiting GHG emissions is restricting fossil fuel use.

Restricting fossil fuel use, however, presents many challenges especially in developing areas. Many developing regions use burnable fuels as their primary electricity source and typically have limited electricity production already [1,27]. The United Nations estimates that over two billion people do not have access to reliable electricity [41]. The need to develop reliable electricity production is especially prevalent in regions such as Sub-Saharan Africa, South Asia, and Latin America; these regions ideally need to produce enough electricity to serve their population without using fossil fuels [13,37,43].

Water power has been used for centuries and is now most commonly harnessed by large industrial dams to power cities and communities over large areas. People living in rural, off-grid areas or in developing regions, however, cannot feasibility construct or gain access to these large structures due to size and cost constraints [25]. Recently, research and development has focused on creating hydropower plants that do not require dams and instead use the natural flow of the water, called hydrokinetic power plants [24].

The goal of this project was to optimize the design and determine the feasibility of a hydrokinetic river power plant with a novel turbine design. The turbine was designed as a hollow cylinder with blades extending inwards in contrast with a traditional design in which blades extend radially outwards from the axis of rotation. The gearbox and electric generators were linked to the outside of the cylinder, theoretically providing more torque due to larger displacement from the axis of rotation.

This high torque, low rotational rate design would theoretically produce as much, or more, power as a traditional turbine design, while improving durability and being usable in slower waters. Inspiration for the design came from the outrunner motor, a type of DC brushless motor. Outrunner motors rotate the outer casing around the winding and shaft, producing high torque and low rotation rates in comparison to a traditional inrunner motor.

Throughout the project, models were developed and modified based on test results. Initial design parameters were chosen arbitrarily and kept fixed throughout the project to limit the factors affecting the design. The fixed parameters were a turbine inner radius of 0.75 m and an absolute water velocity of 2.5 m/s. A generic base model was constructed based off of these parameters. Other parameters were tested in simulation software including ANSYS Fluent and MATLAB, as well as physical tests with scale models in a water tunnel. In addition to turbine optimization, a preliminary design for the turbine casing was modeled.

2 - Background

The purpose of this chapter is to introduce hydroelectric technology and determine the effects of different turbine designs on performance. The chapter begins with a brief overview of why hydropower is needed. Following this overview, conventional hydropower systems are discussed. Finally, hydrokinetic turbines are introduced, as are some of the factors that are important in designing a hydrokinetic power plant.

2.1 - Hydroelectric Power

To reduce fossil fuel use, the foremost solution is the use of renewable energy sources such as sunlight, wind, and water. Of the many choices for clean energy, many governments and international organizations have increased focus on water, or hydroelectric, power [24]. In 2016, hydroelectric power provided over 16% of electricity generated worldwide, and accounted for over 60% of renewable electricity generation (see Figure 1) [18].

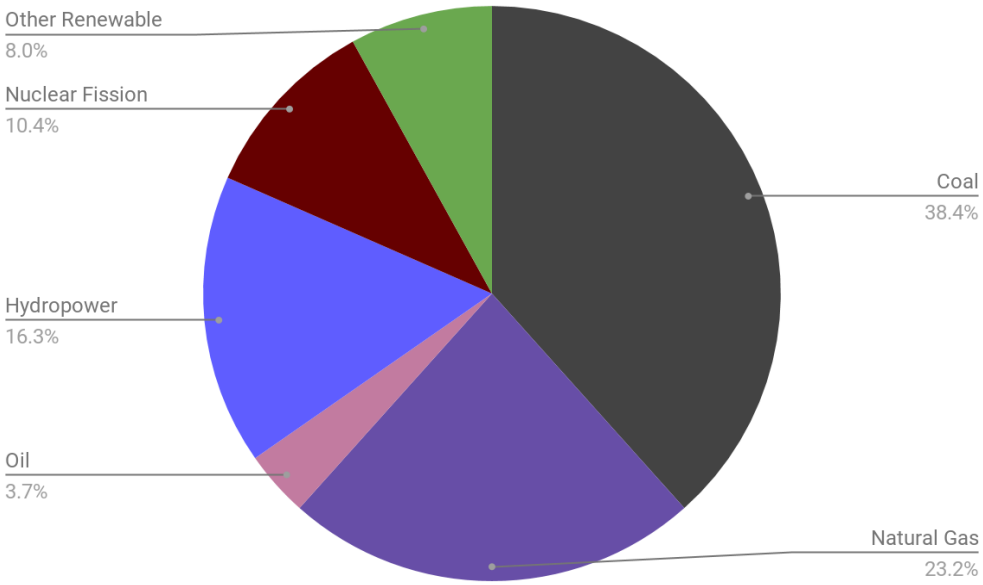

Figure 1: Worldwide electricity generation by resource [18]

The global hydropower capacity is 1100 GW, largely from Asia and Latin America, with more than 150 GW of hydropower capacity currently under construction [5,42]. As of 2017, 7.4% of electricity generated in the United States comes from hydropower [40]; other countries, such as Norway and Paraguay, generate over 90% of their electricity with hydropower [6,17].

Hydropower has many benefits that make it a suitable choice to help decrease GHG emissions. Water is a clean resource that does not use combustion to power generators, eliminating direct contribution to GHG production [5]. The water cycle also replenishes water storages at a constant and predictable rate, reducing concerns about fuel shortages and providing increased reliability. Furthermore, water is a domestic resource, allowing countries to produce electricity without dependence on foreign fuel supplies [4]. Hydropower can also provide electricity to rural communities disconnected from the power grid without having to create large amounts of infrastructure to support it [28]. Smaller benefits provided by hydropower include relatively easy maintenance and possibly increased tourism.

Hydropower systems are also quite flexible and can be built in a variety of sizes to fit the necessary application. While there are no official classifications, the International Renewable Energy Agency (IRENA) breaks hydropower plants into six categories based on size. The largest is large-hydro, and encompasses systems capable of producing 100 MW or more; an example of a large-hydro plant is the Three Gorges Dam in China, the largest hydropower plant in the world with an installed capacity of 22500 MW. Following in decreasing size are: medium-hydro (20 MW - 100 MW), small-hydro (1 MW - 20 MW), and mini-hydro (100 kW - 1 MW). Power plants in these three classifications generally feed into a grid, although mini-hydro plants sometimes help power small, rural communities. Finally, micro-hydro (5 kW - 100 kW) and pico-hydro (< 5 kW) are often used to power small communities or households away from power grids [19].

2.1.1 - Conventional Hydropower

Conventional large hydropower plants use dams to create reservoirs of water. The reservoir increases water pressure by raising the elevation of water before the turbine, creating an artificial “hydraulic head.” Per Bernoulli’s principle (see Eq. 1), the increase in pressure and elevation result in a higher water velocity through the turbine, which in turn generates more electricity.

$$\frac{p}{\rho} + g z_h = \frac{1}{2} c^2 \qquad \text{Eq. 1}$$

Due to the artificial hydraulic head, conventional hydropower plants have the capability of generating vast amounts of electricity [11]. The Three Gorges Dam, which uses a conventional design, produces enough energy to reduce coal consumption by 31 million metric tons per year. Out of the twenty largest power plants in the world, twelve are conventional

hydropower plants. Smaller power plants with a conventional design may use a canal to keep water from upstream at a certain elevation to provide hydraulic head before reaching the power plant (see Figure 2) [39].

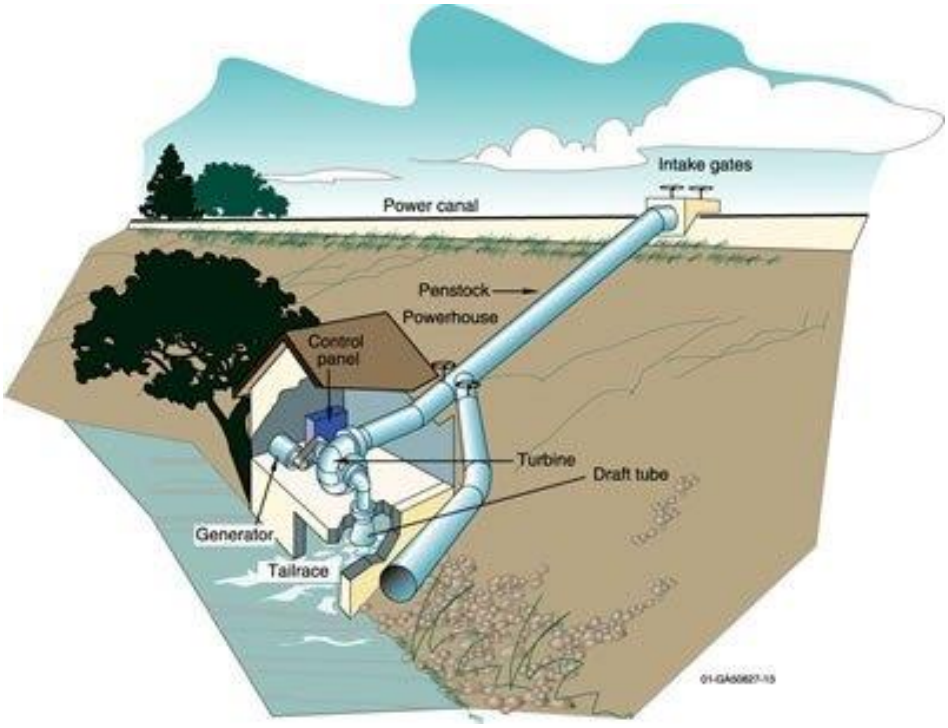

Figure 2: Hydraulic head for small conventional hydropower plant [39]

The dam and reservoir have many benefits that make conventional hydropower attractive. The electricity generated by conventional hydropower plants can be easily controlled by regulating the water flow, with gates on the dam, to the turbine. This allows for the electricity generation to be adjusted based on the current electricity demand. In large hydropower plants, reservoirs are often multipurpose, and used for applications from flood control to recreation. Additionally, the water stored in the reservoir can be used for crop irrigation; in the United States, 10% of cropland is irrigated using reservoir water [3].

2.1.2 - Disadvantages of Large Dams

Despite the benefits, conventional hydropower plants also introduce some significant drawbacks. One of the most obvious is the financial investment into the construction of the power plant and related expenditures. The Three Gorges Dam cost over US$35 billion, over US$12 billion above the projected cost [16]. Developing countries are unable to finance such large projects, leaving many to continue using fossil fuels for electricity production.

Another problem is the creation of the dam and reservoir itself, which is necessary to provide the large hydraulic head needed to drive the turbines. Creating such a reservoir involves flooding a large area of land which negatively impacts the local ecosystem, cause environmental disasters, and displace thousands of people. The construction of the Three Gorges Dam created a reservoir occupying over four hundred square miles. The reservoir displaced over 1.3 million people, increased risks of landslides in the area, and flooded several cultural and archaeological sites. Due to these and many other reasons, many conventional hydropower projects have firm public opposition to them [10,23].

The impacts of creating large water reservoirs are not limited to flooding; microscopic biological activity in reservoirs may have a significant effect on GHG emission. Algae and bacteria, which thrive in the relatively shallow, stagnant waters in reservoirs, produce large quantities of methane through their biological cycles. Recently, researchers estimated that reservoirs around the world release the equivalent of one billion tons of carbon dioxide per year, over 1% of total annual GHG emissions. While conventional hydropower does not directly burn fossil fuels and release GHGs, the effects of the reservoir reduce the positive environmental impact hydropower can provide [29].

2.2 - Hydrokinetic Power

A different type of hydropower configuration can be used to mitigate the problems encountered with conventional hydropower: hydrokinetic power. Hydrokinetic systems use the natural movement of water to produce electricity, eliminating the need to create artificial hydraulic head [26]. The absence of dams or elevated canals significantly decrease the cost and environmental impact of the power plant [34]. However, the lack of an artificial hydraulic head also significantly decreases the possible power generation; there are only three hydrokinetic power stations considered large-hydro by the guidelines discussed above.

2.2.1 - Possible Applications for Small Scale Hydrokinetic Plants

Despite the power limitations, hydrokinetic power plants are attractive because they can easily be installed any body of water with sufficient movement, the most common being rivers, tides, and ocean currents [26]. Other potential sources include man-made channels, industrial outflows, or irrigation canals [21]. These sources often have size or elevation restrictions, but hydrokinetic power plants are very flexible in size and do not use an artificial hydraulic head [19].

The amount of electricity produced by one large, or a series of smaller, micro-hydrokinetic turbines can fit the needs of small communities or extremely rural neighborhoods. Households in developing countries typically use very small amounts of electricity - sometimes as low as 200 W. Therefore, a turbine generating 20 kW could feasibly generate enough electricity to power a community of fifty or more households [28].

Due to the relatively low cost, hydrokinetic power can be cheaply used in conjunction with other power sources, such as wind or sunlight. During the day, a household or community could use the electricity generated by the solar panels. Meanwhile, the electricity generated by the turbine could be stored in a series of batteries, which can then be used at night or during overcast days. These applications, among others, make hydrokinetic turbines a feasible solution to providing developing communities and rural households with electricity [25].

2.2.2 - Hydrokinetic Configurations

While many types of hydrokinetic systems are currently in development, the most common are turbines in either a vertical or horizontal orientation. In vertical flow turbines, the axis of rotation is perpendicular to the surface of the water. Turbines of this design are simple to create, quiet, and easy to couple with a generator; however, they have low torque and efficiency. In horizontal, or axial flow turbines, the axis of rotation is parallel to the oncoming flow. These turbines are self-starting and do not exhibit the problems vertical turbines do to the same degree. Furthermore, studies and experiments done with wind turbines can be extrapolated to help develop axial turbines [35]. For these reasons, the rest of this paper will discuss axial hydrokinetic turbines.

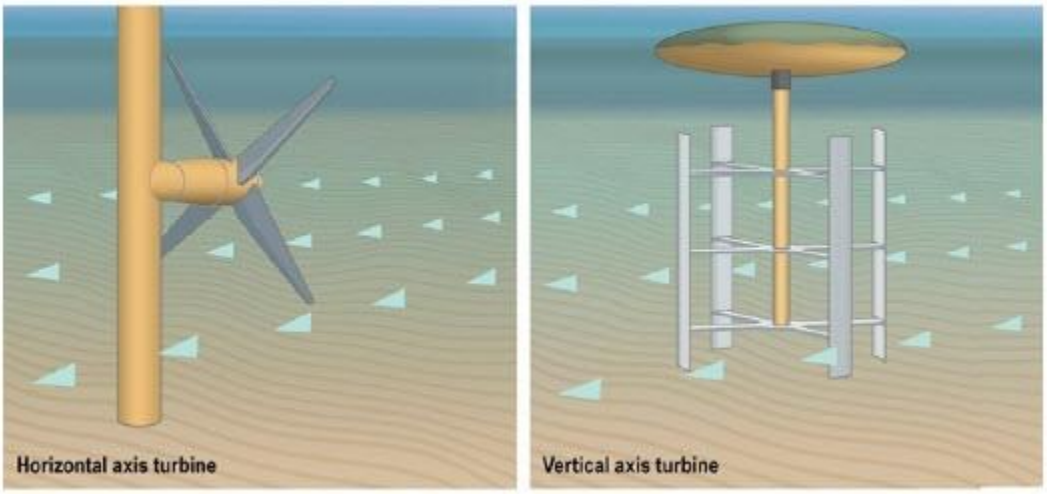

Figure 3: Horizontal and vertical axis turbine examples [38]

One important consideration is the mounting of the turbine in the water. For axial turbines, three primary methods are used: (1) bottom structure mounting (BSM), (2) floating structure mounting (FSM), and (3) near-surface structure mounting (NSM) (see Figure 4) [34].

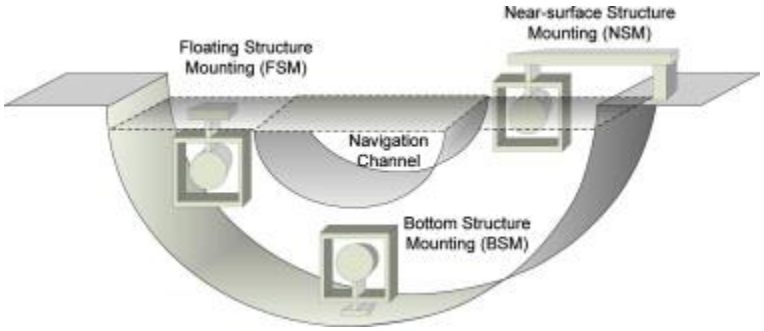

Figure 4: Primary mounting methods for axial turbine [34]

There are several advantages and disadvantages to each mounting method. Rivers and tides have faster water velocities near the surface, meaning that turbines mounted with FSMs or NSMs may be able to generate more power than those mounted with BSMs. However, the energy output from turbines mounted with NSMs may fluctuate depending on the water level. Furthermore, turbines mounted with FSMs and NSMs may get in the way of other river applications, such as naval shipping, recreational boating, or other uses. FSMs also lead to construction challenges, whereas BSMs have abundant civil engineering precursors. On the other hand, turbines mounted with BSMs are difficult to repair or inspect and have larger ecological effects due to their locations. Other factors include the size and mass of the turbine and the constraints on the hardware such as gearboxes and generators [21].

Another consideration related to mounting is the debris management. All bodies of water carry litter, branches, and other waste matter which can damage or reduce the performance of turbines due to collisions or build up over time. A simulation study by Richmond et al. found that 15-30% of debris that enters a turbine will hit a blade [31]. Debris guards redirect large debris to avoid the blades and are significantly more freely designed since they do not have major impacts on the turbine performance. The basic structure of debris guards is a thin metal skeleton in a cone or pyramid shape, with wires connecting from the skeleton to the rim of the turbine case. This keeps large debris out while allowing water to pass through the turbine.

2.2.3 - Flow to Power

Regardless of the hardware used, one of the most important factors in power generation is the velocity of the water flow and the cross-sectional area of the turbine. By increasing the

area of the turbine inlet and placing it in a fast-moving body of water, the power flowing through the turbine is increased (see Figure 5).

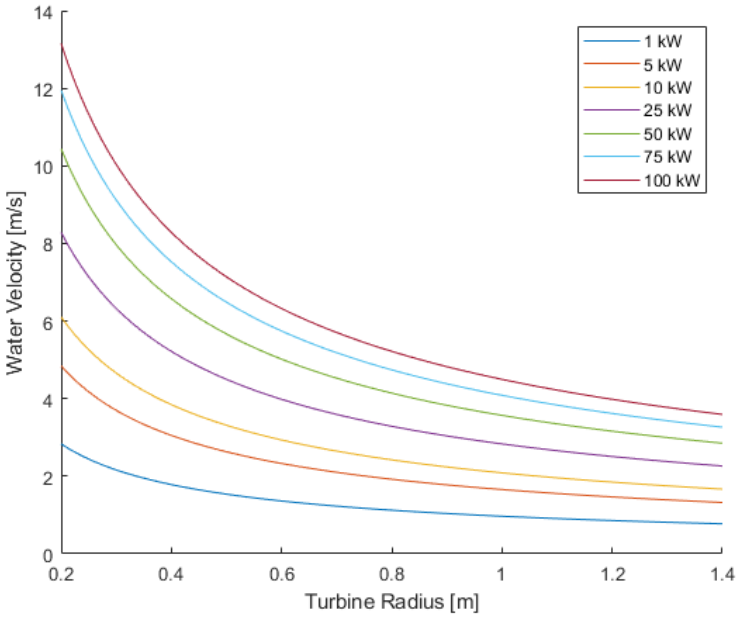

Figure 5: Available water power at different speeds and radii

However, according to studies and simulations performed by Ngo-Duc et al. and Schulze et al., river water velocity negatively correlates to cross sectional area. Therefore, fast moving water is unsuitable for large turbine inlets, and rivers that are deep enough for large turbine inlets typically do not have fast water velocities [30,33]. For these reasons, most hydrokinetic turbine projects focus on small turbines in fast moving rivers or extremely large turbines in ocean waters.

2.3 - High Torque, Low Velocity: the Outrunner Motor

A majority of axial hydrokinetic turbines use a wind turbine-like design, with blades extending from the center. These designs focus on maximizing angular velocity to generate power. However, as discussed above, river water velocity is typically inversely proportional to cross sectional area. In rivers with a large cross section, slow moving water decreases the angular velocity attainable by the blades. To generate more power, the length of the blades needs to increase, which increases manufacturing costs and fragility.

One option to maximize power in slow moving waters is to use a design based on the outrunner motor. Outrunner motors are a type of brushless DC electric motor in which the inner shaft is stationary, and the outside shell rotates. Since the outside shell, which has a larger

radius than the inner shaft, rotates, it rotates slowly but with a very high torque. Since power is proportional to both angular velocity and torque, the decreased angular velocity and increased torque counteract each other.

Figure 6: Rotor (left) and shaft (right) of an outrunner motor. Note that power is applied to the outer magnets, not the axle, of the rotor [9]

3 - Turbine Physics and Performance

This section discusses the physics behind turbomachinery and what parameters can affect performance. It begins with an overview of basic physics that are important for turbomachinery. Blades are then discussed, specifically focusing on the angles and shapes of the blades, using blade element momentum theory. Finally, auxiliary mechanisms that can help improve performance are introduced and discussed.

3.1 - Torque, Energy, and Power

One of the most important parameters in turbine performance is torque, the force on an object that causes rotation about an axis. In its simplest form, torque is dependent on the linear force applied to the object, the distance between the applied force and the axis, and the angle between the position and force vectors:

$$\tau = Fr\ sin\theta \quad \text{Eq. 2}$$

Therefore, an object generates higher torque with increasing radius size, all else being equal.

If torque acts through a rotational distance, it does work:

$$W = \int_{\theta_1}^{\theta_2} \tau\ d\theta \quad \text{Eq. 3}$$

Following the work-energy principle:

$$W = \Delta KE = \frac{1}{2} I({\omega_2}^2 - {\omega_1}^2) \quad \text{Eq. 4}$$

While the calculation of the moment of inertia, *I*, varies depending on the geometry of the rotating body, the square of the radius is invariably a factor. Therefore, to increase the rotational kinetic energy of an object, the necessary work increases with increased radius; that is to say, objects with larger radii have reduced angular velocities given the same work or magnitude of kinetic energy.

In a turbine, torque calculations are more complicated. One of the most fundamental equations in turbomachinery is Euler's turbine equation:

$$\tau = \dot{m}(V_{\theta 2} r_2 - V_{\theta 1} r_1) \quad \text{Eq. 5}$$

This equation uses the conservation of angular momentum to determine the amount of energy imparted to the blades. The greater the difference in tangential velocity, V_θ, before and after the turbine, the more energy is used to create torque.

Power is given as:

$$P = \tau\omega \quad \text{Eq. 6}$$

For a given power output, torque and angular velocity are inversely proportional; the higher the torque, the lower the angular velocity and vice versa. This means that a turbine with a large radius that rotates slowly can generate as much power as a turbine with a small radius that rotates quickly.

Another possible method of determining power output from a hydrokinetic turbine is to use the power equation for a wind turbine:

$$P = \frac{1}{2} C_P \rho A V^3 \eta \quad \text{Eq. 7}$$

This equation finds the total possible energy from the fluid stream and factors in the efficiencies of the turbine, C_p, and other losses, η [11].

3.2 - Turbine Blade Load Analysis

Another extensively used method of determining the torque and power of a turbine is to use the shape of the blades and the flow through the rotor plane. This calculation method is known as the blade element momentum theory (BEMT). BEMT combines blade element theory (BET) and blade momentum theory (BMT), each of which gives a series of equations to be solved iteratively.

3.2.1 - Airfoil Characteristics

Two of the most important characteristics of an airfoil are its lift and drag coefficients, which vary with cross sectional shape and angle relative to the flow. Despite the many different shapes and applications airfoils can have, they all have the same basic features, some of which are listed in Table 1 and displayed in Figure 7 [8].

Table 1: Basic parameters of airfoil shapes

Feature	Sym.	Description
Angle of Attack	α	Angle between flow and chord line
Chord		Straight line connecting leading and trailing edge
Camber line		Locus of midpoints between upper and lower surfaces
Camber		Distance between camber line and chord
Flow Angle	φ	Angle between flow and rotation plane
Pitch	s	Lateral spacing between blades
Solidity	σ	Ratio of chord length to pitch
Stagger	ξ	Angle between axial and chord lines
Max Thickness	t	Maximum thickness

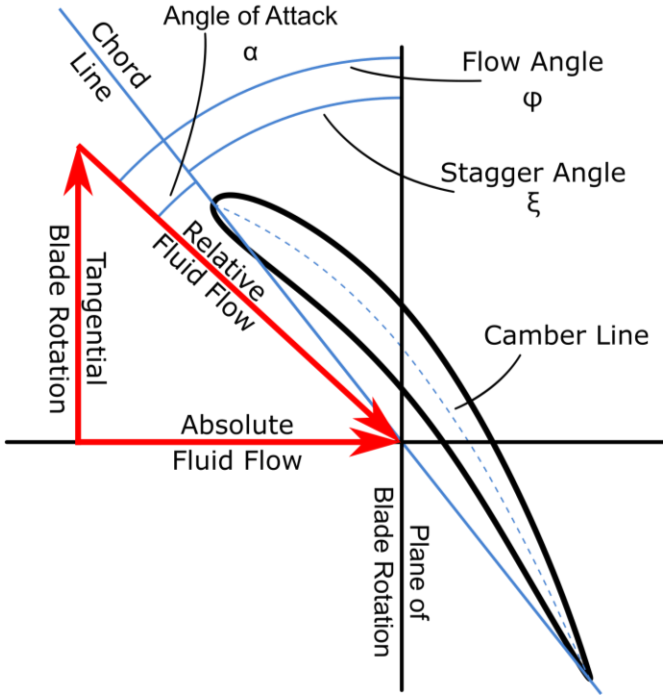

Figure 7: Airfoil characteristics with velocity triangle

Airfoils with no camber are referred to as symmetrical airfoils and produce no lift at an angle of attack of zero. Cambered airfoils have a camber in the direction of lift, and some can produce lift at shallow negative angles of attack.

The simplest airfoil is a flat plate, a type of symmetrical airfoil. Due to their simplicity, the lift and drag coefficients can be estimated much easier than most other airfoils. Equations for estimation can be seen in Table 2.

Table 2: Estimations for airfoil characteristics of flat plate

Equation	Application
$C_l = 2\pi sin\alpha$	Coefficient of lift at low angles of attack
$C_l = sin(2\alpha)$	Coefficient of lift at high angles of attack
$C_d = 2sin^2\alpha$	Coefficient of drag

The boundary between high and low angle of attack is between 15° and 20° [20].

Other airfoils cannot be estimated as easily. Therefore, specialized software programs are used to determine lift and drag coefficients for a given airfoil profile at specified Reynold's numbers and angles of attack.

Other problems with airfoils is the generation of the airfoils themselves due to the large number of variations possible. Some organizations, such as the University of Illinois at Urbana-Champaign (UIUC), host databases with hundreds of premade airfoil profiles. An option for custom generation of airfoils is using a National Advisory Committee for Aeronautics (NACA) airfoil generator (see Appendix A).

3.2.2 - Blade Element Theory

BET describes the forces on the blades by breaking the blades into small parts and determining the incremental forces on each element (see Figure 8).

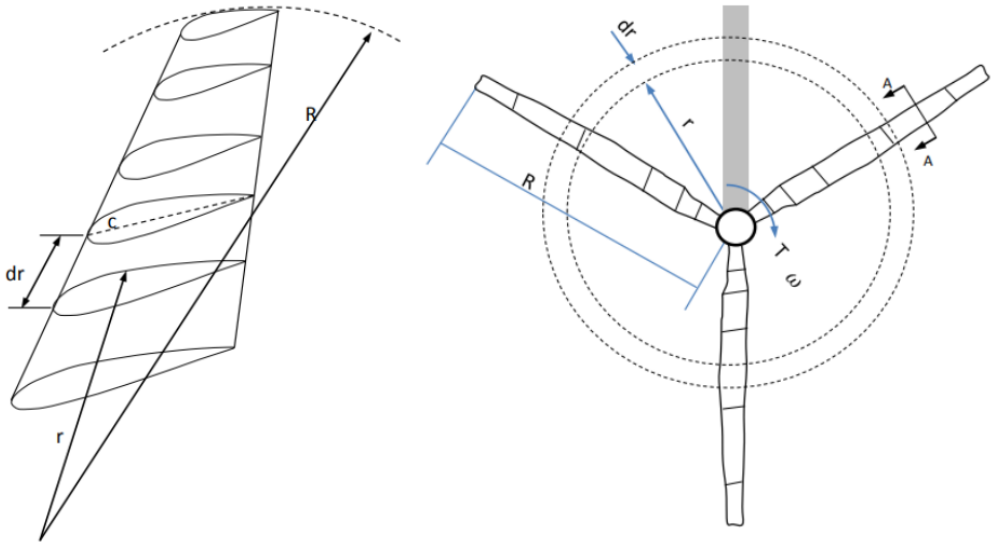

Figure 8: Wind turbine blades broken into elements of thickness dr [8]

The loads on the blade element are assumed to be solely a result of the lift and drag characteristics of the airfoil shapes.

The flow over the blades is the combined vectors of the axial flow into the turbine and the difference between the rotation of the fluid swirl at the rotor plane and the rotor itself. Based on the blade stagger angle, angle of attack, and the relative fluid flow angle, the loads on the blade element can be found (see Figure 9):

$$dT = \sigma\pi\rho\frac{c^2(1-a)^2}{sin^2\varphi}(C_l cos\varphi + C_d sin\varphi)rdr \quad \text{Eq. 8}$$

$$d\tau = \sigma\pi\rho\frac{c^2(1-a)^2}{sin^2\varphi}(C_l sin\varphi - C_d cos\varphi)r^2 dr \quad \text{Eq. 9}$$

where

$$\sigma = \frac{Nb}{2\pi r} \quad \text{Eq. 10}$$

$$\varphi = tan^{-1}[\frac{1-a}{(1+a')\lambda_r}] \quad \text{Eq. 11}$$

$$\lambda_r = \frac{\omega r}{c}$$ Eq. 12

where λ_r is the local tip speed ratio (TSR) [35].

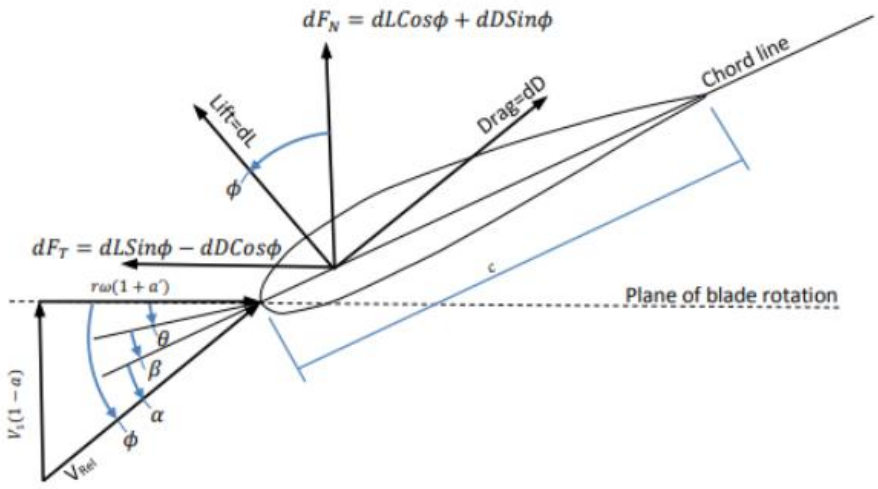

Figure 9: Free body diagram of loads on airfoil [8]

3.2.3 - Blade Momentum Theory

BMT describes the flow of a fluid through an ideal actuator disk, such as a rotor, and determines the thrust and torque of the object through conservation of momentum in a control volume. As the flow approaches and passes through the disk, it imparts some kinetic energy unto the blades and slows down (see Figure 10).

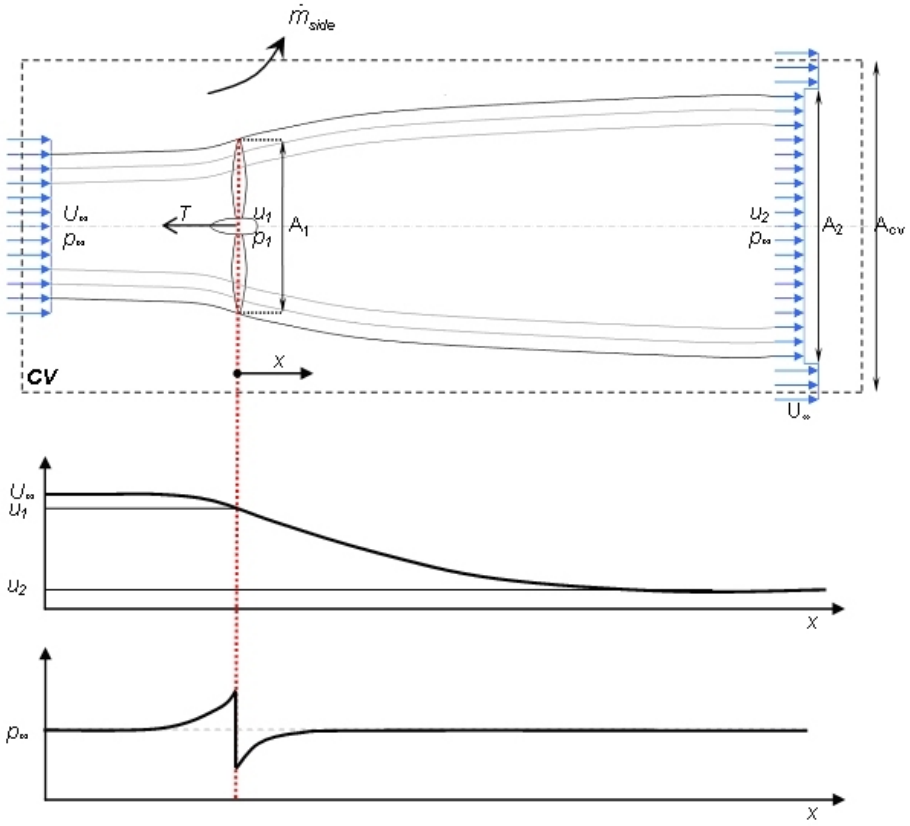

Figure 10: Velocity and pressure through ideal rotor [13]

In its simplest form, the power extracted by the turbine is given as:

$$P = \frac{1}{2}\dot{m}({c_\infty}^2 - {c_2}^2) \qquad \text{Eq. 13}$$

The relationship between the wake speed and the free-stream speed is known as the axial induction factor:

$$a = \frac{1}{2}\frac{c_\infty - c_2}{c_\infty} \qquad \text{Eq. 14}$$

The axial induction factor is also the fractional reduction in flow speed between the free-stream and disk. Another parameter, the tangential induction factor a´, is the ratio of the wake rotation speed to the disk rotation speed and is found through iteration [35].

However, BMT relies on many assumptions, some of which are not practical: 1D, inviscid, incompressible, and isentropic flow; infinitesimally thin disk with an infinite number of blades; uniform thrust and velocity over disk; static pressure far upstream and downstream are equal to ambient static pressure; and no frictional drag [32]. While there are many methods of

accounting for these assumptions, one of the most common is by applying Prandtl's tip loss factor:

$$F = \frac{2}{\pi} cos^{-1}[exp(-\frac{N(R-r)}{2rsin\varphi})] \quad \text{Eq. 15}$$

The Prandtl tip loss factor compensates for a finite number of blades, the largest source of error in BMT [11].

Including the tip loss factor, the equations for incremental thrust and torque are given as:

$$dT = 4\pi Fa(1-a)\rho c^2 r dr \quad \text{Eq. 16}$$

$$d\tau = 4\pi Fa'(1-a)\rho c\omega r^3 dr \quad \text{Eq. 17}$$

3.2.4 - Blade Element Momentum Theory

From BET and BMT, Equations 8 and 9 are set equal to Equations 16 and 17, respectively. From these relations:

$$\frac{a}{1-a} = \frac{\sigma(C_l cos\varphi + C_d sin\varphi)}{4Fsin^2\varphi} \quad \text{Eq. 18}$$

$$\frac{a'}{1+a'} = \frac{\sigma(C_l sin\varphi - C_d cos\varphi)}{4Fsin\varphi cos\varphi} \quad \text{Eq. 19}$$

Equations 11, 18, and 19 need to be solved simultaneously and iteratively to find accurate values for *a*, *a´*, and φ. Once values for these parameters are found, they are plugged back into either Equation 9 or 17 to find the torque for the specified blade element; by repeating this process for the entire blade, the overall torque is found [35].

3.3 - Auxiliary Devices

In 1919, Albert Betz calculated the maximum power coefficient for a simple turbine in a flow stream to be approximately 0.593, known as the Betz limit. Modern day turbines achieve less than 80% of the Betz limit in efficiency [7]. Furthermore, the power generated by the system is also dependent on other efficiencies, such as the gearbox. According to a report by the World Energy Council, a typical overall efficiency for a simple turbine is around 0.35, meaning only one

third of the available kinetic energy in a stream flow is converted to electricity [43]. While the turbines themselves are constrained by the Betz limit, there are ways to increase the power coefficient by adding auxiliary devices.

3.3.1 - Duct Systems

Ducts, used as diffusers or funnels, are among the simplest devices to add to turbines for increased performance. A diffuser is a cone with a smaller inlet than exit that is attached to the back of a turbine. As fluid flows through a diffuser, it flows along the cone walls and creates vortices near the exit. These vortices draw in most of the fluid, creating a low-pressure zone in the middle behind the turbine. Due to the difference in pressure between the front and back of the turbine, fluid flow through the turbine significantly increases. A funnel can have a similar effect if it is attached to the front of the turbine; a high-pressure zone formed in front of the turbine can force fluid through the turbine at a higher rate. Additionally, both a diffuser and a funnel can be used on the same turbine to take advantage of the Venturi effect: the reduction in pressure and increase in velocity that occurs when a fluid flows through a constricted section in a pipe.

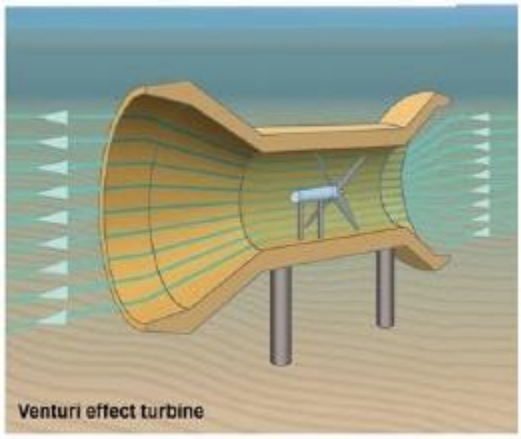

Figure 11: Example of Venturi effect turbine [38]

Turbines that use ducts require larger bodies of water to function correctly, since the entire duct should be submerged to operate as designed. Therefore, they are ideal to use in deep, slow moving rivers where flow rate is a major limitation for power generation. These mechanisms can increase water flow rate by 1.67 times the free stream velocity; with a high-performance diffuser or funnel, a power coefficient of up to 1.69 is possible, far exceeding the Betz limit [22].

3.3.2 - Pre-Swirl Stators

Another method of increasing turbine performance is minimizing post-turbine wake rotation, which is indicative of rotational losses. One possible method of achieving this is the utilization of pre-swirl stators, stationary blades that redirect flow before it reaches the rotor. By generating a fluid swirl opposite of the wake created by the turbine, the efficiency of the system increases. Such systems have been used with marine propellers, resulting in a decrease in fuel consumption of around 5% [45].

In turbines, pre-swirl stators redirect flow in the direction of blade rotation, increasing load on the blades and increasing torque, comparable to a fictitious increase in fluid velocity. Amin & Xiao reported a possible increase of up to 13% in the coefficient of power with the addition of pre-swirl stators after a series of computational tests (see Figure 12) [2].

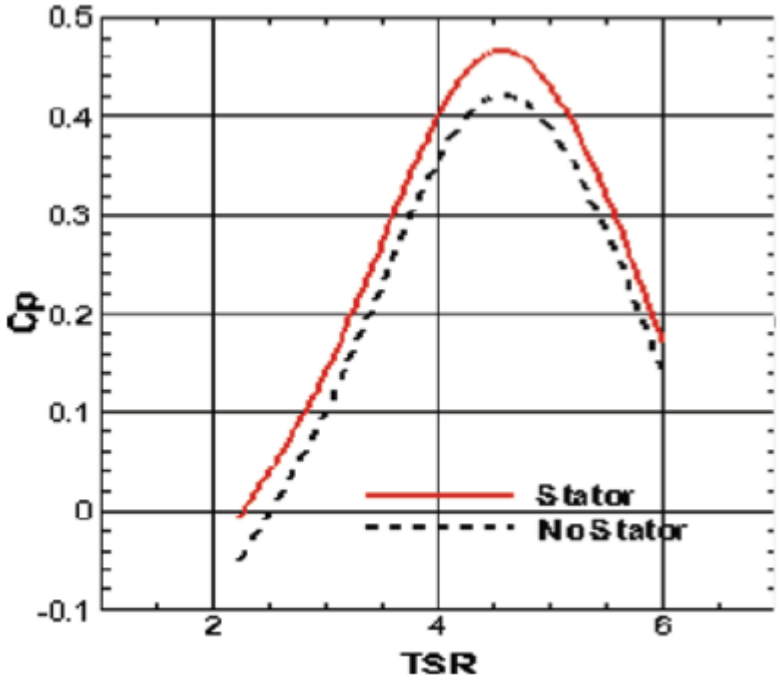

Figure 12: Power coefficients at different tip speed ratios [2]

Pre-swirl stators do not require larger bodies of water and are typically the same diameter or only slightly larger than the turbine blades, allowing for more flexibility than duct systems. They can also be used in conjunction with ducts to maximize the coefficient of power. However, since both systems significantly increase drag, the anchoring system needs to be stronger to compensate [15].

4 - Methodology

The goal of this project was to optimize and determine the feasibility of a hydrokinetic power plant with an outrunner motor-style turbine. The hydraulic turbine was designed as a rotating tube with turbine blades extending inwards in contrast with a traditional design in which blades extend radially outwards from the axis of rotation. While axial hydrokinetic turbines share many similarities with wind turbines and have been researched extensively, no literature was found discussing an outrunner-style turbine mechanism. Therefore, simulations and tests were performed starting with very basic parameters and progressed to more specialized parameters.

4.1 - Early Ideation with Fixed Design Parameters

The first step was to create initial models of the turbine. These early designs drew inspiration from outrunner motors, wind turbines, and turbine engines. In order to reduce variability between models, a list of fixed design parameters was created. The fixed parameters were:

- Outside turbine diameter of 1.6 m
- Inside turbine diameter of 1.5 m
- Water velocity of 2.5 m/s
- Three gears encircling the turbine to drive the generators

While the last two fixed parameters did not affect the design of the turbine itself, they were used during simulations and outer shell design, respectively. Many different turbine designs were modeled; however, all of the designs shared a simple cylindrical shell, with blades radiating inward from the shell towards the center of the geometry. There was also no central axle at the center of the cylinder; instead, there was an opening through which water was allowed to pass.

One of the most important aspects of these original designs was ensuring that the SolidWorks models were easy to manipulate, so that necessary variables could be changed depending on acquired data. For this reason, almost all of the variables, including the length of the turbine, the diameter of the turbine, the angle of the blades, the number of blades, the diameter of the central hole, and many others, were easily adjustable.

4.2 - Software Simulations

To determine whether the outrunner design turbine could produce sufficient power, the performance of the turbine needed to be improved. Performing turbine calculations by hand would be prone to inaccuracies and mistakes. Therefore, simulations were performed in ANSYS Workbench, XFOIL, and MATLAB to determine properties and values of parameters that maximize turbine performance.

4.2.1 - ANSYS Workbench

ANSYS Workbench was used to determine the effects of varying different parameters on torque and power generated by the turbine. To perform these analyses, the “Fluid Flow (Fluent)” analysis system was used. The ANSYS Workbench academic version was used, since a professional license was not available.

The simulations performed in Fluent all used the same setup to provide standardization and mitigate external variability. The fluid domain was set to a cylinder with a radius that is five times greater than the outer diameter of the turbine, as seen in Figure 13.

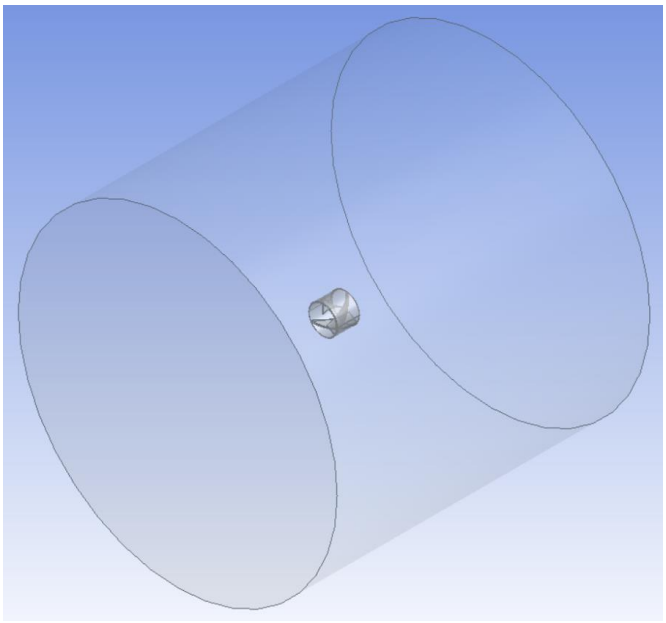

Figure 13: Turbine inside fluid domain in ANSYS Fluent

Fluent was set to the following settings: pressure-based, steady-state, and absolute velocity-based. The inlet was set to a velocity inlet, the outlet set to an outflow, and the outer area of the fluid domain set to a wall. The reference values can be seen in Figure 14. One thousand iterations, with a ten-step hybrid initialization was used.

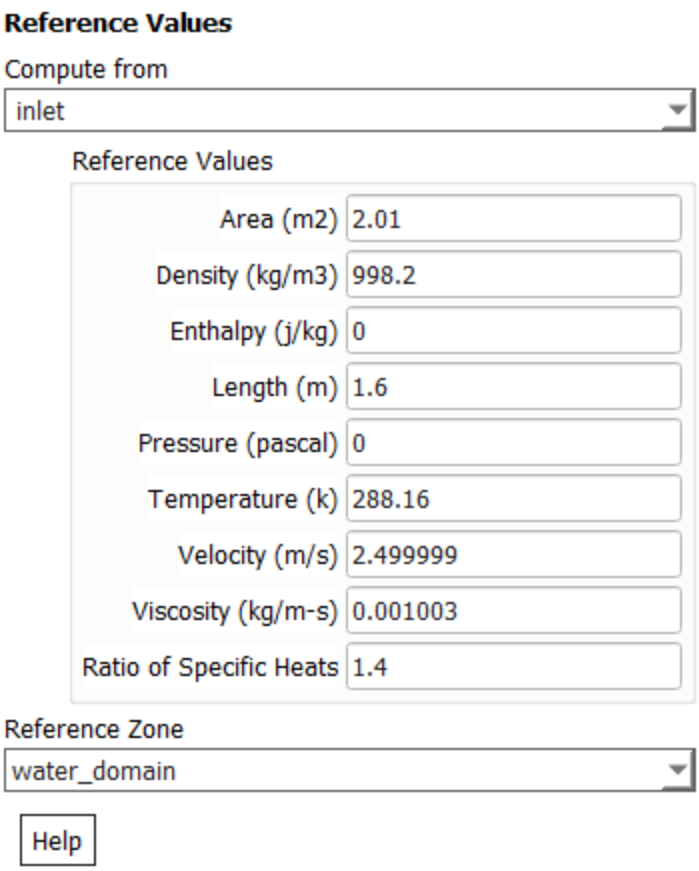

Figure 14: Reference values in ANSYS Fluent

ANSYS Fluent was used to provide an initial understanding of important turbine parameters and adjust them accordingly to maximize performance. However, problems were encountered during some of the tests, which are discussed in Appendix B.

Initial Tests

Initial tests were performed to determine the effects of different blade angles on torque generation. Since these tests were performed early in the development process, the importance of stagger angle was not known at the time, and the tests instead used 'total swept blade area,' calculated from 'traveled angle per blade.' When the turbine is viewed along its axis of rotation, the leading and trailing edge of each blade is offset by an angle; this is the traveled angle per blade (see Figure 15).

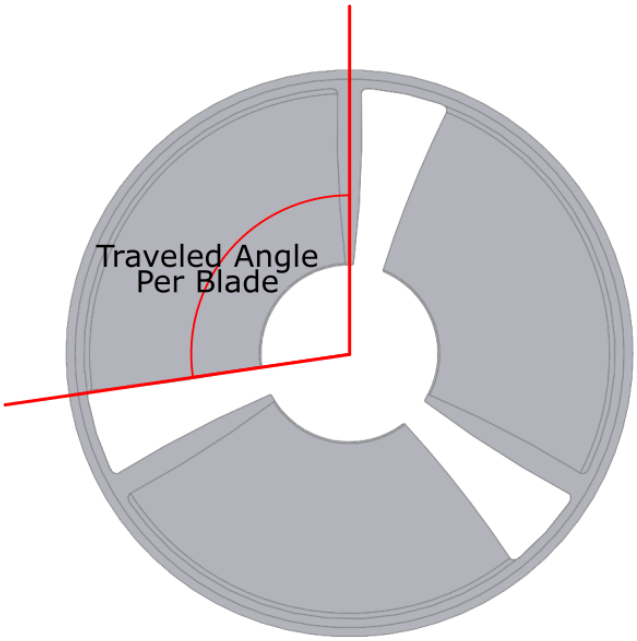

Figure 15: Turbine viewed along axis of rotation to demonstrate traveled angle per blade

In terms of stagger angle, traveled angle per blade can be found with:

$$\varphi = \frac{Ltan\xi}{R}\left(\frac{180}{\pi}\right) \quad \text{Eq. 20}$$

Total swept blade area is then found with:

$$A_{bl} = \pi N \frac{\varphi}{360}\left(R^2 - (R - z_{bl})^2\right) \quad \text{Eq. 21}$$

The purpose of the first test was to determine the effects of the number of blades. Fluent simulated flow through eight different turbine models with one through eight blades, each with a total swept blade area of 360°. Since all turbine models had the same total swept blade area but different number of blades, the models all had different traveled angles per blade.

The purpose of the second test was to determine the importance of traveled angle per blade over total swept area. A total of 48 models were tested. The models had between two and six blades and between 22.5° and 180° traveled angles per blade, in increments of 22.5°. The results from these two tests were used to standardize the number of blades.

Stagger

After performing initial tests, the effects of changing stagger angle on torque generation was explored. Fifteen models, with stagger angles between 8° and 78°, were tested to

determine stagger for optimal torque generation. Examples of the models can be seen in Figure 16 below.

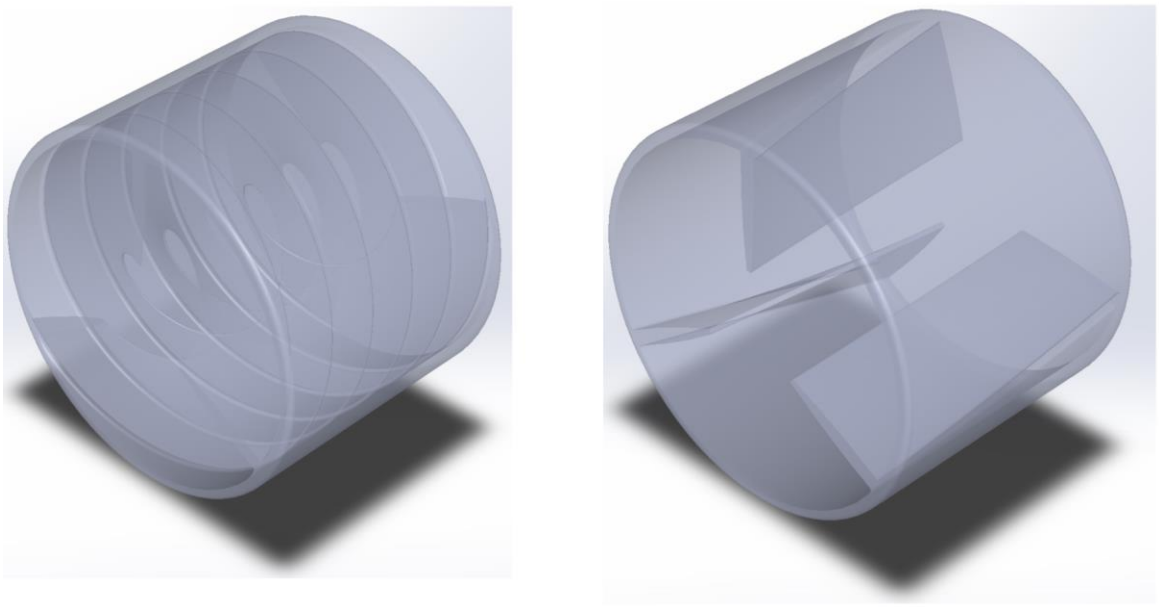

Figure 16: Models with 8° (left) and 78° (right) stagger angles

In contrast with the initial tests, the models used in these tests had a length of 1.25 m instead of 2.5 m to improve physical fabrication speed; this was due to complications with physical water tunnel testing and is discussed further in Appendix C.

Length and Water Speed

To ensure that changing model lengths had no adverse effects on turbine performance, several models of different lengths were tested in different water velocities. The model lengths ranged between 0.25 m to 2.5 m in increments of 0.25 m, while the water velocities ranged between 0.5 m/s and 5 m/s, with increments of 0.5 m/s. Examples of the models can be seen in Figure 17 below.

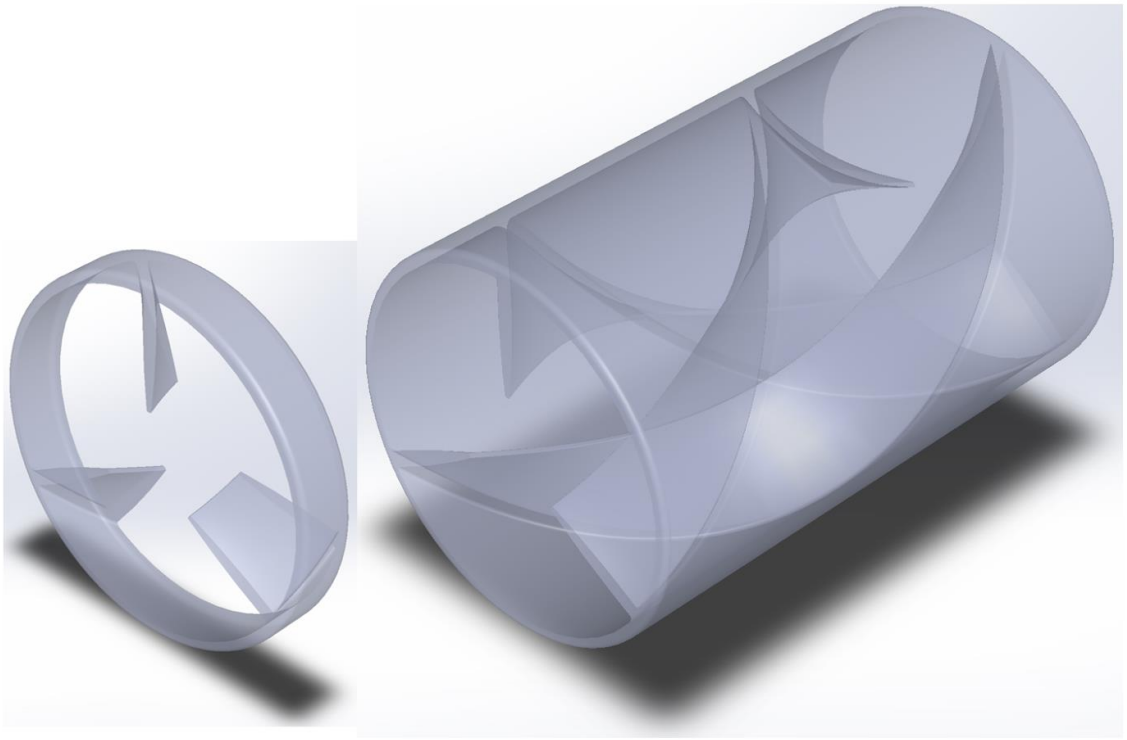

Figure 17: Models with 0.25 m (left) and 2.5 m (right) lengths

With the data collected from these simulations, the effects of different turbine lengths on torque generation was determined for different water velocities. The efficiency of the turbines was then calculated to determine whether the turbine yields different efficiencies at different water speeds. Maximum torque was defined as the torque achieved if all water pressure flowing through the turbine exerted force on the blades only on the maximum radius, normal to the axis of rotation:

$$\tau_{max} = \frac{1}{2}\pi\rho c^2 R^3 \qquad \text{Eq. 22}$$

leading to the expression for efficiency:

$$\eta_\tau = \frac{2\tau_{act}}{\pi\rho c^2 R^3} \qquad \text{Eq. 23}$$

Blade Height

Next, the effects of changing blade height was determined. Ten different models were tested, with blades extending from 0% to 90% of the turbine radius in 10% increments. Examples of the models can be seen in Figure 18 below.

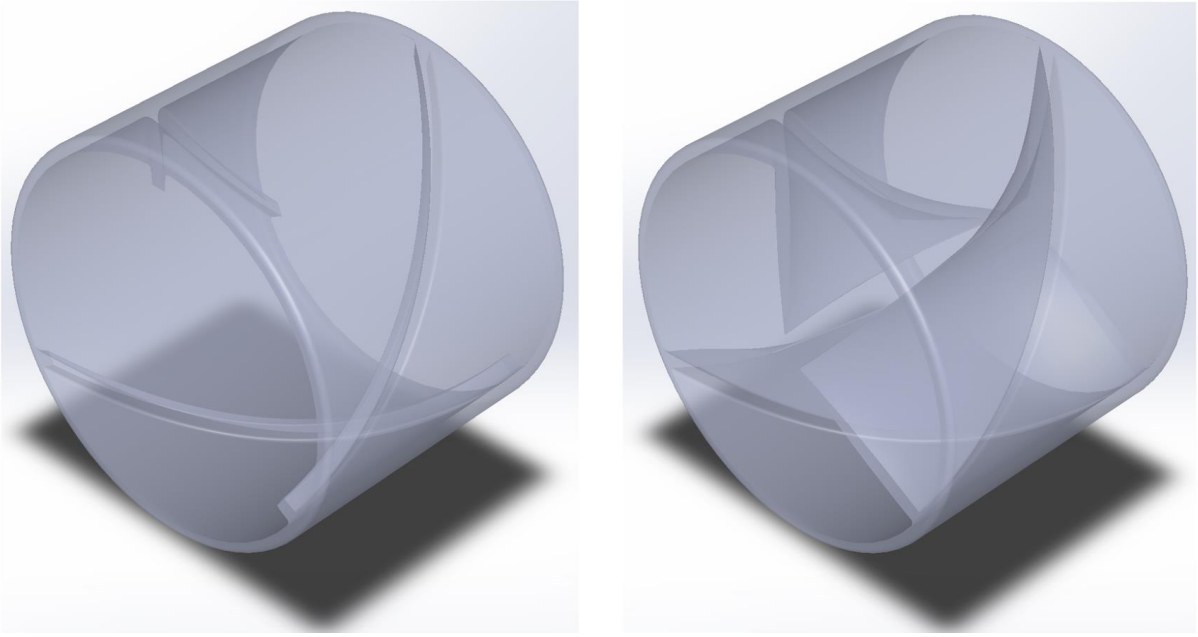

Figure 18: Models with 10% (left) and 90% (right) blade heights

This test measured induced drag in addition to torque, since excessive drag necessitates stronger fixtures and can lead to faster failure. The torque to drag ratio was also calculated for these blade heights to minimize drag, if necessary.

Ducts

The effects of funnels and diffusers were then tested to determine whether they can provide a profitable increase in performance. Due to limitations with the academic version of ANSYS Workbench and for ease of modeling, the ducts were attached directly to the turbine model, resulting in one composite model. The duct geometry was defined by two parameters: duct angle and radius ratio, which can be seen in Figure 19 below.

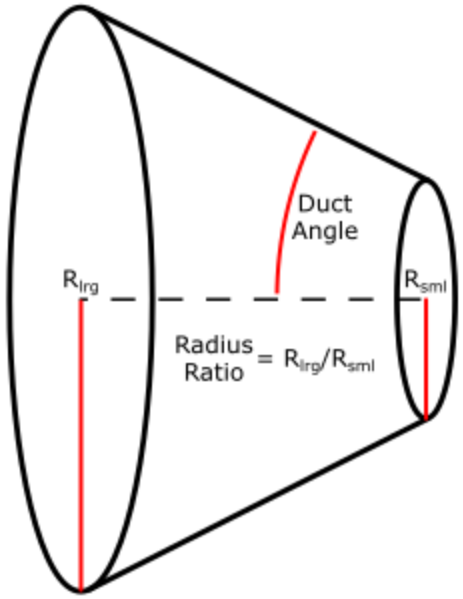

Figure 19: Duct geometry parameters

The duct angles used in this test ranged from 15° to 75° in increments of 15°, while the radius ratios ranged from 2 to 5. Examples of the models can be seen in Figure 20 below.

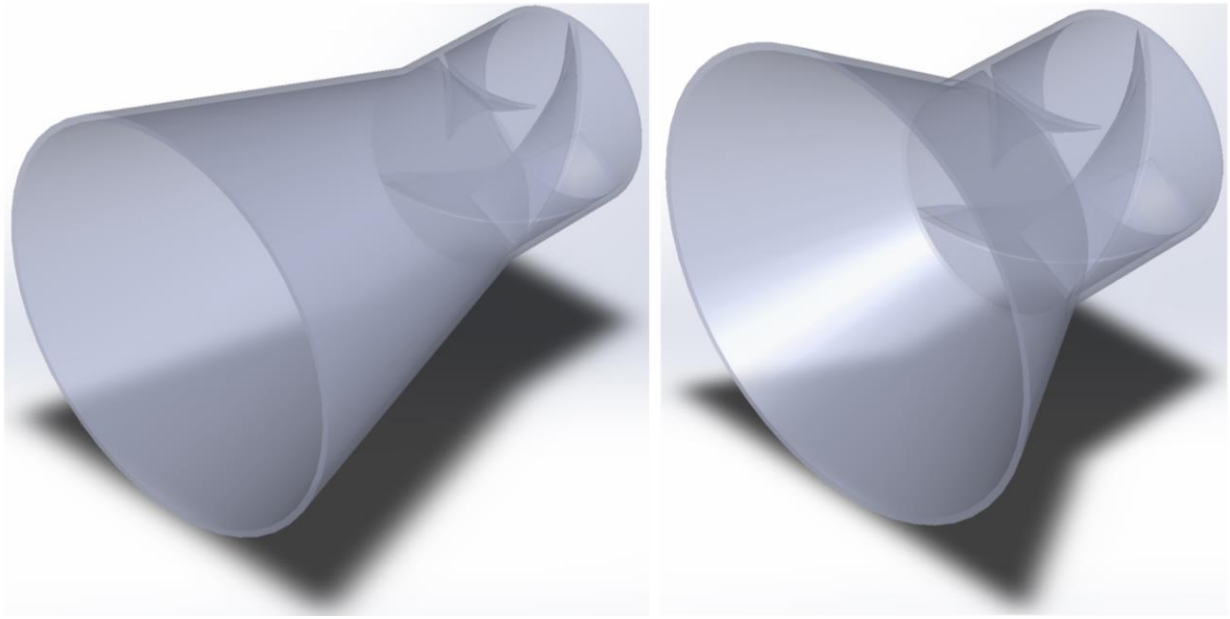

Figure 20: Models with radius ratios of 2 and duct angles of 15° (left) and 30° (right)

Similar to the blade height tests, drag forces were calculated during these simulations. The drag data was compared to the torque data and the benefits of using duct systems were determined.

Nose Cone

A short test to determine the effects of a nose cone was conducted next. Only one model was tested, which can be seen in Figure 21 below.

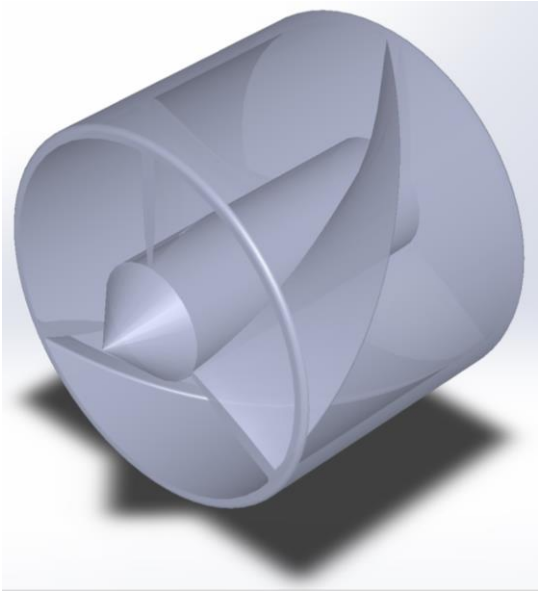

Figure 21: Model with nose cone

The nose cone was modeled as a cylinder occupying the center hole with a tip at 90°. The torque generated by the model with the nose cone was compared to the base model to determine whether nose cones can provide any significant performance improvement.

Angular Velocity

The previous tests were performed with a stationary model. This allowed for simple testing between model variation, but prevented power from being calculated since power requires angular movement (see Eq. 6). To find the angular velocity for maximized power, the model was rotated at different rates between 0 RPM and 36 RPM. The power was then calculated by finding the torque at a rotation rate and multiplying it against the given angular velocity. In order to ascertain the effects of friction on power generation, five different friction torques were subtracted from the generated torque.

Next, the relationship between water speed and optimal angular velocity was explored. Over one hundred tests were run for ten water speeds to determine the optimal angular velocity, measured to the closest tenth of an RPM, for power generation for each water speed.

Airfoil Profiles

The turbines tested to this point used flat plate airfoils as blades. To test the effects of airfoil profiles with different characteristics, three simplified blade profiles, designated test1 through test3, were created and compared to the default flat plate (see Figure 22).

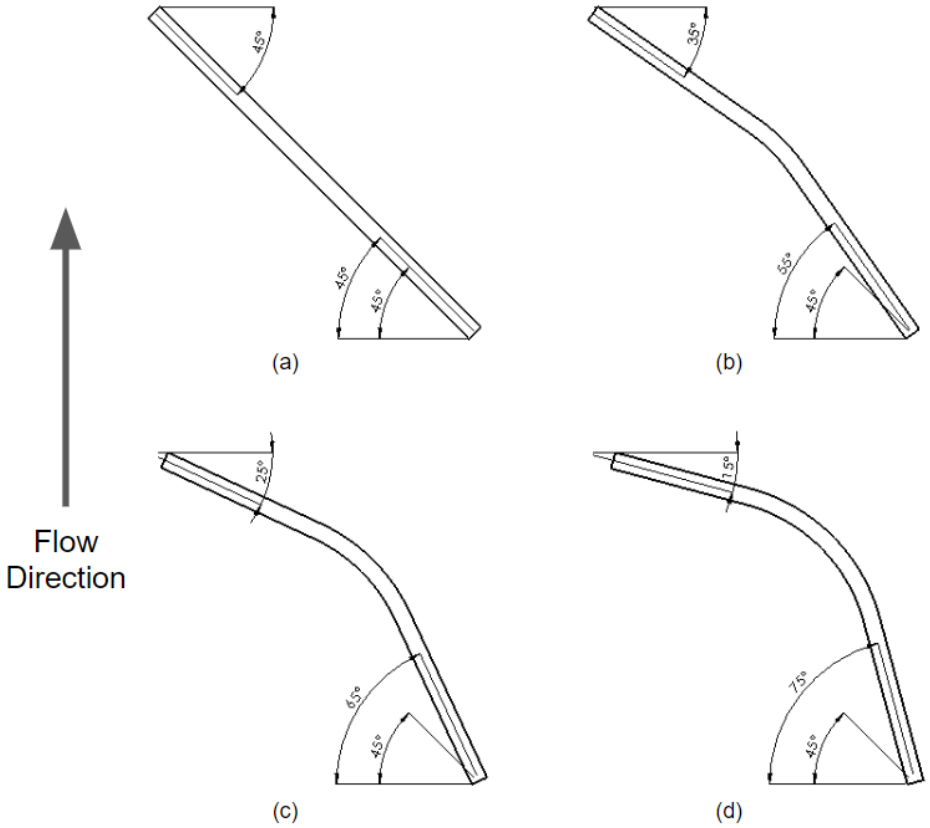

Figure 22: Tested profiles: (a) default; (b) test1; (c) test2; (d) test3

The profiles of the airfoils take the form of a flat plate with a bend in the middle. The reason for the simplified design is the limitations of the ANSYS Workbench academic version, which was not able to create meshes for blades with more complicated curvature. Examples of the models can be seen in Figure 23 below.

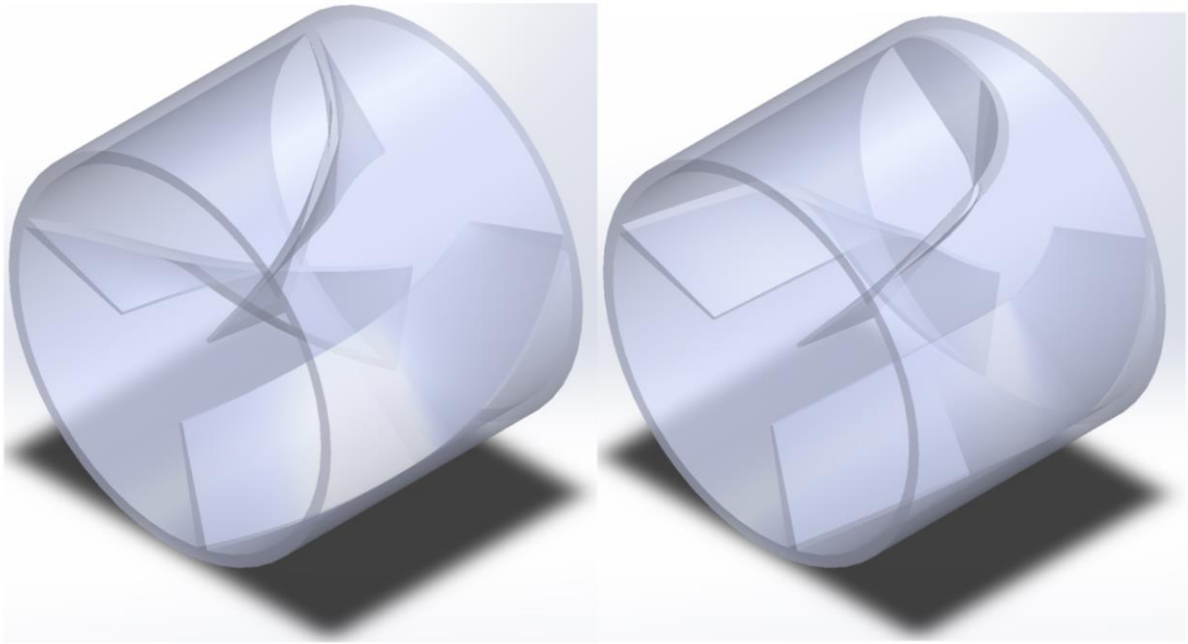

Figure 23: Models of test1 (left) and test3 (right)

These airfoils have exaggerated maximum cambers to increase the difference between their simulations. Real airfoils rarely have maximum cambers exceeding that of test1 since airfoils such as test2 and test3 are extremely prone to turbulent separation, reversed flow, and high drag.

4.2.2 - XFoil and MATLAB

Due to limitations with the ANSYS Workbench academic version, airfoils with smoothed profiles could not be tested. To better understand the effects of airfoil profiles on the performance of the turbine, XFOIL was used to procure the aerodynamic characteristics of selected airfoils. Eight of the tested profiles were found on the UIUC Airfoil Coordinate Database, and the last used the flat plate characteristic equations found in Table 2.

All the airfoils were tested with the same settings. Once a specified airfoil was loaded into the program, the paneling was modified to increase the accuracy of the calculations. The number of panel nodes was changed to 240 for increased resolution and the trailing to leading edge panel density ratio was changed to 1 for increased accuracy in the front and back of the airfoil. The program was set to calculate viscous flow with a Reynolds number of 5,000,000 and a Mach number of 0. These numbers were chosen as a representation of approximate values the airfoil would experience in water.

After setting up the program, the airfoil was tested at different angles of attacks. Each started at 0° and incremented by 1° until it reached 12°, when possible (see Figure 24).

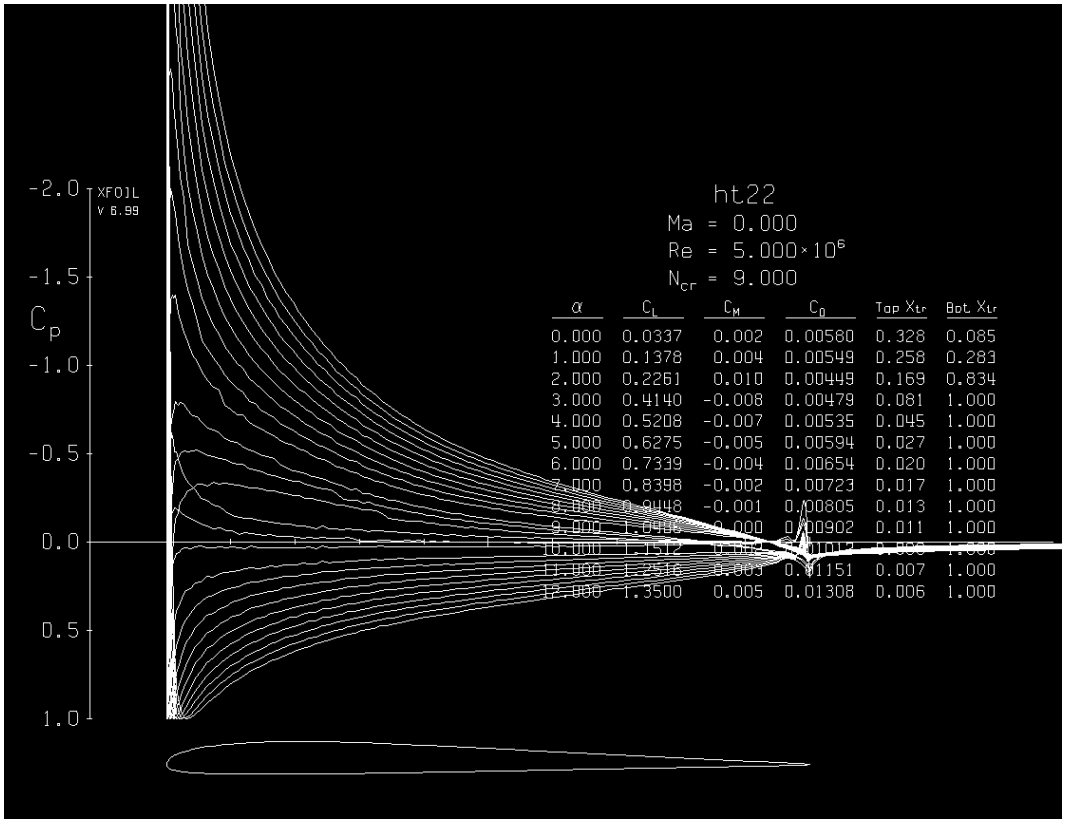

Figure 24: Tested angles for airfoil HT22 with pressure coefficient plots

The lift and drag coefficients for each test were recorded, and the lift-to-drag ratio was calculated as well. If spikes or other abnormal features were discovered, additional tests near the angle of attack of interest were conducted.

To analyze the effects of the airfoil characteristics on turbine torque, a MATLAB program was written that uses BEMT (see Appendix D). To determine whether the program was sufficiently accurate to draw meaningful conclusions from it, the program was run simulating a turbine with flat plates for blades at various rotational velocities. The torque and power outputs from these tests were compared to the results from the angular velocity tests run in ANSYS Fluent.

After confirming that the MATLAB program was sufficiently accurate, the eight airfoils were tested. To test each airfoil, the trend line equations for the lift and drag coefficients were found; a linear relation was used for the lift coefficient, while a second-degree polynomial was used for the drag coefficient. The equations for the trend lines were plugged into the program so that it could calculate the approximate lift and drag coefficients as needed. Neither the lift nor drag coefficients follow their respective trends over a large range of angles of attack, but none of the angles of attack in the calculations were observed to exceed 10°, allowing for a close

estimation. The program iteratively calculates the axial induction factor, tangential induction factor, flow angle, lift coefficient, drag coefficient, Prandtl tip loss factor, and angle of attack. The power generated by a turbine using each airfoil was calculated and compared to each other.

After discerning the effects of different airfoils on torque generation, the MATLAB BEMT program was modified to determine the optimal airfoil characteristics (see Appendix E). The modified program iterates over a specified number of values for coefficient of lift, coefficient of drag, and rotational velocity and calculates the torque and power from every combination. It then returns the combination that resulted in the highest power as the optimum solution. Since performing the calculations takes exponentially longer with more tested values, the number of different values for each parameter was set to a low number, and the returned values were refined by adjusting the upper and lower bounds of each parameter as needed.

4.3 - Water Tunnel Testing

To test the real-world viability of the design, numerous tests were conducted in a water tunnel. These tests occurred throughout the duration of the project, and a wide variety of different turbine designs were tested. To conduct these tests, scaled down versions of the most current SolidWorks design were used. These designs were then manufactured using a 3D printer, seen in Figure 25 below.

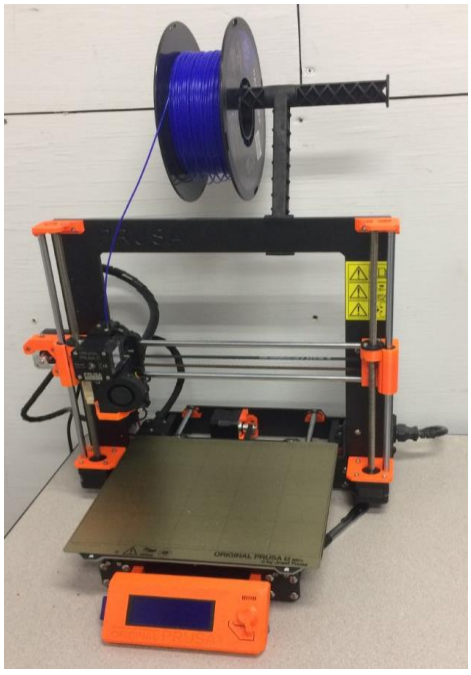

Figure 25: Prusa i3 Mk2

For the original tests, scaled down prototype turbines with a diameter of 5 cm and a length of 7.8 cm were used, a 1:32 scale model. The shell and bearings used to mount and secure these prototypes were also 3D printed. However, none of these early prototypes were successful. This was primarily because of the large amount of friction in the preliminary prototypes.

To remedy this issue, later experiments were conducted differently. The diameter of the model was increased to 10 cm, and the length was kept at 7.8 cm, increasing the size to a 1:16 scale. This significantly decreased the overall effect of friction on the turbine. Additionally, the shell was changed as well; while the bulk of the design remained 3D printed PLA, the contact surface with the turbine was changed to a PVC pipe with a diameter of four inches. The PVC pipe has a smooth inside surface, which led to a significant reduction in friction when compared to 3D printed roller bearings. Additional PLA printed inserts were used to separate the turbine from the back wall of the shell, reducing friction between the turbine and the outside shell. After completing these changes to the prototype design, the tests began producing successful results.

The models were tested in the water tunnel in Higgins Laboratories at Worcester Polytechnic Institute. Due to faulty equipment, the water speed was stuck at 5.23 in/s; this speed is geometrically similar to a water speed of 2.12 m/s for a full-scale model. While slightly slower than the target velocity of 2.5 m/s, the speed was deemed sufficient for testing. However, the scale test was neither kinematically nor dynamically similar to a full-scale environment since Reynolds number was not matched; assuming a Reynolds number of 5 million, a fluid with a kinematic viscosity of 2×10^{-9} m^2/s or a water velocity of 57 m/s would be necessary. Neither are achievable; therefore, while the scaled water speed was sufficient to match target velocities, no numerically specific conclusions could be drawn from the tests.

However, the physical tests still provided valuable proofs of concept. Throughout the project, models were printed and tested to determine whether the turbine could rotate in the experimental conditions. Physical tests were especially important in testing the pre-swirl stator. The pre-swirl stator adds another component to the system and the limitations with the ANSYS Workbench academic version prevented both structures from being loaded. Similarly, the pre-swirl stator could not be tested in MATLAB due to the complexities of rotating one component while keeping the other stationary. A model of the pre-swirl stator was printed, along with a truncated model of the turbine; this was done so a new, larger fixture would not have to be printed. The stator was held in place by wads of paper towels to prevent it from rotating, while the turbine component was supported and held in place by two PVC sections.

When the turbine model was in the water tunnel, a camera was used to record a video of it rotating. The video was analyzed, and the rotational velocity was determined. While the rotational velocity of the physical model differs from a full-scale model, it was still useful for determining whether or not the stator increased performance of the turbine. The rotation rate of the turbine with the stator was compared to a previous test without the stator for this reason.

4.4 - Turbine Casing Development

As the turbine model was developed, a casing was designed to house it for power generation. The designed shell is only preliminary and meant to demonstrate the complete power plant concept. The shell was created using SolidWorks and was largely based on the fixed design parameters. It also incorporates some of the data collected from the ANSYS Fluent tests.

5 - Results and Final Design

The results of the experiments and simulations are important to create optimizations that will be incorporated into the final design. The results of the simulations are presented and discussed.

5.1 - ANSYS Fluent General Design Simulations

As discussed above, ANSYS Fluent was used to optimize the performance of the turbine. The results of the tests are discussed in this section.

Initial Tests

The first set of data compared the performance of turbines with a different number of blades, but with the same swept area. The results of this test can be seen in Figure 26 below

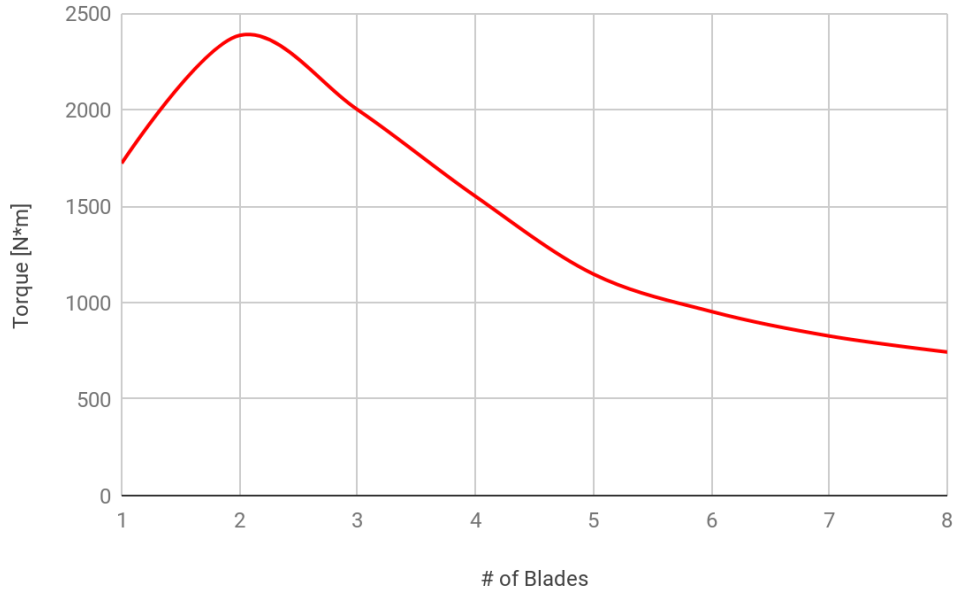

Figure 26: Torque vs. number of blades, with the same swept area

It was originally hypothesized that total swept blade area was the main factor that controlled the performance of the turbine. However, the test shows a significant difference in the torque created by turbines with a differing number of blades, despite having the same total swept blade area.

To determine whether the decisive factor in turbine performance was number of blades or traveled angle per blade, simulations of turbines with different combinations of blade numbers and swept angles per blade were run. The results of this test can be seen in Figure 27 below.

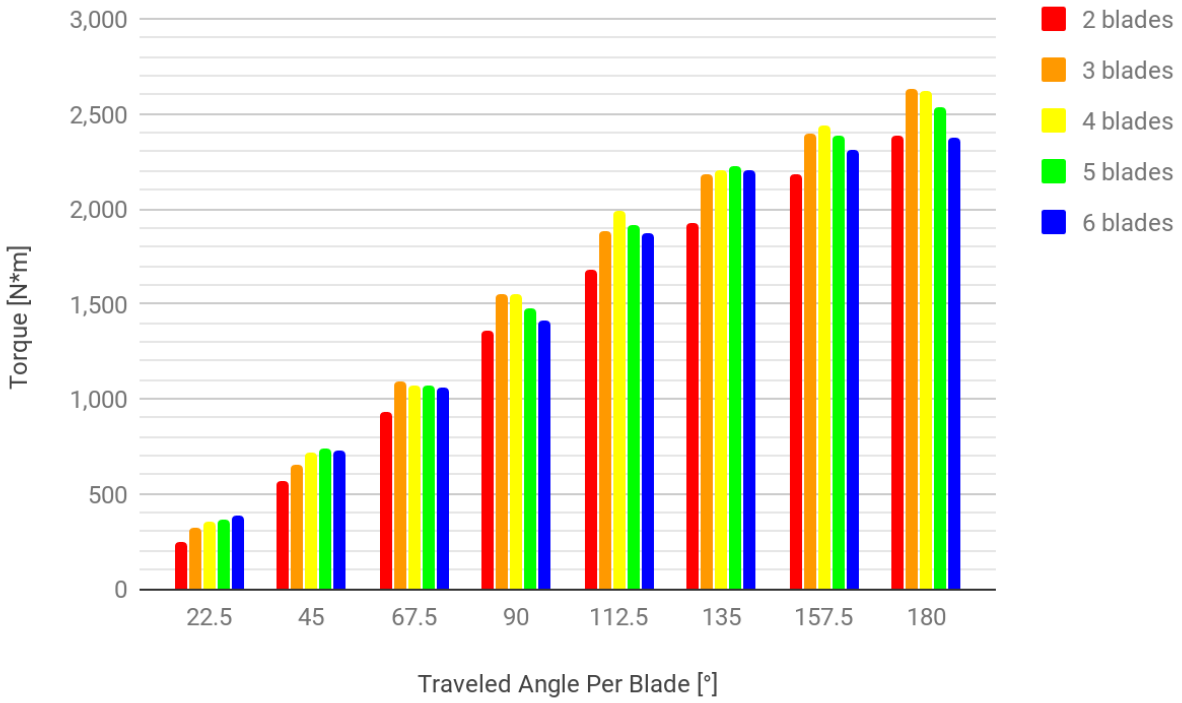

Figure 27: Performance of number of blades and traveled angle per blade

The simulations showed that traveled angle per blade was the most significant factor in torque generation for a turbine. The models with small traveled angle per blade performed significantly worse than those with a higher traveled angle per blade. However, the data still indicated that the number of blades has some effect on the torque generated. For most of the traveled angle per blade groupings, the models with three or four blades performed noticeably better than the other models. While models with four blades performed better in some cases, adding another blade would add manufacturing costs for an insignificant performance increase. Taking this information into account, the base model was updated to have three blades.

Stagger

From the initial tests and literature review, it was determined that the angle of the blade against the water has a significant effect on turbine performance. Instead of using traveled angle per blade, however, stagger angle was tested instead, since stagger angle is independent

from the length of the turbine. The results of the stagger angle tests can be seen in Figure 28 below.

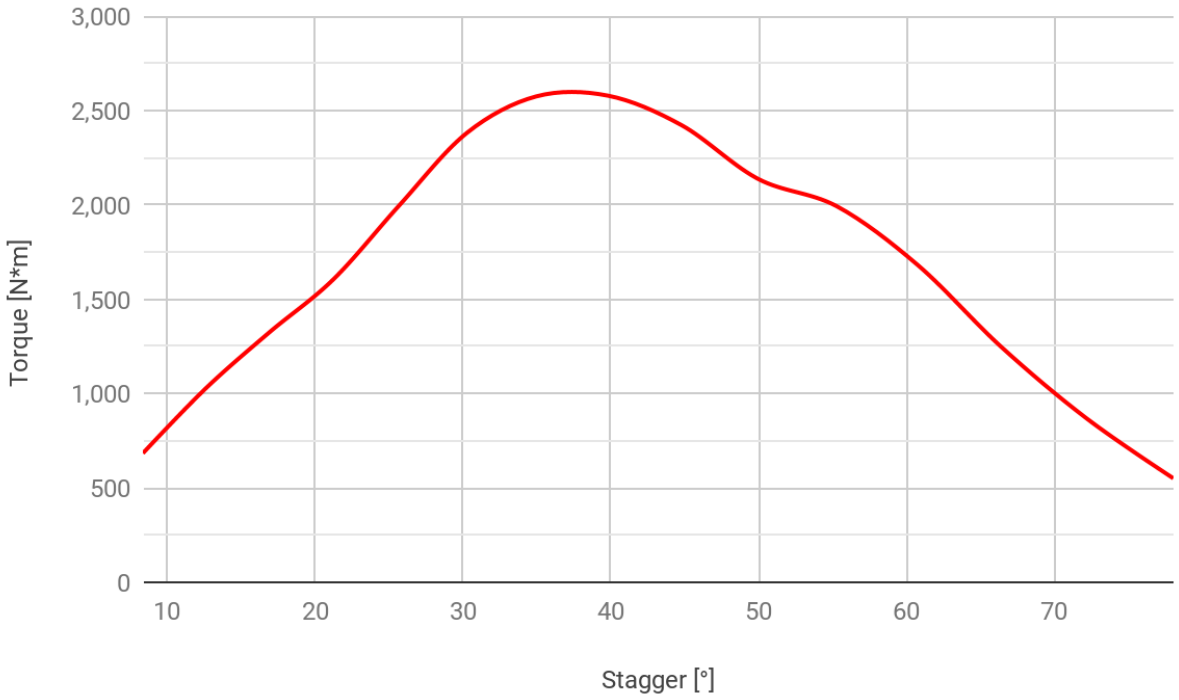

Figure 28: Performance of different stagger angles

The simulations showed that the optimal stagger angle for the turbine is between 35° and 40°. However, due to computational errors, the optimal pitch was initially believed to be 45°; additionally, as mentioned in section 4.2.1 above, the models used in this section had a length of 1.25 m instead of 2.5 m. These faults are further discussed in Appendix B. Nonetheless, the base model was updated to have a stagger of 37°.

Length and Water Speed

To determine whether changing the length of the turbine had significant effects on its performance, models of different lengths were tested at different water speeds. The results of the test can be seen in Figure 29 below.

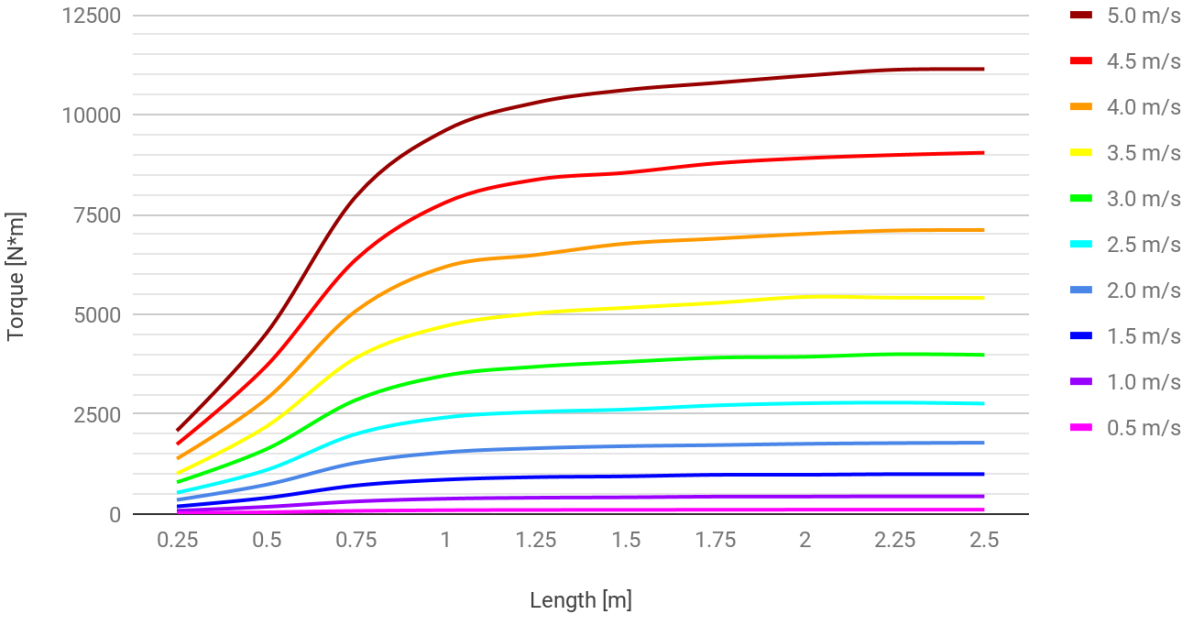

Figure 29: Performance of different turbine lengths and water speeds

The simulation data demonstrates that torque production is positively correlated with length. However, the torque eventually seems to reach an asymptote at approximately 1.25 m, which coincidentally coincides with the new turbine length. To determine whether the efficiency of the turbine was dependent on the water velocity, the maximum torque for a given speed was calculated and the efficiencies for each test were determined. The results of these calculations can be seen in Figure 30 below.

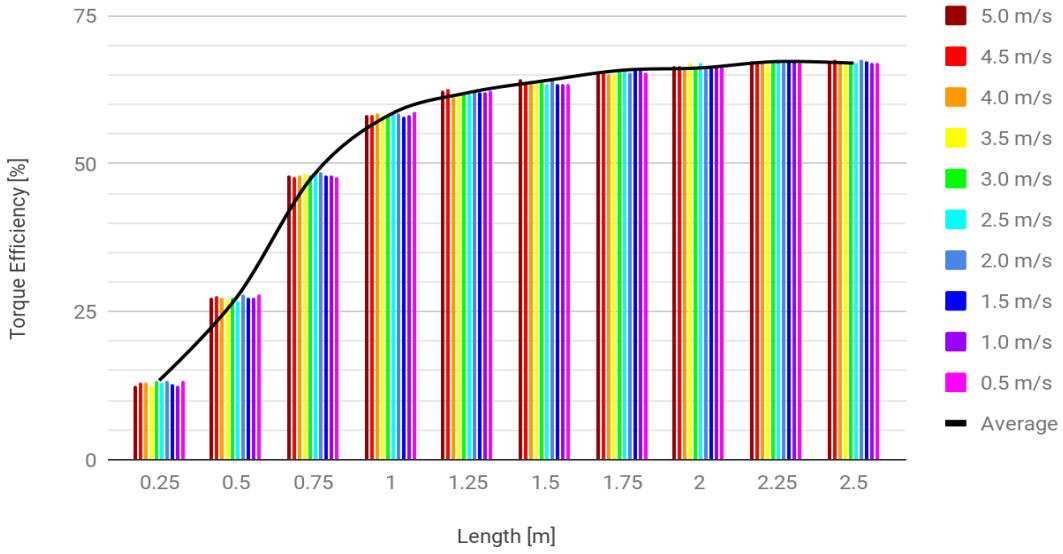

Figure 30: Efficiencies of different turbine lengths and water speeds

The efficiency of the turbine approaches an asymptote of about 68% efficiency, independent of water velocity, flattening out around a length of 2 m. From this data, the base model was kept at 1.25 m long; while the efficiency could be increased by lengthening the turbine slightly, increasing the length of the turbine increases production costs and has increasingly diminishing returns.

Blade Heights

The performance of different blade heights was tested. The results of these simulations can be seen in Figure 31 below.

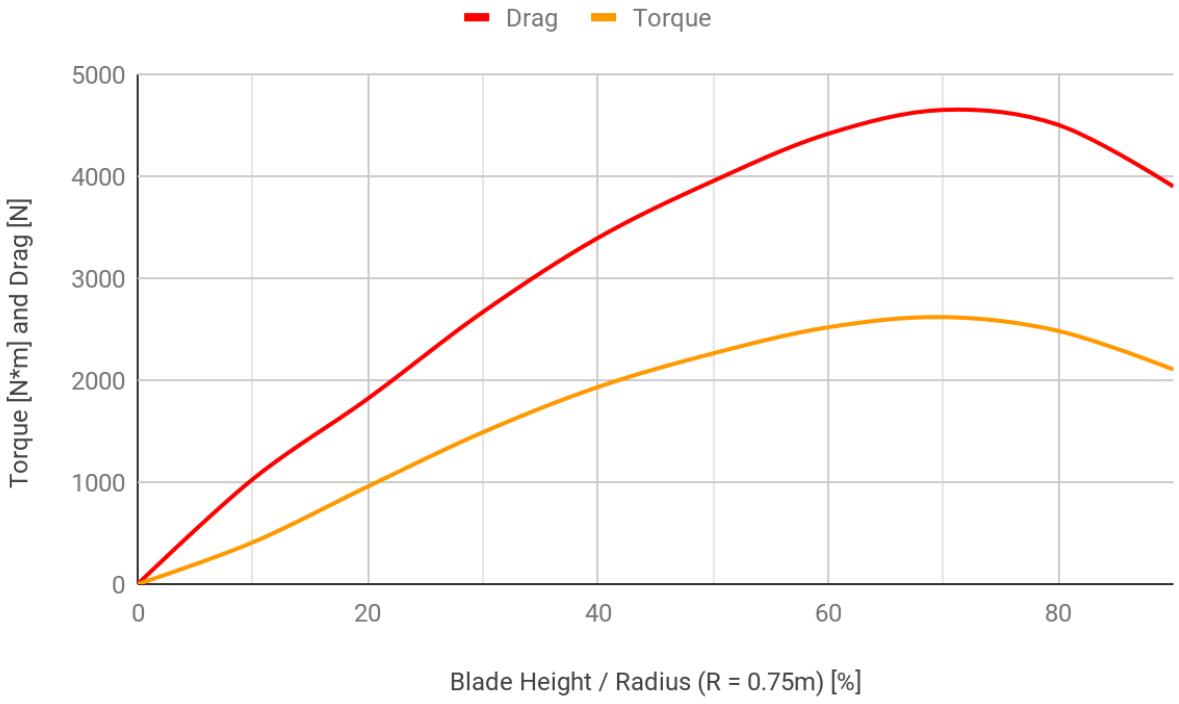

Figure 31: Torque and drag performance of different blade heights

At smaller blade heights, torque and drag increase predictably; larger blades contact more water, increasing force on the blades which increases both torque and drag. At around 70% blade height, however, both torque and drag begin to decrease. The decrease continues as the blade height increases. The decrease in torque and drag may be due to increased viscous forces and back pressure through the turbine as a result of increased surface area in contact with the water. The resistance caused by the back pressure forces water around the turbine, rather than through, decreasing overall torque and drag.

Since increased drag necessitates stronger fixtures and can hasten wear of the turbine elements, it was important to determine whether there was an optimal blade height for maximized torque with minimized drag. The results of the torque-to-drag ratio as a function of the blade height can be seen in Figure 32 below.

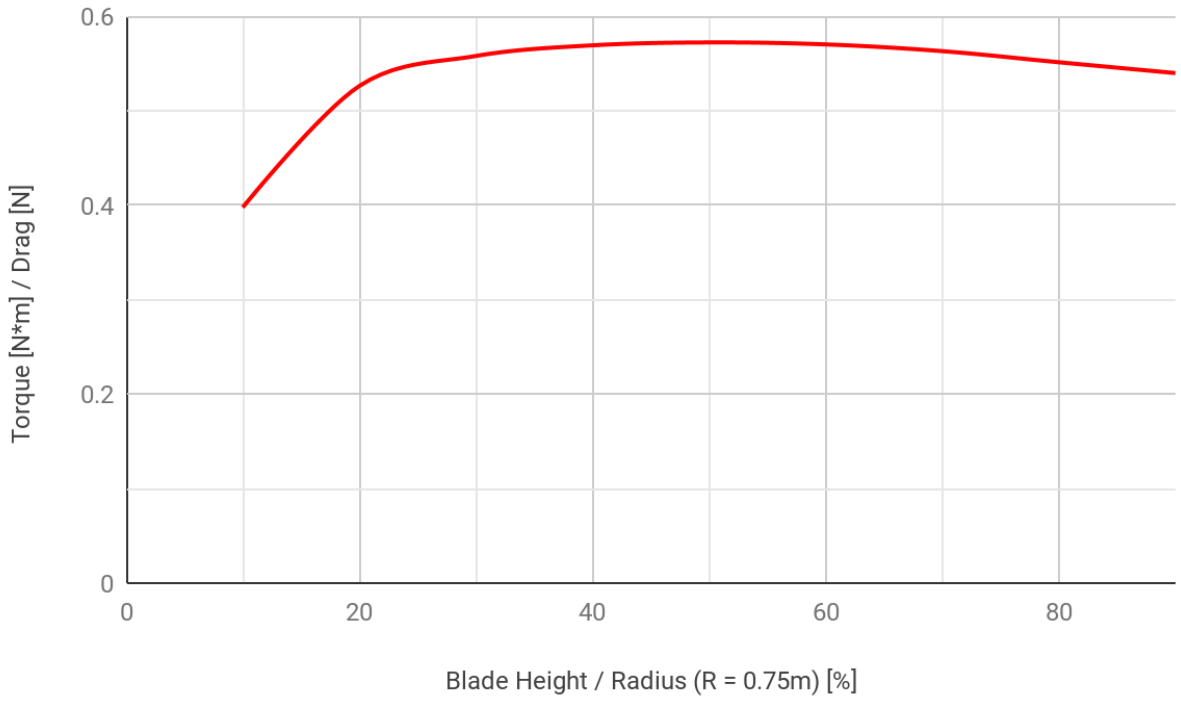

Figure 32: Torque to drag ratio for different blade heights

The torque-to-drag ratio increases from 10% to 50% blade heights, with the most significant increase occurring from 10% to 20%. After 50% blade height, the torque-to-drag ratio begins to decrease. Regardless of whether it is increasing or decreasing, the torque-to-drag ratio changes very little between 20% and 90%. This indicates that the change in torque and drag are proportionate to the change in blade height, and that torque-to-drag ratio is not a factor that is predominant in designing the turbine. From this data, the blade height on the base model was kept at 67%; this value was close enough to the maximum torque value of 70% that changing it was deemed unnecessary.

Ducts

Ducts were tested to determine if they could increase performance by a significant amount. Funnels were tested first, with four different radius ratios and five different duct angles. The results of the test can be seen in Figure 33 below.

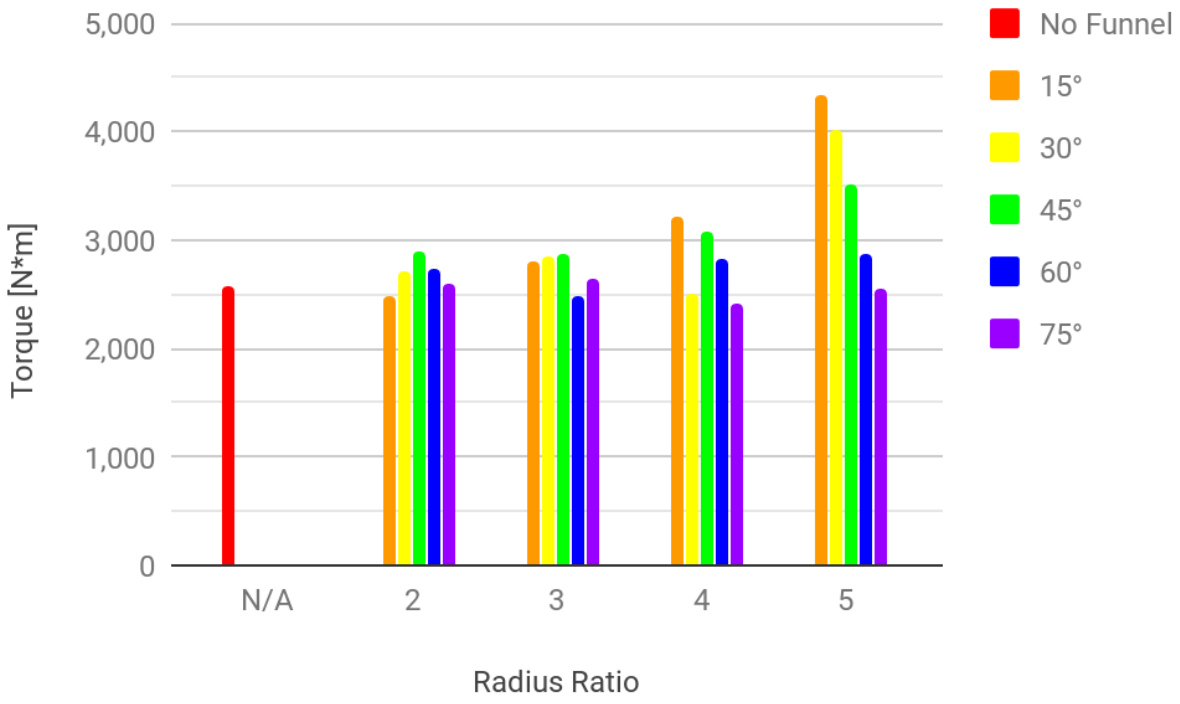

Figure 33: Performance increase from different funnel geometries

In comparison to the turbine without a funnel, many of the models with funnels performed slightly better. The best performing funnel had a radius ratio of 5 and duct angle of 15°; however, this funnel would be extremely impractical. The opening would have a diameter of 7.5 m and the length of the duct would reach over 11 m. The other funnels do not provide as much performance improvement as one might predict, possibly due to viscous forces and back pressure limiting flow through the turbine. In addition, the funnels also incur significant drag, as seen in Figure 34 below.

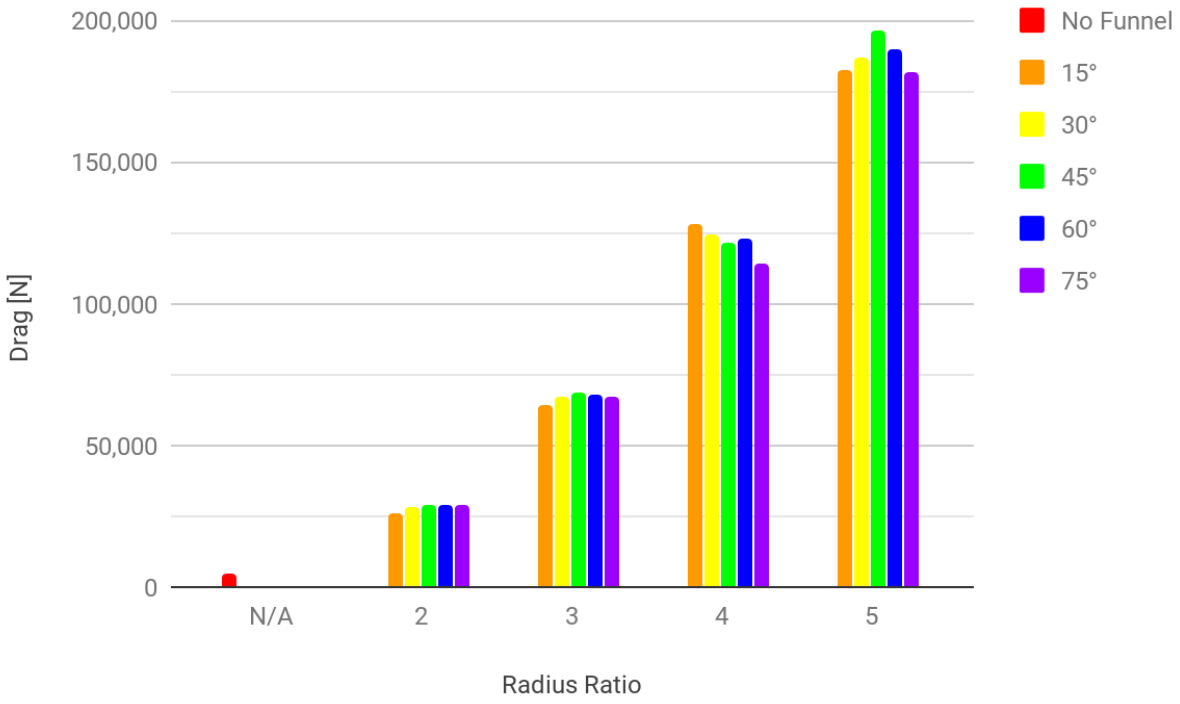

Figure 34: Drag of different funnel geometries

The drag simulations demonstrate the massive amounts of drag produced by funnels of different sizes. In addition to being impractically sized, funnels with a radius ratio of 5 produce up to 43 times as much drag as a turbine without a funnel. Smaller funnels also produce significant amounts of drag, and do not increase turbine performance enough to justify their use. Drag experienced by these funnels would require fixtures several times stronger than a turbine without a funnel and would cause component degradation at a higher rate without any substantial payoff.

Diffusers were tested next; however, they were only tested with a radius ratio of 2, since the other sizes are largely impractical. The results of this test can be seen in Figure 35 below.

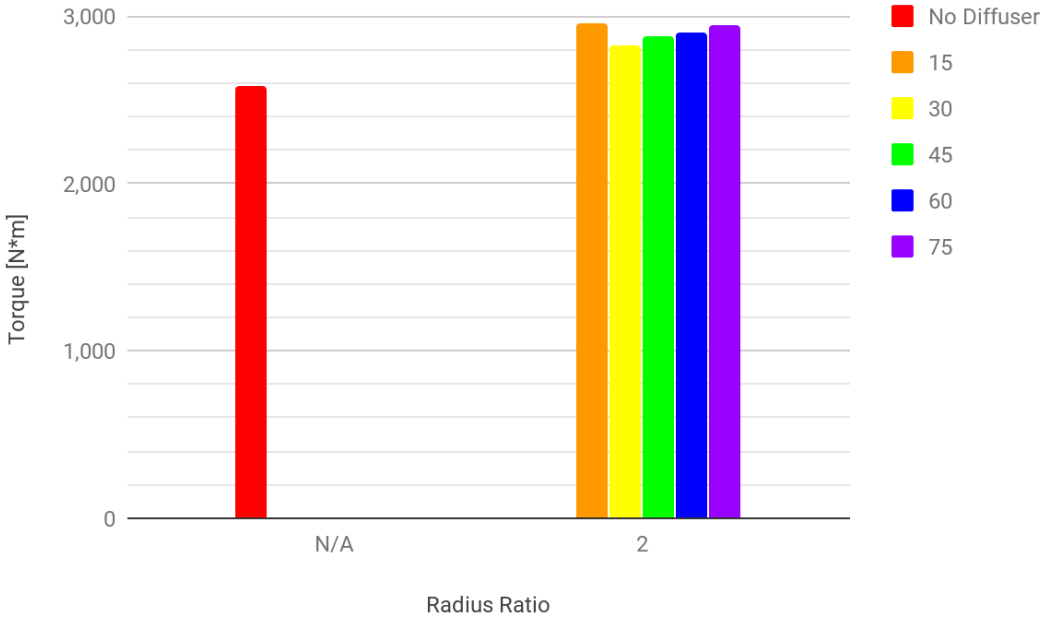

Figure 35: Performance increase from different diffuser geometries

The performance increase from diffusers is larger than the increase from funnels of the same size. It also appears to be somewhat independent of duct angle. The drag, however, is dependent on duct angle, as seen in Figure 36 below.

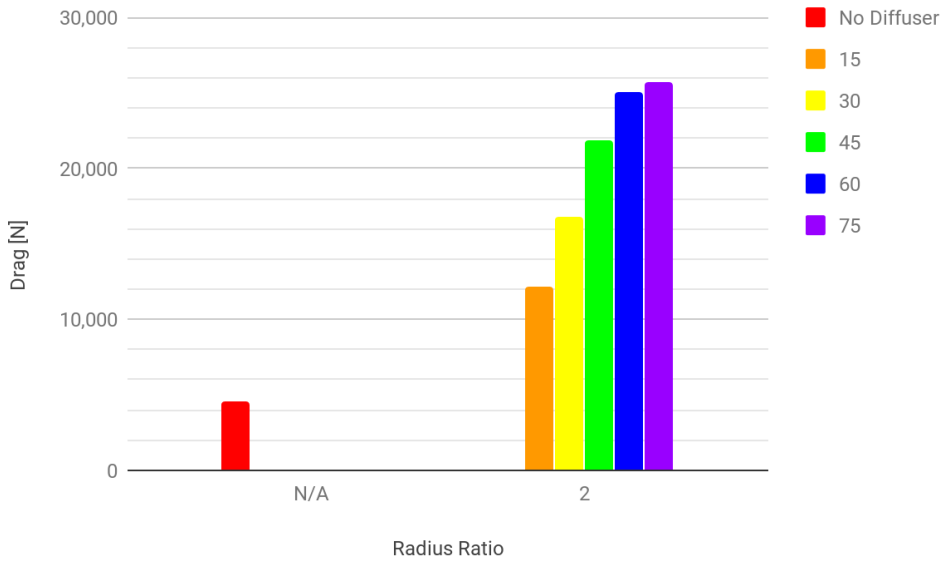

Figure 36: Drag of different diffuser geometries

Shallower duct angles decreased drag on the geometry, since smoother inclines result in less turbulent flows. Even for the steepest duct angle, the induced drag is significantly less than funnels of the same size and duct angle produce; a diffuser with a duct angle of 75° produces

25 kN, while the funnels with a radius ratio of 2 produce 28 kN. This information was incorporated into the turbine shell instead of the turbine itself. The turbine exit acts as a diffuser with a radius ratio smaller than the ones tested by staying within the radius of the shell. Nonetheless, it provides some performance improvement while generating negligible drag due to its inline design.

Nose Cone

To determine whether a nose cone could be beneficial to turbine performance, a model with a nose cone was tested and compared to the base model. The results of the test can be seen in Figure 37 below.

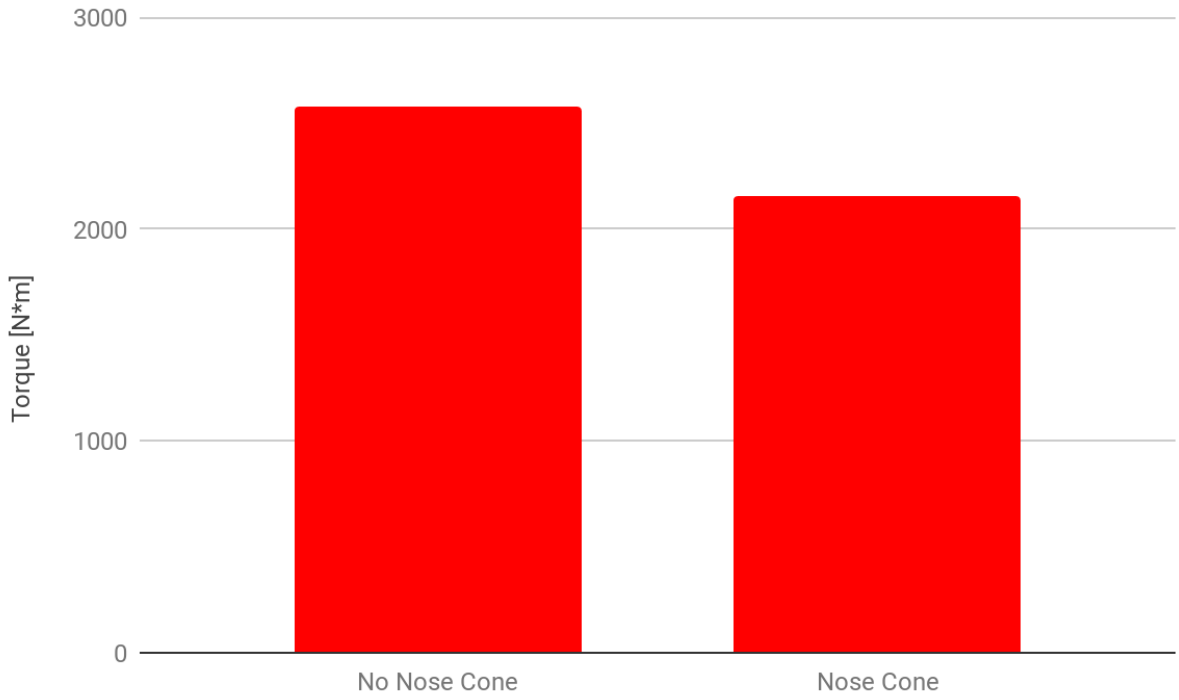

Figure 37: Effect of nose cone on torque generation

The model with the nose cone performed significantly worse than the base model. As a result, no further testing was conducted regarding the effects of different nose cone geometries. The decrease in torque was likely due to increased viscous forces and back pressure, similar to the blade height simulations. The base model was kept the same, due to the drawbacks of the nose cone.

Angular Velocity

To find the optimal rotational velocity of the base turbine, it was tested at different rotation rates to determine which produced the most power. The torque of the turbine at different rotational velocities can be seen in Figure 38 below.

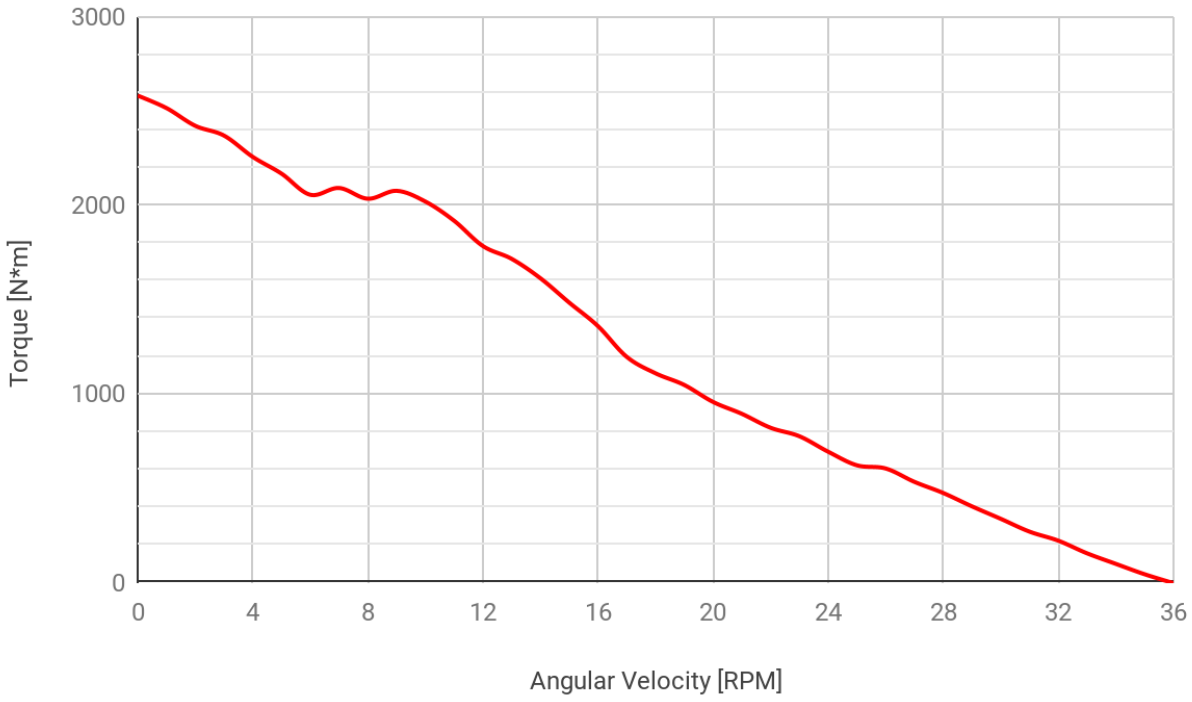

Figure 38: Torque generated from different angular velocities

The torque decreases as the angular velocity increases. Rotation rates faster than 36 RPM require power to be put into the system, meaning that the system is acting as a motor instead of turbine; it is putting energy into the water rather than extracting energy from the water. The roughness in the line may be due to factors such as laminar to turbulent transitions or reversed flow that affect the torque at certain rotation rates. By multiplying the torque by the angular velocity at which it was rotating, the power output of the system is obtained, which can be seen in Figure 39 below.

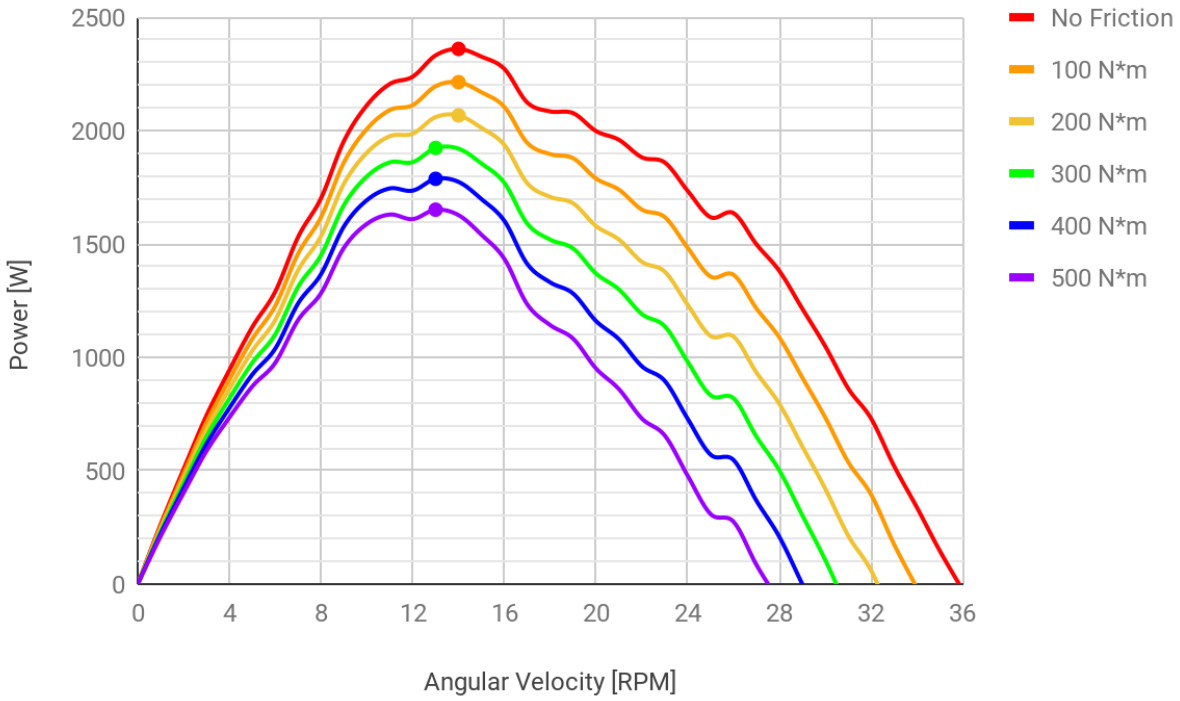

Figure 39: Power production from different angular velocities

The power generation increases and then decreases with angular velocity, demonstrating that there is an optimal rotation rate for maximum power generation. The power generation for different frictional forces was also calculated; they produce similar power profiles, albeit with lower values. The effects of friction are more pronounced at higher angular velocities due to the relationship between torque and power.

Assuming no friction, the optimal angular velocity for the base turbine in a water flow of 2.5 m/s is 14.1 RPM. This angular velocity is ideal for this water speed, independent of the gearbox and generator efficiency. To determine the relationship between optimal angular velocity and water speed, simulations were conducted at different water speeds and angular velocities. The results of this test can be seen in Figure 40 below.

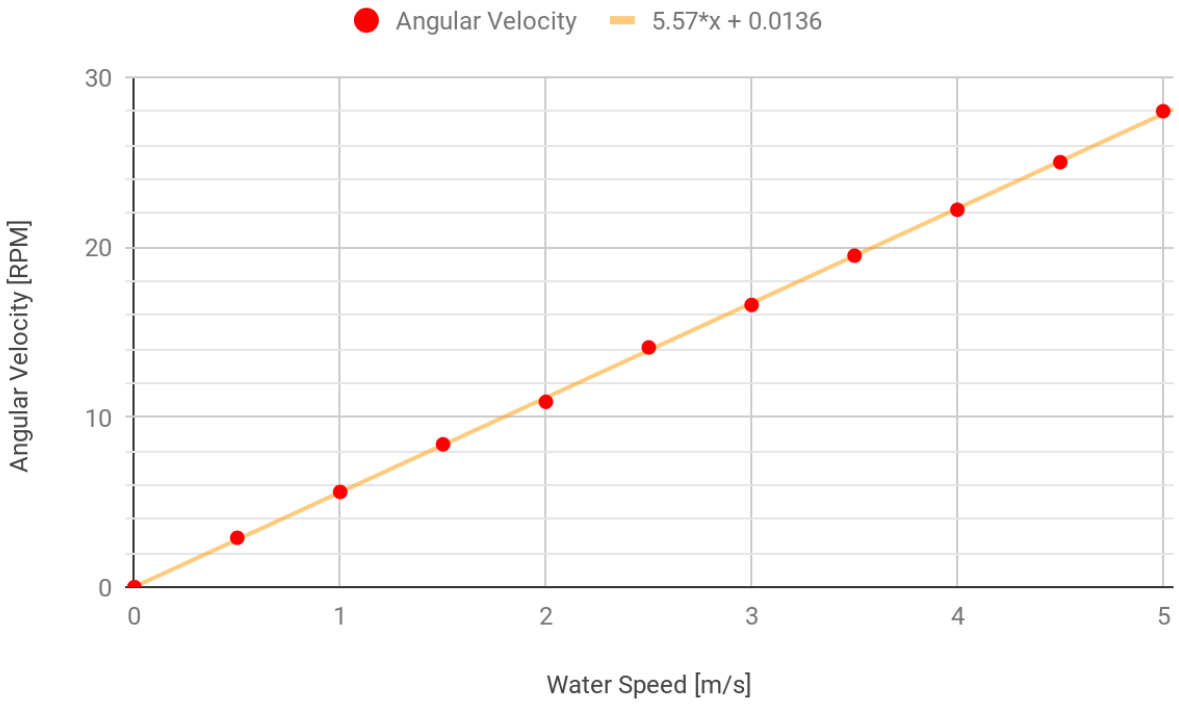

Figure 40: Optimal angular velocity for different water speeds

The correlation between optimal angular velocity and water speed is a highly linear relationship, making it easy to extrapolate to other water speeds. Theoretically, optimal angular velocities could also be easily found for other turbine geometries by finding the optimal angular velocity at one water speed; the line from the origin to that data point should be the relationship between optimal angular velocity and water speed. While this data does not affect the base model, it is important information for fatigue and stress testing.

Airfoil Profiles

The turbines with airfoils mentioned in section 4.2.2 were tested. The three models with modified airfoils were compared to the base model with flat plate blades. The results of this test can be seen in Figure 41 below.

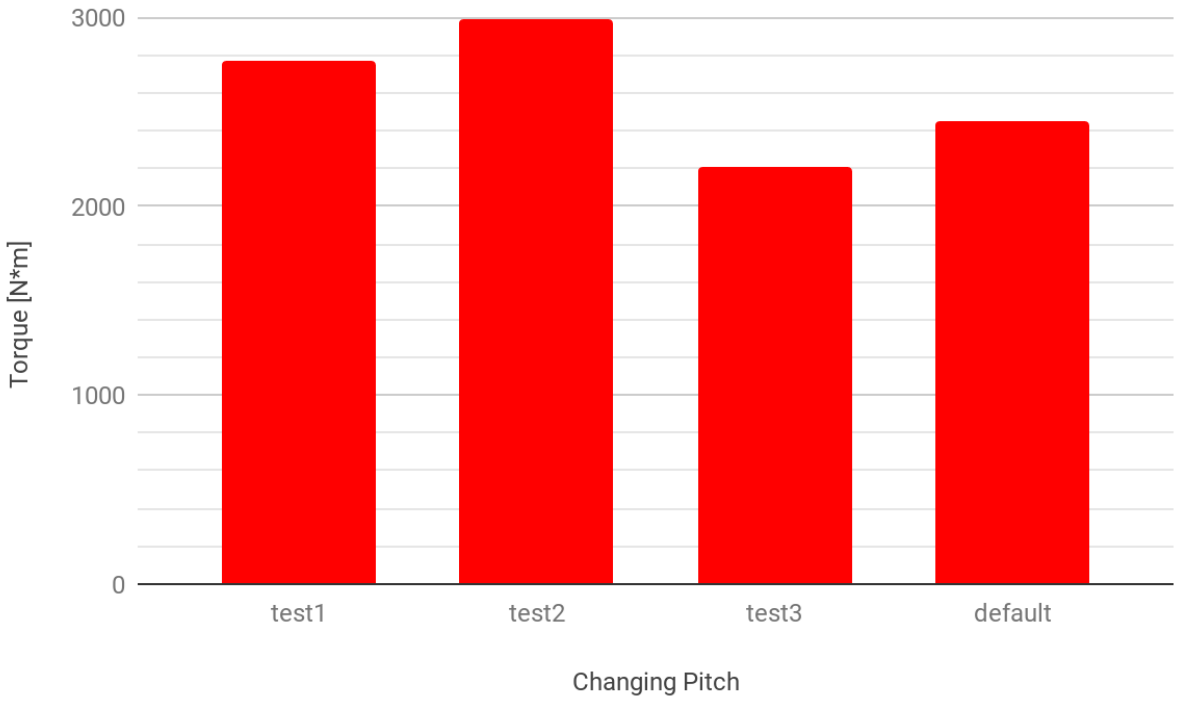

Figure 41: Performance of different airfoil profiles

Both test1 and test2 generated more torque than the flat plate, improving performance by 13% and 22%, respectively. However, test3 generated almost 10% less torque than the flat plate. The decrease in torque was due to the increased drag produced by the larger maximum camber. This also resulted in some turbulent separation and reversed flow, which further decreased the torque. Nonetheless, this test provided ample evidence that turbine performance can be increased with different airfoil profiles.

5.2 - XFOIL and MATLAB Blade Profile Optimization

As a result of the airfoil profile tests, further airfoil optimization was performed. However, due to limitations with the academic version of ANSYS Workbench, the airfoil optimization was performed using XFOIL and MATLAB instead.

XFOIL Blade Characteristic Evaluations

The airfoils listed in Appendix F were tested to ascertain the performance of non-flat plate blade profiles. The lift coefficients of the airfoils from XFOIL compared to the flat plate estimation can be seen in Figure 42 below.

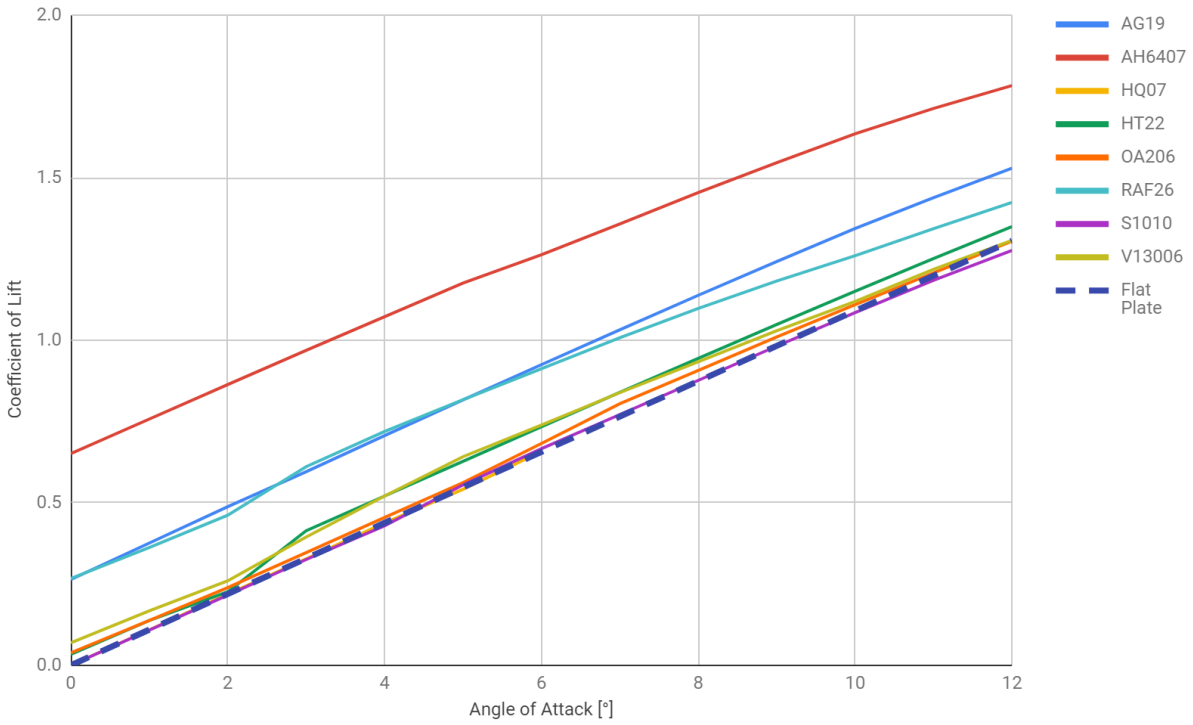

Figure 42: Lift characteristics of tested airfoils at different angles of attack

All of the airfoils tested exhibited a lift characteristic similar, or better, compared to that of the flat plate. AG19, AH6407, and RAF26 exhibit the most significant cambers out of the airfoils tested, and produced the highest coefficients of lift. The only airfoil that performed slightly worse was S1010, a symmetrical airfoil. The other airfoils, which are slightly cambered, demonstrated lift coefficients slightly better than the flat plate.

The drag coefficient of an airfoil is also important for calculating torque in BEMT. The drag characteristics of the airfoils from XFOIL compared to the flat plate estimation can be seen in Figure 43 below.

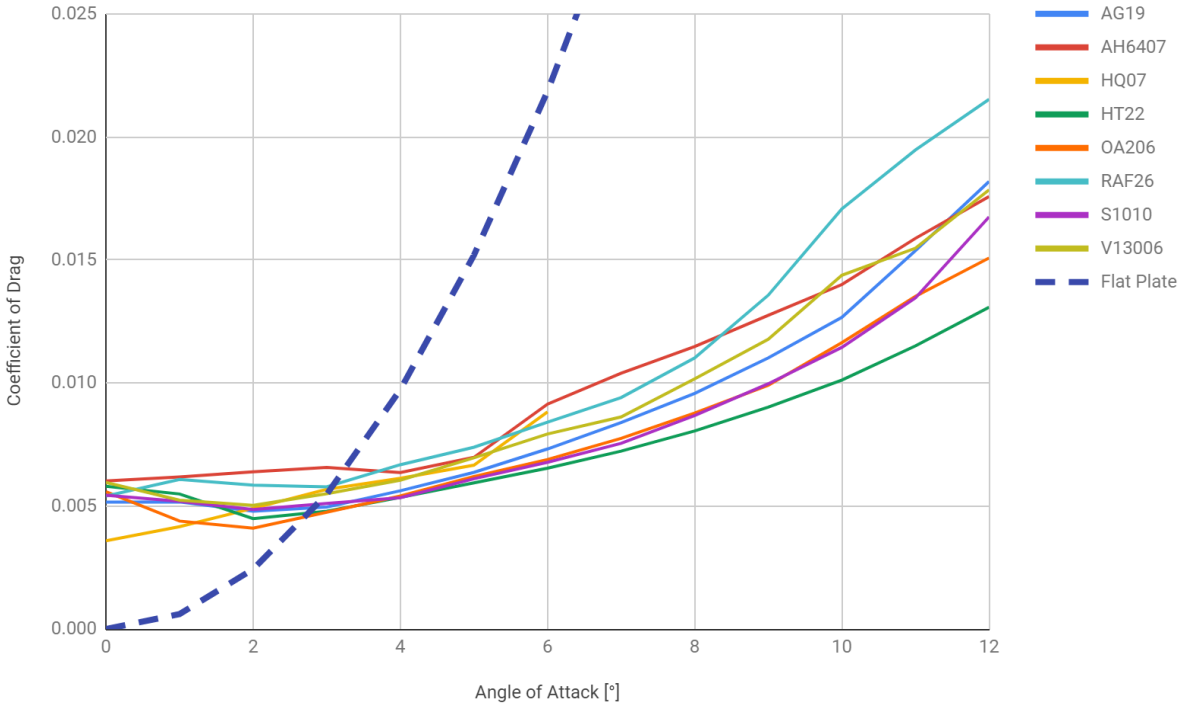

Figure 43: Drag characteristics of tested airfoils at different angles of attack

The advantage of smoothed airfoils is far more apparent when looking at drag characteristics. While the flat plate initially produces less drag than smoothed airfoils, the drag coefficient increases at a significantly higher rate than the smoothed airfoils. The lack of curvature on the plate creates turbulent separation and increases reversed flow, creating more drag. The airfoils with the next highest drag characteristics are those with largest camber. Larger cambers increase the angle near the trailing end of the airfoil in relation to the fluid flow, creating turbulent separation more easily than curved, symmetrical airfoils. Despite this, the cambered airfoils still produced far less drag than the flat plate.

MATLAB Blade Performance Calculations

To determine the accuracy of the MATLAB BEMT program, comparisons were performed against data from the ANSYS Fluent simulations. The torque and power at different angular velocities were calculated, which can be seen in Figures 44 & 45 below.

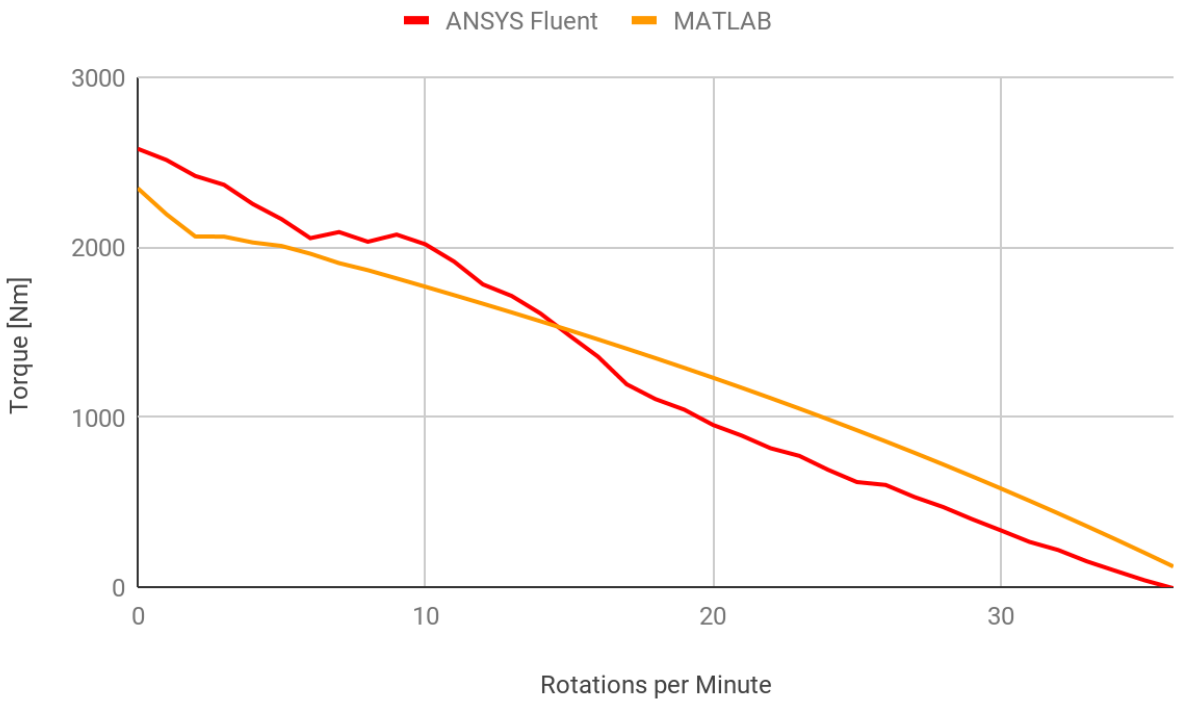

Figure 44: Torque calculation comparison between ANSYS Fluent and MATLAB

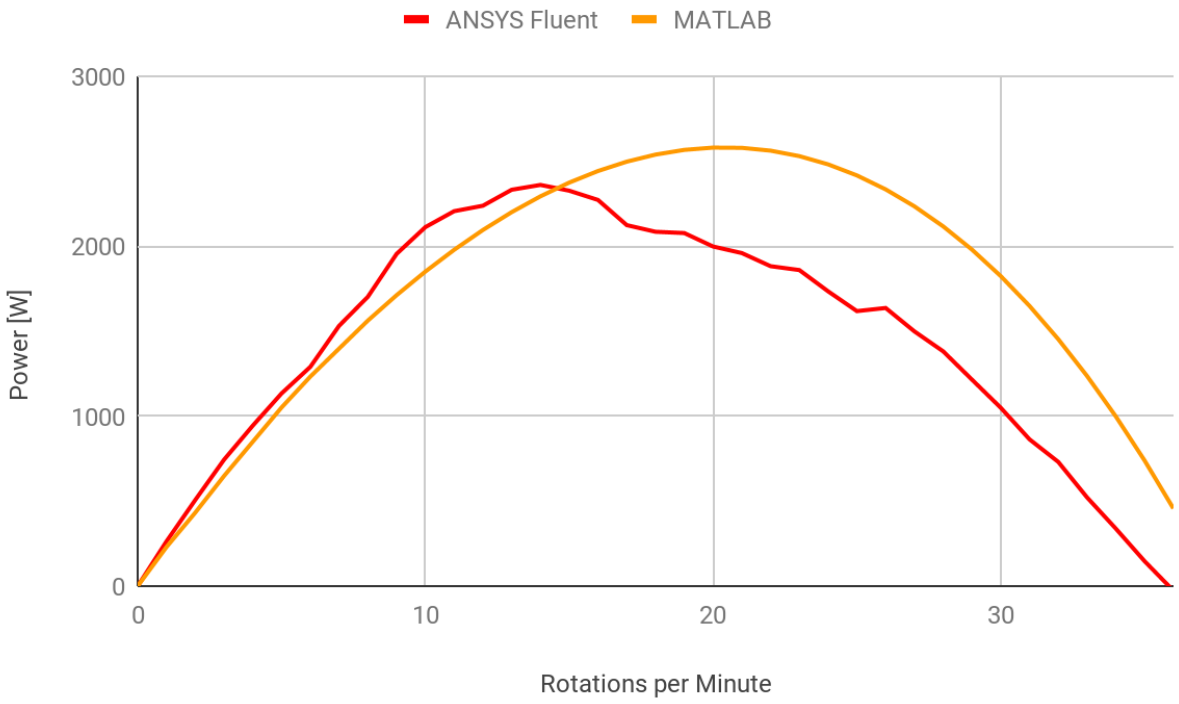

Figure 45: Power calculation comparison between ANSYS Fluent and MATLAB

Due to its simplicity, the MATLAB program is not able to account for complications that may affect the calculations, such as Reynolds number variance with different angular velocities or fluid vortices that may form. This causes some deviation from the ANSYS data, which is especially prominent at rotational speeds faster than fifteen rotations per minute. Despite the discrepancies, it was decided that performing airfoil analysis with the program could still provide valuable insight and help optimize the turbine design. The results of the tests for the nine airfoils can be seen in Figure 46 below.

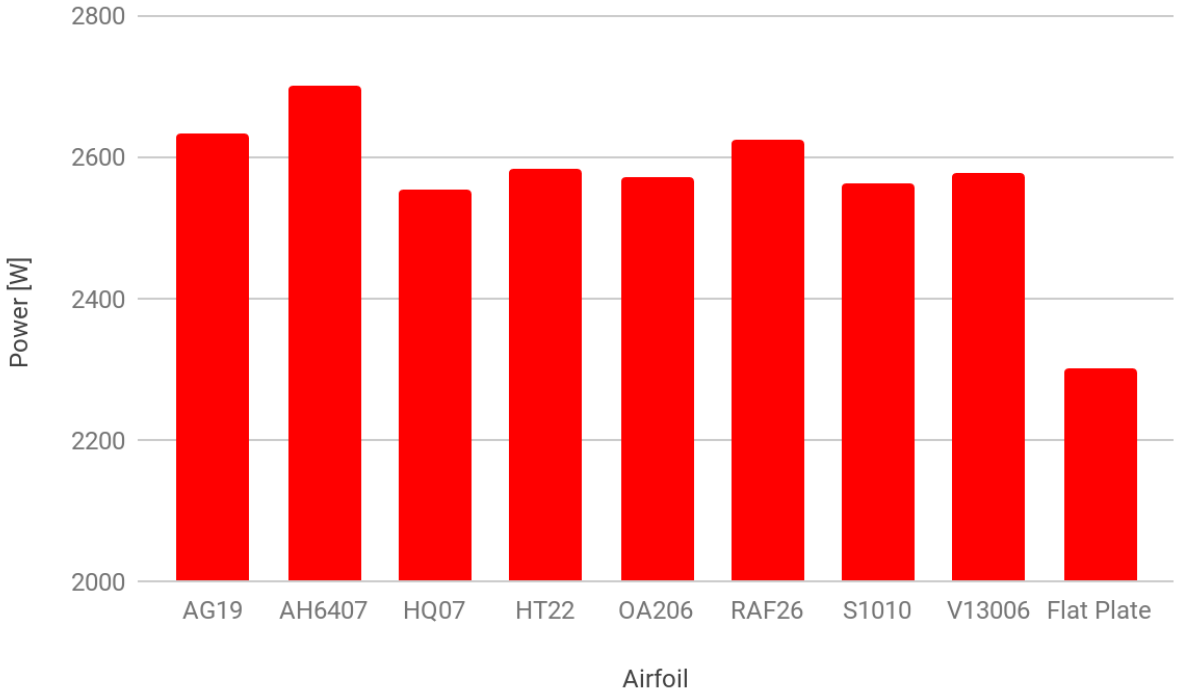

Figure 46: Calculated power generation for tested airfoils

The tests were conducted with an RPM of 14.1, which was determined to be the most efficient rotational velocity through ANSYS Fluent simulations, above. As one might expect, the airfoils with the best performances were AG19, AH6407, and RAF26. The increased performance was likely due to the significantly higher coefficient of lift these airfoils have over the others. However, the other airfoils still performed significantly better than the flat plate; even S1010, which produced less lift in the XFOIL simulations, generated over 250 W more power than the flat plate. The increased performance in comparison with the flat plate was likely due to the significantly lower drag coefficient. Nonetheless, it is evident that varying the airfoil profile can have significant effects of the efficiency and performance of the turbine.

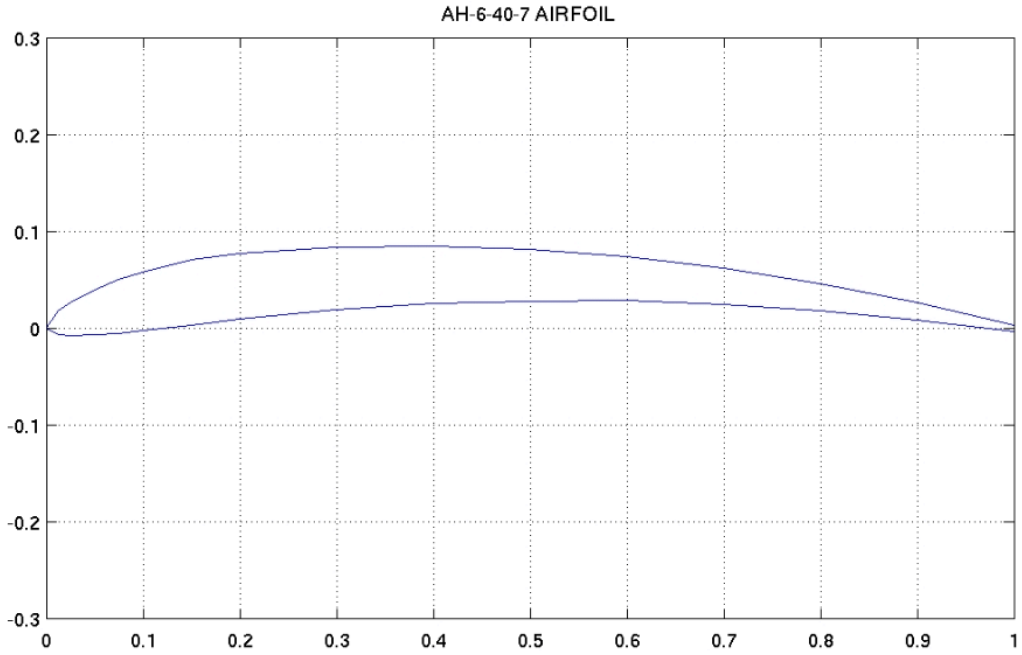

Figure 47: The highest performing pre-made airfoil tested

Inverse Airfoil Design

After determining that differently shaped airfoils can have a significant effect on power output, different rotational velocities and airfoil characteristics were tested to determine optimal values. The torque and power output of the blade profile with the optimal characteristics can be seen in Table 3 below with comparisons to AH6704 and a flat plate.

Table 3: Performance comparison between optimized airfoil, AH6407, and flat plate airfoils

Parameter	Optimized Airfoil	AH6407 (14.1 RPM)	Flat Plate (14.1 RPM)
Torque [Nm]	4840	1842	1560
Power [W]	3050	2700	2300
Coefficient of Power	0.221	0.196	0.167

The optimized airfoil generates a 32% increase in power generation in comparison to the flat plate, significantly improving the efficiency of the turbine and coefficient of power. It also produced 11% more power than AH6407. Since the rotational velocity was adjusted as part of the optimization, the optimized airfoil produces two and three times as much torque as AH6407

and the flat plate, respectively. The rotational velocity, along with the airfoil characteristics, that yielded maximum power can be seen in Table 4 below.

Table 4: Characteristics of optimized airfoil

Parameter	Value
Rotations per Minute (Angular Velocity)	6.01 RPM (0.629 rad/s)
Coefficient of Lift at 0° Angle of Attack	1.051
Coefficient of Drag at 0° Angle of Attack	0.003

The airfoil has a higher coefficient of lift at 0° angle of attack, allowing the turbine to rotate at a slower rate, while producing more torque and power than the tested airfoils. This data can be seen as valid and meaningful due to the low rotational rate of the turbine; the data produced by ANSYS Fluent coincides very closely with the MATLAB program model around 6 RPM. Through trial and error, an airfoil with similar characteristics was found with the following features: maximum camber 9% of the chord length; maximum camber placement at 45% of the chord; and maximum thickness 4.5% of the chord length. The NACA designation for this airfoil is NACA 9404, and its characteristics can be seen in Table 5 below.

Table 5: Comparison between optimized airfoil and possible real-world counterpart

Parameter	Optimized Airfoil	NACA 9404
Coefficient of Lift	1.051	1.055
Coefficient of Drag	0.003	0.005
Power [W]	3050	2920
Coefficient of Power	0.221	0.211

The coefficient of drag on NACA 9404 is slightly higher than that of the optimized airfoil, resulting in a power loss of around 130 W. However, this performance is still superior to the performance of the flat plate and AH6704. As a result of these tests, the base model was updated to use NACA 9404 as its blades, instead of a flat plate. NACA 9404 can be seen in Figure 48 below.

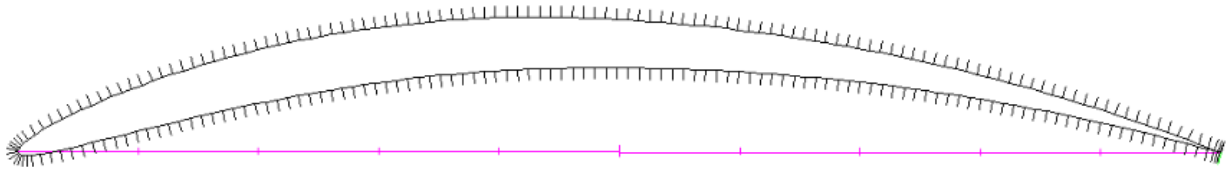

Figure 48: Profile of NACA 9404

5.3 - Physical Pre-Swirl Stator Testing

Most of the tests performed in the water tunnel were informal tests to determine whether or not the turbine would rotate instead of testing features that could affect the performance of the turbine. The exception to this was the test of the pre-swirl stator. The control turbine model maintained a rotational velocity of 34.3 RPM. The turbine with the stator, however, achieved a rotational velocity of 43.1 RPM, an improvement by over 25%. This indicates that the addition of a pre-swirl stator may have a significant effect on the performance of a turbine. This drastic improvement in performance is especially notable due to the fact that the turbine model used with the pre-swirl stator is significantly shorter than the control turbine model: 4.7 cm to 7.8 cm, respectively. As established in section 5.1 above, longer turbines are more efficient and produce more torque; this means that the pre-swirl stator compensated for this decreased efficiency and further surpassed the performance of the control stator.

However, as discussed in section 4.3 above, the testing environment was neither kinematically nor dynamically similar to a full-scale model. While this does not mean that the results of the water tunnel test are insignificant, precaution must be taken when analyzing the test results. The only meaningful conclusion drawn from this test was that the addition of a pre-swirl stator can improve the performance of a turbine. Interpretations regarding the magnitude of performance increase or stator properties that produce the largest performance improvement cannot be made with any reasonable level of confidence.

5.4 - SolidWorks Turbine Casing Design

As optimum performance values were determined for different parameters, the base SolidWorks model was updated accordingly. Once the final update was performed, the model was modified to be able to drive generators. This was accomplished by encompassing the base of the turbine in gear teeth, effectively changing part of the turbine into a large gear which can be seen in Figure 49 below.

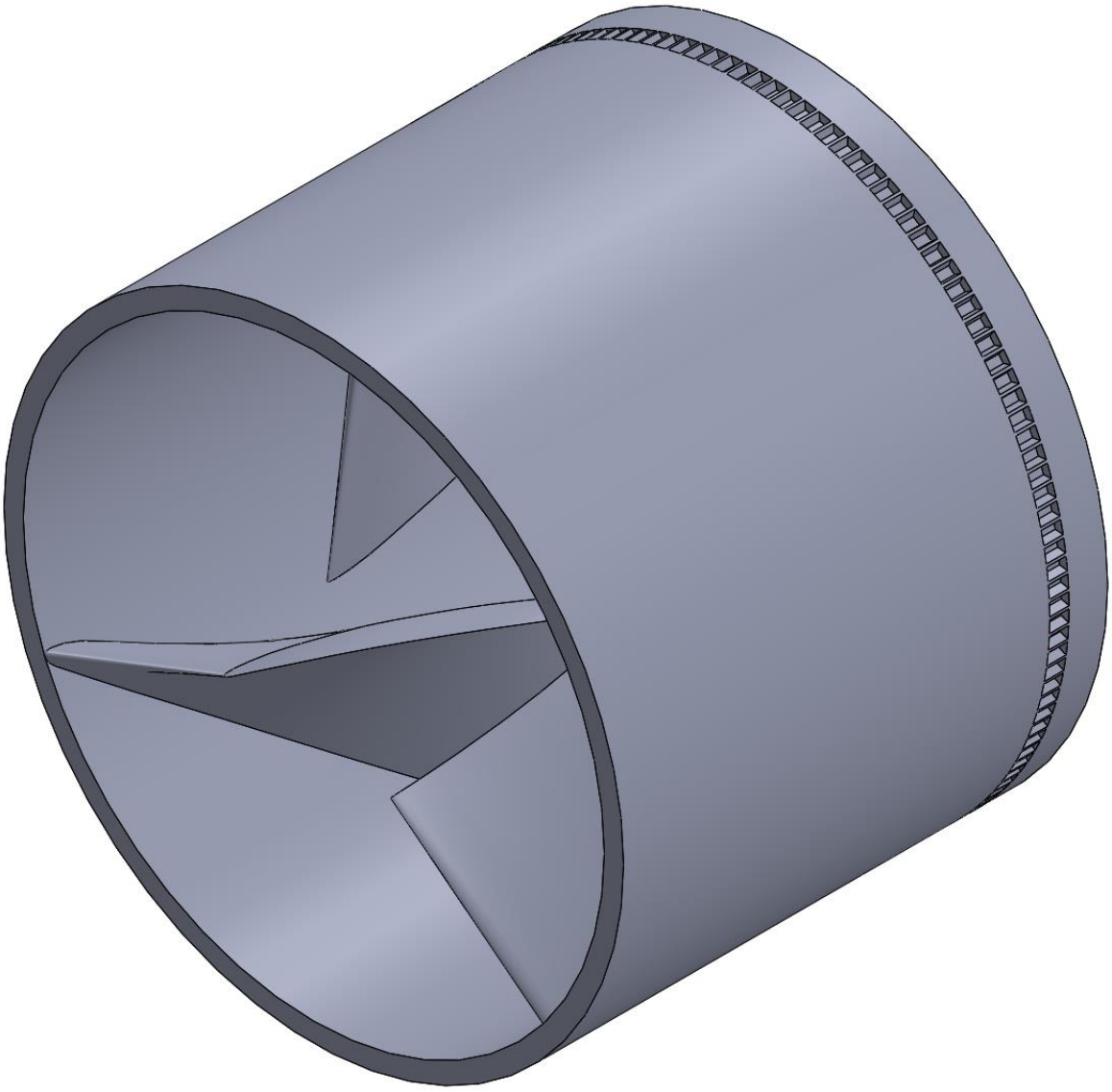

Figure 49: Final turbine design with gear ring

The gear has 132 teeth to drive three planetary gears which are equally spaced around the perimeter of the turbine. The planetary gears are each attached to electric generators which derive energy from the system. The turbine and generators are housed in an external casing, a prototype of which can be seen in Figure 50 below.

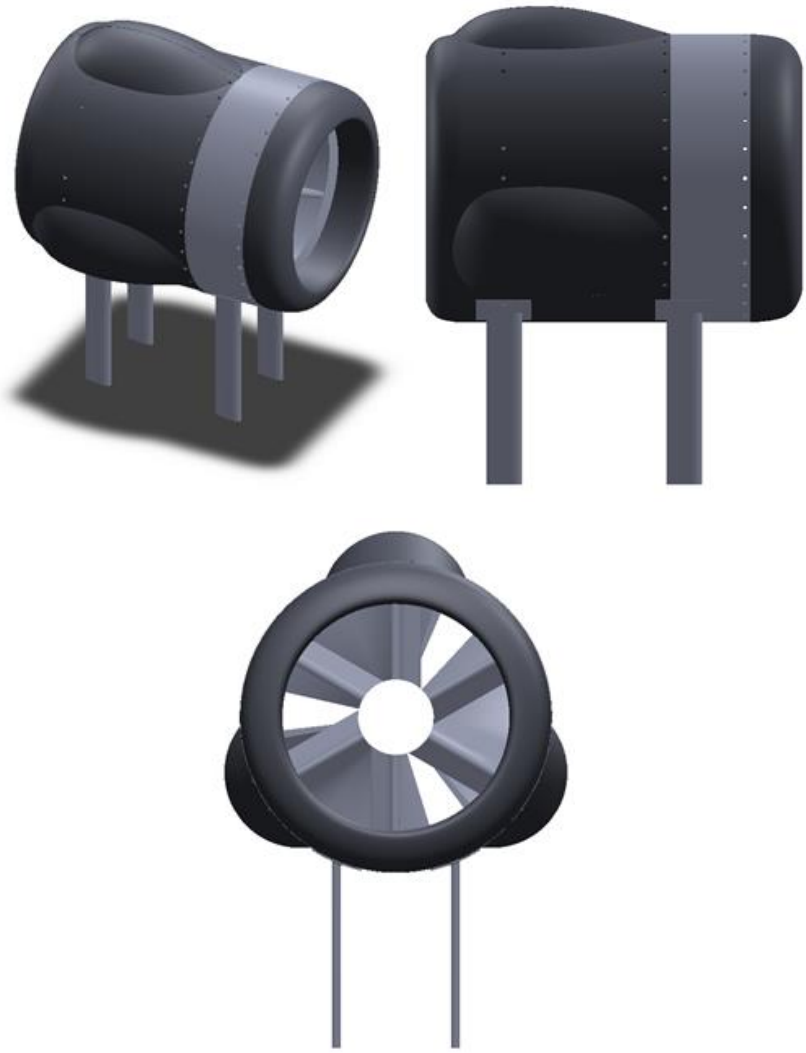

Figure 50: Multiple views of mock-up casing design

This design is not intended to be a final or optimal design, but rather a basic outline of a possible shell that could be used to house and generate power from the turbine itself. For this reason, no necessary material properties or cost-benefit analyses were undertaken. The main components of the casing are discussed below.

Roller Bearing Holder

One of the most important components of the casing is the roller bearing holder, seen in Figure 51 below.

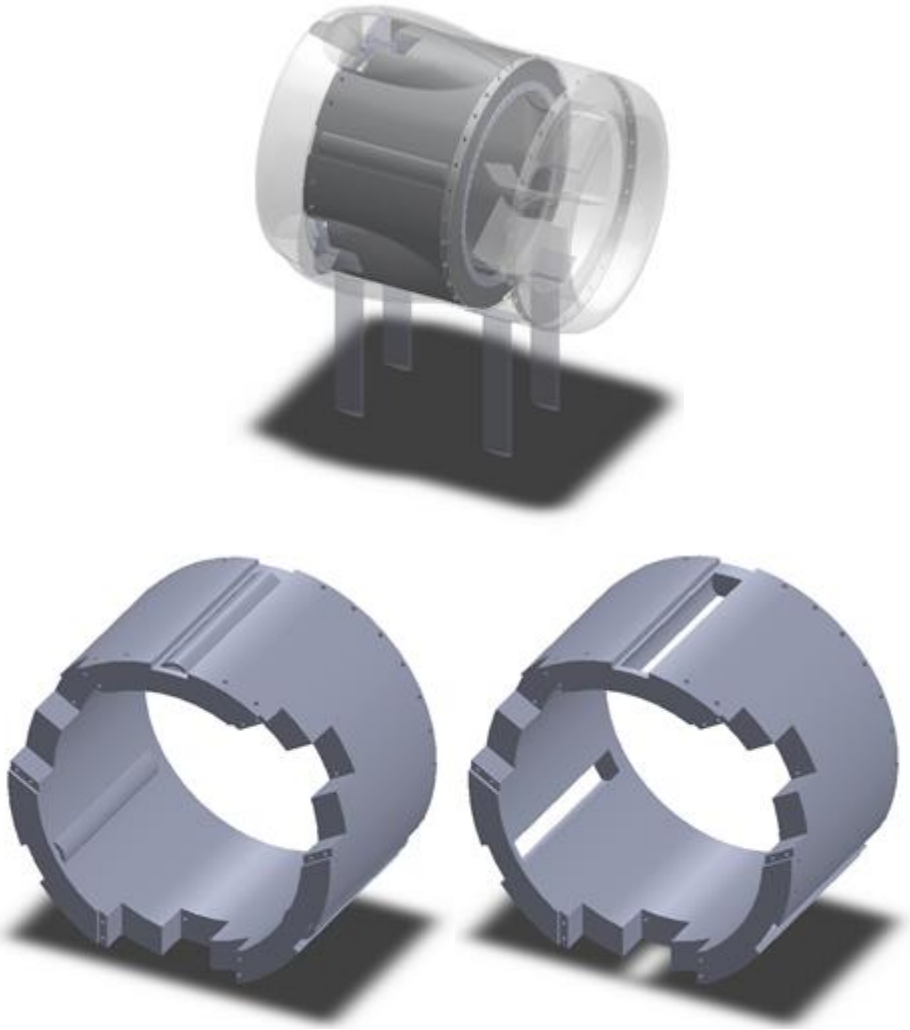

Figure 51 counterclockwise from top: Roller bearing holder in casing, with rollers, and without rollers

The roller bearing holder is positioned in the center of the casing and acts as the skeleton of the structure; most components are fixed to the roller bearing holder in some way and the holder also secures the turbine, limiting its movement to rotations. The notches cut out of one the sides are the housings for the generator and gearbox and can be resized as needed.

Casing Front

The largest structure of the casing is the exterior, which is divided into four modular components. Making the exterior modular allows for easier manufacturing and maintenance and

can decrease costs due to the lack of large parts molded around interior components. The first piece, the front component, can be seen in Figure 52 below.

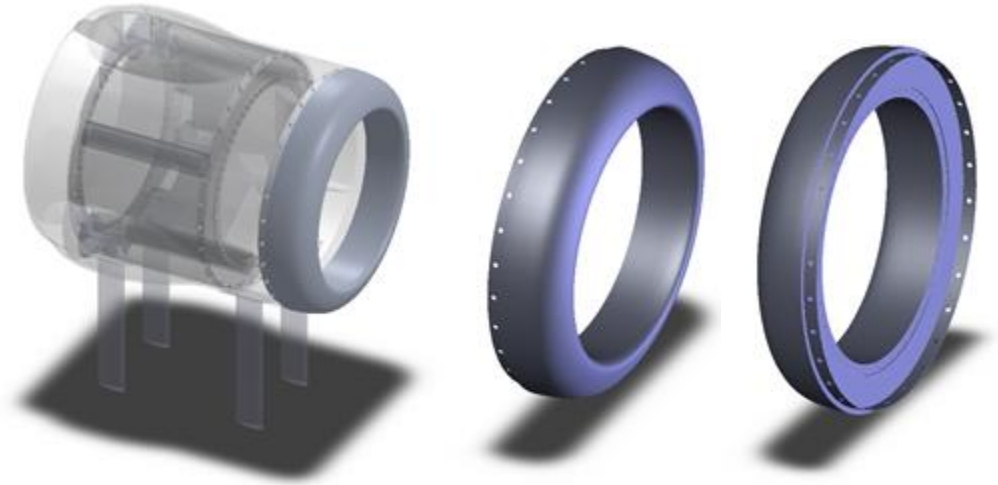

Figure 52 from left to right: Front component in place, front view, and back view

The rounded surface was designed to mitigate turbulent separation that could occur from fluid interaction with the turbine and its casing. In turn, this reduces drag from the water on the casing, decreasing the loads on the casing fixture.

Casing Back

The next two exterior components cover the back of the casing. They are the largest components of the entire casing and each cover half of the turbine. These components can be seen in Figure 53 below.

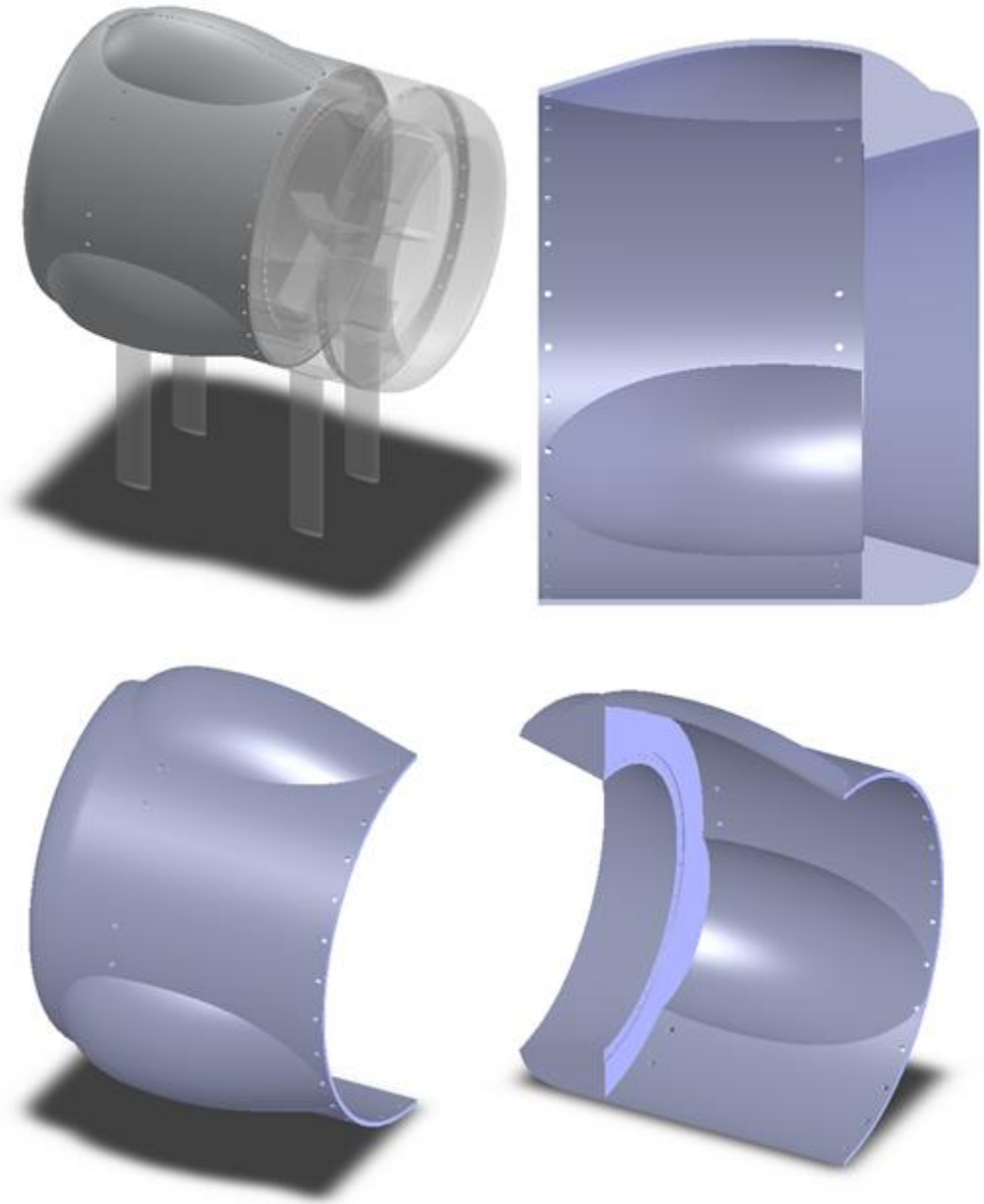

Figure 53 clockwise from top left: Rear components in place, side view of left rear component, and interior and exterior views

These pieces are mostly hollow and mainly act as a protective cover for the more important components inside. They are designed to maintain a waterproof seal and protect against debris in the water. The curvature of the rear components was designed to minimize drag from the water to reduce loads on the fixture, while providing enough volume for the components inside. The three evenly spaced protrusions seen on the outside of the shell are designed to fit the over the planetary gears and generators without creating substantial drag.

The rear components are also designed to act as a small diffuser, which is most easily seen in the side profile in Figure 53. Since diffusers were determined to be beneficial, a small diffuser with a duct angle of 15° was modeled into the back of the rear components. The radius ratio of this diffuser is significantly smaller than any of the diffusers tested in section 5.1, but incurs minimal drag due to not increasing the drag profile of the casing, meaning any performance gain from the diffuser is beneficial.

Pre-Swirl Stator Insert

The final component of the external case is a section that contains a pre-swirl stator. This component can be seen in Figure 54 below.

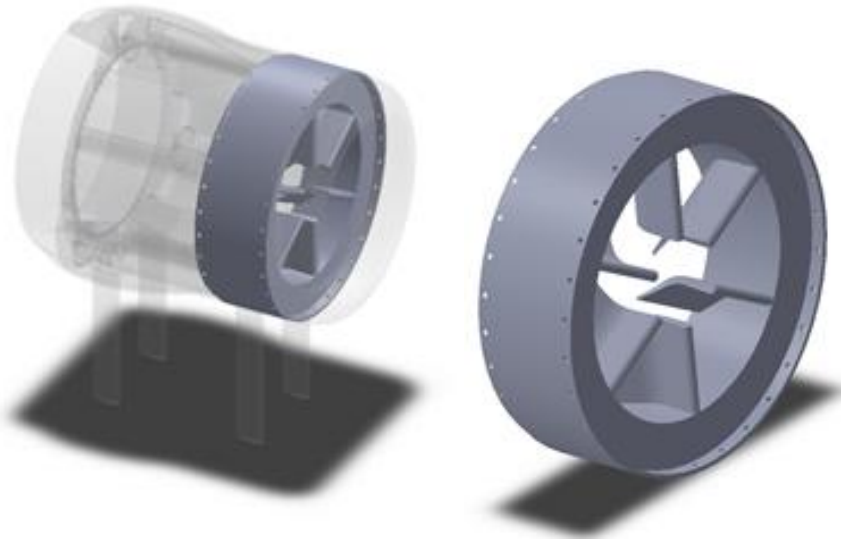

Figure 54: stator section in-place (left) and isolated (right)

Due to the performance benefits from pre-swirl stators, the casing was designed to be able to incorporate the stator section. Since the magnitude of performance benefit could not be determined with sufficient confidence, however, the inclusion of the pre-swirl stator section is optional; the front component can be attached directly to the roller bearing holder if it is determined that the drag produced by the stator section outweighs the benefits it provides.

Power Generation

The purpose of designing the turbine and casing was to generate power, which would be accomplished by the gear trains and generators, seen in Figure 55 below.

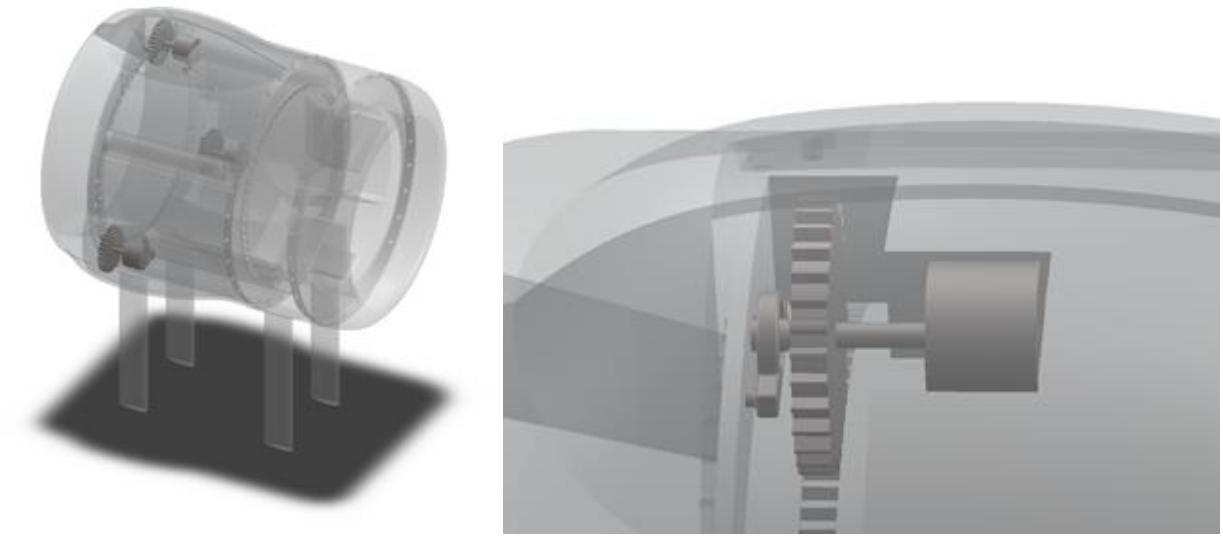

Figure 55: Gears and generator in-place (left) and close-up (right)

As mentioned above, the gear trains and generators are located inside the protrusions in the rear components of the exterior casing. The gears in this design have 30 teeth, resulting in a gear ratio of 15:66. The generator displayed here is a simple placeholder, representing a small generator with a length of 150 mm and diameter of 200 mm. Depending on the needs of the user, the roller bearing holder could be modified to fit generators of different sizes and gearboxes with different gear ratios to adjust power output.

Axial Roller Bearings

Additional components within the casing are ring roller bearings, seen in Figure 56 below.

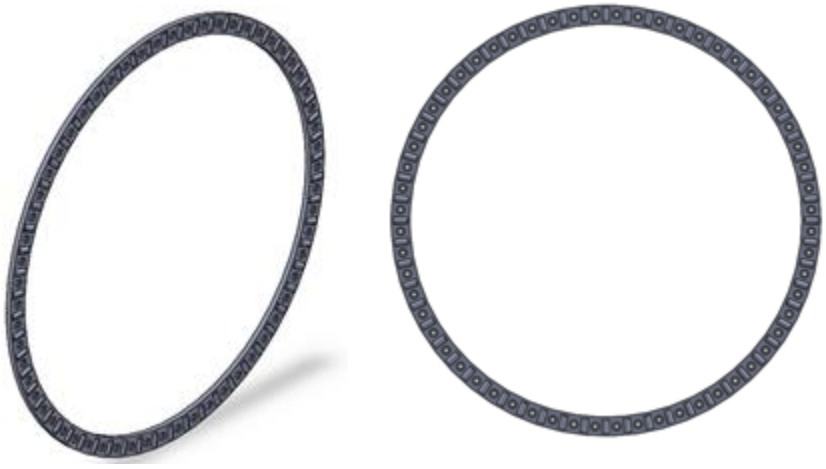

Figure 56: Ring roller bearings isolated

These components are included to decrease the frictional interaction between the front and back walls of the casing with the turbine during rotation, increasing torque and power generation. They are built to fit into indentations in the front component and rear components.

Mounting

The entire casing needs to be secured in place to operate properly. The simplest fixture to implement are legs, seen in Figure 57 below.

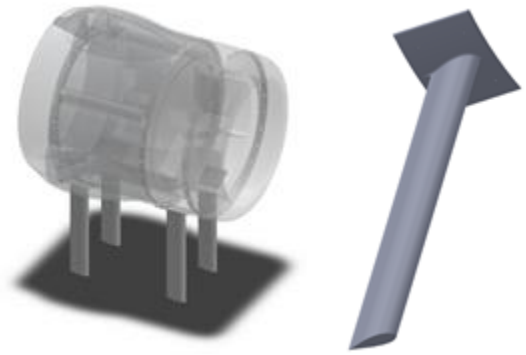

Figure 57: Leg fixtures in-place (left) and isolated (right)

As mentioned in section 2.2.2, there are three main methods for mounting axial hydro turbines. Due to the decreased fluctuation in power generation with water level change and abundant engineering experiences, BSM was chosen as the most suitable mounting method. The legs would need to be strong enough to counteract the drag forces on the entire turbine system without buckling or fatiguing; however, since all river bottoms are different and turbines in different rivers will experience different loads, anchoring methods were not developed since they should be designed on a case by case basis. The profile of the legs was designed as a symmetric airfoil to reduce drag forces.

Debris Grate

The final major component of the turbine casing is the debris grate, seen in Figure 58 below.

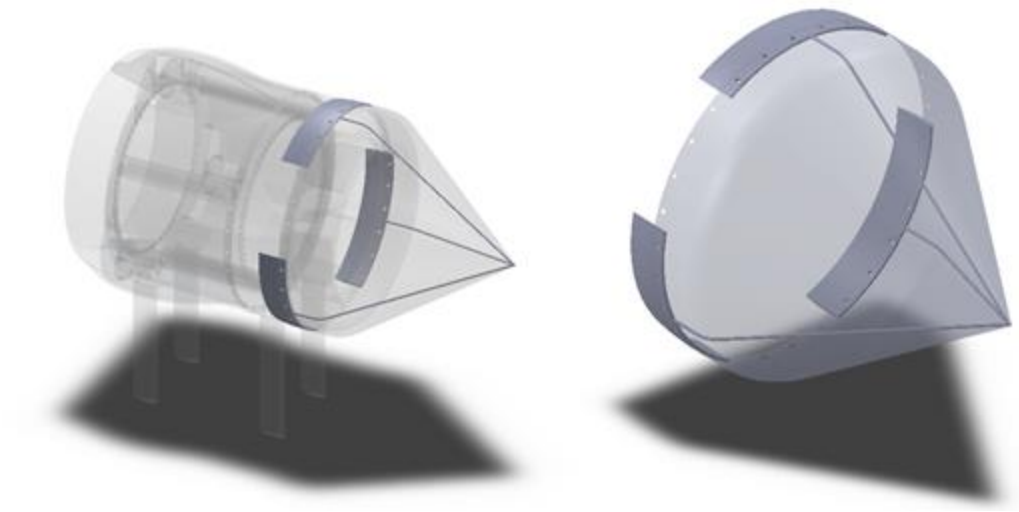

Figure 58: Debris grate in-place (left) and isolated (right)

The debris grate is a cone shaped structure attached to the front of the shell to prevent fish and debris from entering the turbine and damaging any of the components contained within. While the model displays a translucent filter-like cover for the grate, an actual debris grate would likely be constructed from stainless steel wires spaced widely such that the grate has minimal effect on the water flow into the turbine. The three-pronged structure in the grate acts as a skeleton, both providing support for the finer wires and reducing or preventing structure deformation after collisions with large debris.

5.5 - Final Turbine Design

The specifications of the final turbine design can be seen below.

Table 6: Specifications for final turbine design

Parameter	Value
Inner Radius	0.75 m
Outer Radius	0.80 m
Stagger Angle	37°
Length	1.25 m
Blade Height	0.5 m
Nose Cone	None
Airfoil	NACA 9404

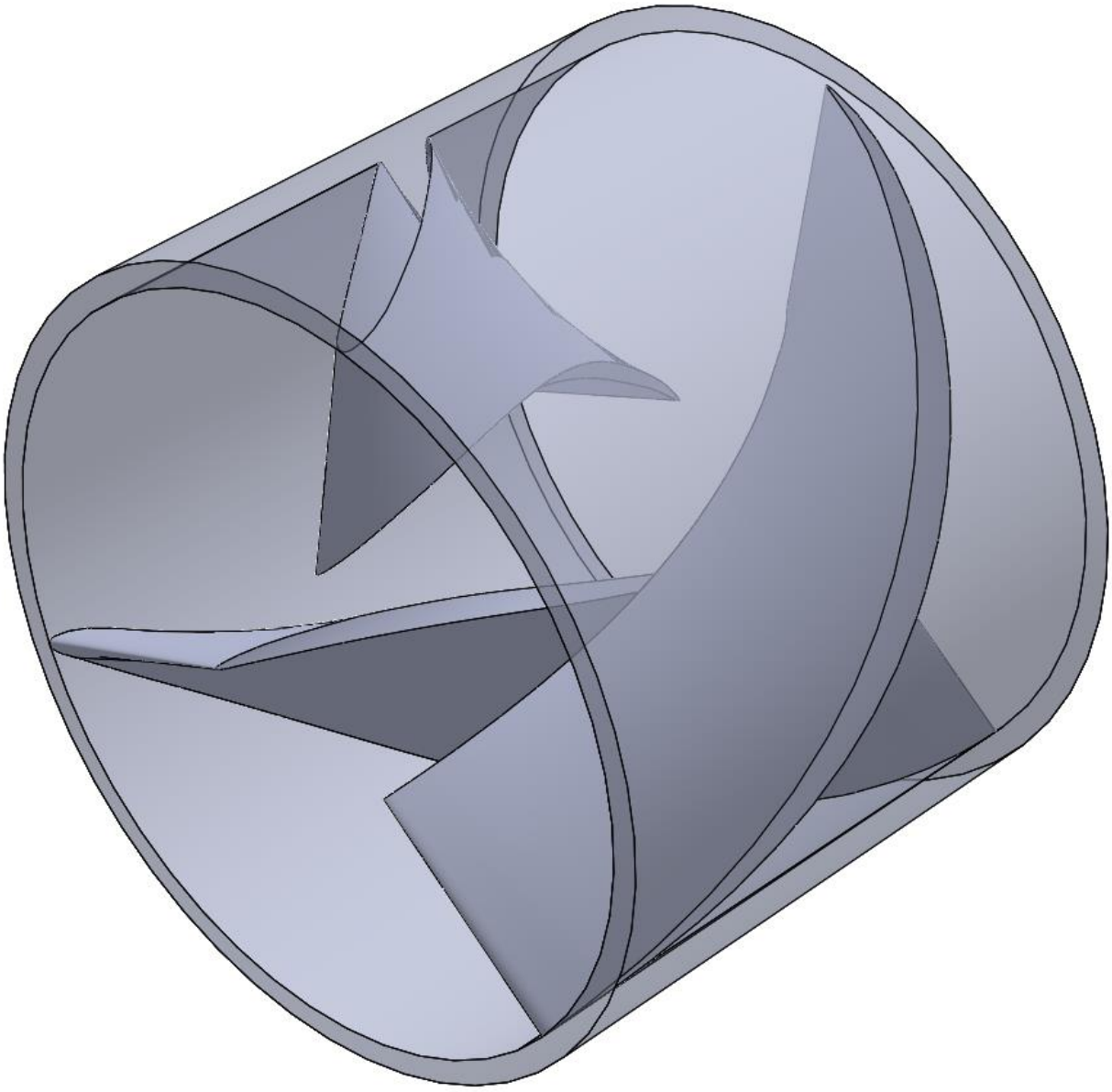

Figure 59: Model of final turbine design

6 - Conclusions

As the population of the world increases, the demand for electricity and the need for clean power generation increase as well. In comparison to dammed power plants, hydrokinetic power plants are relatively unexplored. However, due to their relatively low cost and near-ubiquitous applicability, their development and optimization can help bring clean power to communities in rural and developing regions.

This project focused on the design and optimization of a hydrokinetic power plant, with a novel coreless, outrunner motor-based turbine design. The focus of the project was primarily on the optimization of the turbine design to determine if the power plant would be capable of producing enough electricity to power a small off-grid community or neighborhood. Most of the optimizations were performed in simulation software, such as ANSYS Fluent and MATLAB, although some physical tests were performed with scale models in a water tunnel. A secondary focus was the development of a design for the turbine casing, which was performed using SolidWorks.

The parameters that were tested include: stagger angle, turbine length, blade height, effects of ducts and nose cones, angular velocity, and blade profiles. The final design was developed by modifying the base model as a result of these tests and is capable of producing almost 3 kW of power, which can be increased with the addition of a pre-swirl stator and a duct system. This is sufficient to power ten or more households in developing regions, or two rural homes with average American power use [28].

This design holds several advantages over traditional turbine designs. Since the turbine is designed to generate torque, rather than velocity, it can theoretically operate in slower moving waters more effectively. Additionally, due to the slow rotation rate of the turbine, the lifespan of the components can be lengthened since they are subject to less stress. The turbine and casing design is also much more resistant to damage from impacts and debris.

Due to time and software constraints, testing was limited, and should be explored further if this project is continued. Some of the most important areas to investigate include structural and material analysis. Since the focus of this project was on performance optimization for the turbine, these two areas were neglected. Similarly, a cost-benefit analysis should be performed to determine whether the production of these turbines would be worthwhile. The fixed parameters could be varied to determine turbine size for optimal production cost to power generation ratio. More blade profile optimization should also be performed and larger scale models should also be tested to observe the real-world performance of the design. Finally, the

design of the casing should be explored and further developed to enhance the performance of the turbine and provide the necessary housing and support.

Overall, this project was successful. It explored the feasibility of the outrunner-based turbine design to show that the design is capable of providing enough electricity to power a small community or neighborhood. The high torque focused design provides power with a lower angular velocity than traditional designs, which can increase longevity. However, existing hydrokinetic turbines of similar sizes have similar or greater power production. Therefore, to increase potential for commercial development, more research should be conducted to maximize performance. If future project groups investigate the areas discussed above, however, the efficiency and performance of the power plant could be improved, and the usability of this design could increase. Additional studies could then be performed to determine if the device is competitive with alternative existing products.

7 - References

[1] African Energy Industry Report :: 2018, An. (2018). Retrieved from https://www.futureenergyafrica.com/media/1751/1-mir-africa-mir-18-2-es_685804715-05-2018.pdf

[2] Amin, I. & Xiao, Q. (2013). *Numerical simulation of a horizontal axis tidal turbine with a pre-swirl stator*. Paper presented at Developments in Maritime Transportation and Exploitation of Sea Resources, Spain. London, UK: Taylor & Francis Group.

[3] Benefits of Dams. (2018). Retrieved from https://www.fema.gov/benefits-dams

[4] Benefits of Hydropower. (2018). Retrieved from https://www.energy.gov/eere/water/benefits-hydropower

[5] Berga, L. (2016). The Role of Hydropower in Climate Change Mitigation and Adaptation: A Review. *Engineering*, 2(3), 313-318.

[6] Binge and purge. (2009). Retrieved from https://www.economist.com/briefing/2009/01/22/binge-and-purge

[7] Burton, T., Jenkins, N., Sharpe, D., & Bossanyi, E. (2011). Wind Energy Handbook. John Wiley & Sons, Ltd.

[8] Chica, E., Pérez, F., Rubio-Clemente, A., & Agudelo, S. (2015). Design of a hydrokinetic turbine. *WIT Transactions on Ecology and the Environment*, 195, 137-148.

[9] Dambis, K. (Photograph). Maytech 5055 75kV BLDC outrunner motor rotor and stator. Retrieved from https://www.flickr.com/photos/kasparsdambis/28137980911

[10] Debatty, R. (2007). Flotsam, Jetsam and the Three Gorges Dam. Retrieved from https://web.archive.org/web/20080706022236/http://www.worldchanging.com/archives/007682.html

[11] Dixon, S. L. (1998). *Fluid Mechanics, Thermodynamics of Turbomachinery*. Woburn, MA: Butterworth-Heinemann.

[12] El kchine, Y. & Sriti, M. (2017). Tip Loss Factor Effects on Aerodynamic Performances of Horizontal Axis Wind Turbine. *Energy Procedia*, 118, 136-140.

[13] Ferguson, R., Wilkinson, W., & Hill, R. (2000). Electricity use and economic development. *Energy Policy*, 28(13), 923-934.

[14] Froude's Momentum Theory for an Actuator Disk. Retrieved from http://www.esru.strath.ac.uk/EandE/Web_sites/05-06/marine_renewables/technology/Froude.htm

[15] Gish, L. A., Carandang, A., & Hawbaker, G. (2016). *Numerical optimization of pre-swirl stators for horizontal axis hydrokinetic turbines*. Paper presented at OCEANS 2016 MTS/IEEE Monterey, Monterey, CA, USA. Annapolis, MD: United States Naval Academy.

[16] Graham-Harrison, E. (2009). China says Three Gorges Dam cost $37 billion. Retrieved from https://www.reuters.com/article/idUSPEK84588

[17] Hydropower in Paraguay. (2019). Retrieved from https://www.worldenergy.org/data/resources/country/paraguay/hydropower/

[18] International Energy Agency. (2018). *Key World Energy Statistics*.

[19] International Renewable Energy Agency. (2012). *Renewable energy technologies: cost analysis series - Hydropower*. Retrieved from https://www.irena.org/DocumentDownloads/Publications/RE_Technologies_Cost_Analysis-HYDROPOWER.pdf

[20] Jiang, H., Li, Y., & Cheng, Z. (2014). Relation of Lift and Drag Coefficients of Flow around Flat Plate. *Applied Mechanics and Materials*, 518, 161-164.

[21] Khan, M. J., Bhuyan, G., Iqbal, M. T., & Quaicoe, J. E. (2009). Hydrokinetic energy conversion systems and assessment of horizontal and vertical axis turbines for river and tidal applications: A technology status review. *Applied Energy*, 86(10), 1823-1835.

[22] Kirke, B. (2003). Developments in ducted water current turbines. Retrieved from https://www.researchgate.net/publication/237809015_Developments_in_ducted_water_current_turbines_This_paper_was_originally_written_in_2003_and_published_on_wwwcyberiadnet_This_version_includes_some_updates_on_tests_conducted_in_2005

[23] Kuo, L. (2015). The world's biggest hydropower project may be causing giant landslides in China. *Quartz*, retrieved from https://qz.com/436880/the-worlds-biggest-hydropower-project-may-be-causing-giant-landslides-in-china/

[24] Lago, L. I., Ponta, F. L., & Chen, L. (2010). Advances and trends in hydrokinetic turbine systems. *Energy for Sustainable Development*, 14(4), 287-296.

[25] Ladokun, L. L., Ajao, K. R., & Sule, B. F. (2013). Hydrokinetic energy conversion systems: prospects and challenges in Nigerian hydrological setting. *Nigerian Journal of Technology*, 32(3), 538-549.

[26] Laws, N. D. & Epps, B. P. (2016). Hydrokinetic energy conversion: Technology, research, and outlook. *Renewable and Sustainable Energy Reviews*, 57, 1245-1259.

[27] Lomborg, B. (2013). The poor need cheap fossil fuels. *The New York Times*, Retrieved from https://www.nytimes.com/2013/12/04/opinion/the-poor-need-cheap-fossil-fuels.html

[28] Maher, P., Smith, N. P. A., & Williams, A. A. (2003). Assessment of pico hydro as an option for off-grid electrification in Kenya. *Renewable Energy*, 28(9), 1357-1369.

[29] Mooney, C. (2016, September). Reservoirs are a major source of global greenhouse gases, scientists say. *The Washington Post*, Retrieved from https://www.washingtonpost.com/news/energy-environment/wp/2016/09/28/scientists-just-found-yet-another-way-that-humans-are-creating-greenhouse-gases/?noredirect=on&utm_term=.fae0ffdcfad0

[30] Ngo-Duc, T., Oki, T., Kanae, S. (2007). A variable streamflow velocity method for global river routing model: model description and preliminary results. *Hydrology and Earth System Sciences Discussion*, 4, 4389-4414.

[31] Richmond, M. C., Romero-Gomez, P. D. J., & Rakowski, C. L. (2013). *Simulating Collisions for Hydrokinetic Turbines* (Report No. PNNL-22580). Richland, WA: U.S. Department of Energy.

[32] Riglin, J. D. (2016). *Design, Modeling, and Prototyping of a Hydrokinetic Turbine Unit for River Application*. (Doctoral dissertation, Lehigh University, Bethlehem, PA). Retrieved from https://preserve.lehigh.edu/cgi/viewcontent.cgi?article=3783&context=etd

[33] Schulze, K., Hunger, M., & Döll, P. (2005). Simulating river flow velocity on global scale. *Advances in Geosciences*, 5, 133-136.

[34] Siddappaji, K. (2014). *High Efficiency and Cost-Effective Hydrokinetic Turbines*. (Doctoral dissertation, University of Cincinnati, Cincinnati, OH). Retrieved from https://www.researchgate.net/publication/308021659_High_Efficiency_and_Cost-Effective_Hydrokinetic_Turbines

[35] Siddappaji, K. & Turner, M. G. (2015). *Revolutionary geometries of mobile hydrokinetic turbines for wind energy applications*. Paper presented at ASME Turbo Expo 2015, Montreal, Canada. Cincinnati, OH: University of Cincinnati.

[36] Spera, D. A. (2009). *Wind Turbine Technology: Fundamental Concepts in Wind Turbine Engineering*. New York City, NY: ASME.

[37] Stern, D. I., Burkes, P. J., Bruns, S. B. (2017). *The Impact of Electricity on Economic Development: A Macroscopic Perspective*. UC Berkeley: Center for Effective Global Action. Retrieved from https://escholarship.org/uc/item/7jb0015q

[38] Technology characterization. (2018). Retrieved from https://hub.globalccsinstitute.com/publications/renewable-electricity-futures-study-volume-2-renewable-electricity-generation-and-storage-technologies/95-technology-characterization

[39] Types of Hydropower Plants. (2018). Retrieved from https://www.energy.gov/eere/water/types-hydropower-plants

[40] What is U.S. electricity generation by energy source?. (2018). Retrieved from https://www.eia.gov/tools/faqs/faq.php?id=427&t=3

[41] World Bank Group, The. (2009). *Energy Strategy Approach Paper*. Retrieved from http://large.stanford.edu/courses/2014/ph240/heinz1/docs/Approach-paper.pdf

[42] World Energy Council. (2010). *Survey of energy resources committee membership 2010*. Retrieved from https://www.worldenergy.org/wp-content/uploads/2012/10/PUB_World-Energy-Insight_2010_WEC.pdf

[43] World Energy Council. (2016). *World Energy Resources: Hydropower | 2016*. Retrieved from https://www.worldenergy.org/wp-content/uploads/2017/03/WEResources_Hydropower_2016.pdf

[44] Xiao, S., Xu, M., Zhu, T., & Zhang, X. (2012). The Relationship between Electricity Consumption and Economic Growth in China. *Physics Procedia*, 24(A), 56-62.

[45] Zondervan, G., Holtrop, J., Windt, J., & van Terwisga, T. (2011). *On the Design and Analysis of Pre-Swirl Stators for Single and Twin Screw Ships*. Paper presented at the Second International Symposium on Marine Propulsors, Hamburg, Germany. Wageningen, NL: Delft University of Technology.

Appendix A - NACA Airfoil Generator

NACA airfoils are blade profiles developed by the National Advisory Committee for Aeronautics. The shape of the profile is described by a series of numbers following “NACA,” where the numbers correspond to a value for a certain airfoil parameter. The most commonly used NACA airfoil designations are four-digit and five-digit airfoils.

Four-digit NACA airfoils take numbers for three parameters total. The first number makes up the first digit in the airfoil designation and describes the maximum camber as a percentage of the chord length. The second digit describes the distance of the maximum camber from the airfoil leading edge as a percentage of the chord length. The final two digits describe the maximum thickness of the airfoil, again as a percentage of the chord length. It should be noted that while the designation does not reflect it, the digits can be input into a generator with fractions of percentages. For example, an airfoil with a maximum camber 6.3% of the chord length would start its designation with a 6, but the shape of the airfoil would still place the maximum camber at 6.3% of the chord length.

Five-digit NACA airfoils describe more complex airfoil shapes. The first digit describes the design coefficient of lift, and is found by dividing the design coefficient of lift at optimal angle of attack by 0.15. The second describes the position of the maximum camber, but is found by multiplying the distance as a percent of the chord length by half. The third digit describes whether the airfoil is simple or reflexed, and the final two function identically to the last two digits in a four-digit NACA airfoil.

Appendix B - ANSYS Fluent Limitations and Errors

The educational version of Fluent used had some key limitations. First, there was a geometry limit of 50 bodies and 300 faces. This prevented more complex geometry from being tested, including the turbine with all of its component parts (like the shell, bearings, etc.). There was also a limit for the quality of the mesh. The mesh could not exceed 512,000 elements. In all of the tests, the mesh had a number of elements that was very close to the limit, and testing complex airfoil shapes was completely impossible. The mesh quality limit was still high enough to be acceptable for the data collected.

For the ANSYS Fluent airfoil profile data, the mesh used in the simulation was lower quality. Normally, the mesh for the turbine ends up having a much higher quality than the water surrounding it, but in the case of the airfoil profile data, the meshing program did not increase the mesh quality for the turbine. The reasons for this are unknown, but the mesh should still have a high enough quality for the purposes of this project.

Additionally, many of the simulations for the duct data had floating point exception errors. This is more prevalent with the higher radius ratios and is solved by running Fluent in serial mode (rather than parallel). This limits the program to only use one CPU core. Since only one core is being used, it takes several times longer to create the solution. Time constraints prevented more testing from being performed to determine optimal duct geometry; however, the data received from the tests that were run were enough to make conclusions.

Appendix C - Inconsistencies and Oversights

During the project, some inconsistencies and oversights may have affected the final outcome. Some of the most significant are discussed below.

Turbine Length Adjustment

For the early designs, a turbine length of 2.5 m was used, which was used in the initial tests. However, due to frictional effects during water tunnel testing, the scale model diameter was doubled from 5 cm to 10 cm. To compensate and reduce on printing time, the full-scale length was cut in half to 1.25 m, which is the length used for all of the tests after the initial test. Coincidentally, this length happened to be a near ideal length for performance; however, this change was still important to note.

Stagger Calculation Error

One oversight during this project was the initial calculation of the stagger angles. The formula used initially was incorrect and resulted in the calculated staggers being off by between 5° and 10°. However, much of the data is still valid; the values for stagger were adjusted to reflect actual stagger, rather than the incorrectly calculated stagger. This did affect the airfoil profile data, because the models for these simulations were created with a stagger of 45°, which was what was originally thought to be the optimal stagger.

Appendix D - MATLAB BEMT code

```
%%%%%%%%%%%%%%%%%%%%%%%%bemt.m%%%%%%%%%%%%%%%%%%%%%%%%
close all
clear
clc

global i solid TSRr N R1 r stag omega c airfoil

%% turbine parameters
R2 = 0.75; %blade outer radius
R1 = 0.25; %blade inner radius
N = 3; %number of blades
len = 1.25; %length of turbine
stag = 40; %stagger angle
A = pi*R2^2; %turbine inlet area
RPM = linspace(0,36,37); %turbine rotations per minute
linspace(0,36,37)
omega = RPM./60*2*pi; %angular velocity

%% fluid parameters
c = 2.5; %absolute water velocity
rho = 1000; %water density
Pavail = 1/2*rho*A*c^3; %total possible water power in given area

%% blade parameters
dr = 0.01; %blade element section lengths
r = R1:dr:R2; %array of radii
chord = len/sind(stag); %chord length
solid = (N*chord)./(2*pi.*r); %solidity

% possible inputs:flat,ag19,ah6407,hq07,ht22,oa206,raf26,s1010,v13006
airfoil = 'flat';

%% initializing variables and function
dtau = zeros(1,numel(r));

a = zeros(1,numel(r));
ap = zeros(1,numel(r));
phi = zeros(1,numel(r));
Cl = zeros(1,numel(r));
Cd = zeros(1,numel(r));
F = zeros(1,numel(r));
AoA = zeros(1,numel(r));
```

```
tau = zeros(1,numel(RPM));
P = zeros(1,numel(RPM));

fun = @bemtcalc;
guess = [0.5,0.5,40,1,0.5,0.8,20];
options = optimoptions('fsolve','Display','none','Maxiterations',...
    2e5,'Algorithm','levenberg-marquardt');

%% calculations

for j = 1:numel(RPM) %for testing multiple RPMs
    TSRr = (omega(j).*r)./c; %local tip speed ratio

    for i = 1:numel(r)


        b = fsolve(fun,guess,options);
        a(i) = b(1);
        ap(i) = b(2);
        phi(i) = b(3);
        Cl(i) = b(4);
        Cd(i) = b(5);
        F(i) = b(6);
        AoA(i) = b(7);


        dtau(i) = 4*F(i)*ap(i)*(1-a(i))*rho*c*omega(j)*pi*r(i)^3*dr;


    end

    tau(j) = sum(dtau);
    P(j) = tau(j)*omega(j);

end



%% outputs

fprintf('Power = %.2f W\n',P(j))
fprintf('Cp = %.4f\n',P(j)/Pavail)
fprintf('Torque = %.2f Nm\n',tau(j))
```

```
%%%%%%%%%%%%%%%%%%%%%%%%bemtcalc.m%%%%%%%%%%%%%%%%%%%%%%%%
function b = bemtcalc(x)

global i solid TSRr N R1 r stag

b(1) = (solid(i)*(x(4)*cosd(x(3))+x(5)*sind(x(3))))/...
    (4*x(6)*sind(x(3))^2)-x(1)/(1-x(1));
b(2) = (solid(i)*(x(4)*sind(x(3))-x(5)*cosd(x(3))))/...
    (4*x(6)*sind(x(3))*cosd(x(3)))-x(2)/(1+x(2));
b(3) = atand((1-x(1))/((1+x(2))*TSRr(i)))-x(3);

coef = bemtfunc(x(7));
b(4) = coef(1)-x(4);
b(5) = coef(2)-x(5);

b(6) = (2/pi)*acos(exp(-(N*(r(i)-R1))/(2*r(i)*sind(x(3)))))-x(6);
b(7) = stag+x(3)-90-x(7);

%%%%%%%%%%%%%%%%%%%%%%%%bemtfunc.m%%%%%%%%%%%%%%%%%%%%%%%%
function f = bemtfunc(alfa)

global airfoil


if strcmp(airfoil,'flat')
    if abs(alfa) < 20
        f(1) = 2*pi*sind(alfa);
    else
        f(1) = sind(2*alfa);
    end
    f(2) = 0.04+2*sind(alfa)^2;
elseif strcmp(airfoil,'ag19')
    f(1) = 0.106*alfa+0.277;
    f(2) = 5.32e-3-4.51e-4*alfa+1.24e-4*alfa^2;
elseif strcmp(airfoil,'ah6407')
    f(1) = 0.538+1.62*alfa-0.00507*alfa^2;
    f(2) = 0.00231*exp(0.193*alfa);
elseif strcmp(airfoil,'hq07')
    f(1) = 0.109*alfa-2.86e-5;
    f(2) = 3.61e-3*exp(0.14*alfa);
elseif strcmp(airfoil,'ht22')
    f(1) = 0.111*alfa+0.0502;
    f(2) = 3.44e-3*exp(0.109*alfa);
elseif strcmp(airfoil,'oa206')
```

```
    f(1) = 0.108*alfa+0.0323;
    f(2) = 4.93e-3-2.79e-4*alfa+9.49e-5*alfa^2;
elseif strcmp(airfoil,'raf26')
    f(1) = 0.0973*alfa+0.298;
    f(2) = 5.99e-3-5.23e-4*alfa+1.55e-4*alfa^2;
elseif strcmp(airfoil,'s1010')
    f(1) = 0.108*alfa+5.84e-3;
    f(2) = 5.6e-3-5.56e-4*alfa+1.19e-4*alfa^2;
elseif strcmp(airfoil,'v13006')
    f(1) = 0.105*alfa+0.0827;
    f(2) = 5.59e-3-3.32e-4*alfa+1.14e-4*alfa^2;
elseif strcmp(airfoil,'test')
    f(1) = 0.0944*alfa+1.06;
    f(2) = 4.7e-3-1.61e-4*alfa+3.13e-4*alfa^2;
end
```

Appendix E - MATLAB Inverse Design Code

```
%%%%%%%%%%%%%%%%%%%%%%%%bemtreverse.m%%%%%%%%%%%%%%%%%%%%%%%%
close all
clear
clc

global i1 i2 i3 i4 solid TSRr N R1 r Cl Cd stag

%% testing parameters - change these values only
n = 26; %number of iterations to try - program performs n^4 operations
RPMbounds = [6,6.06]; %lower and upper bounds for rotation rate
Clbounds = [1.035,1.055]; %lower and upper bounds for lift coefficient
Cdbounds = [0.003 0.008]; %lower and upper bounds for drag coefficient

%% turbine parameters
R2 = 0.75; %blade outer radius
R1 = 0.25; %blade inner radius
N = 3; %number of blades
len = 1.25; %length of turbine
stag = 45; %stagger angle
A = pi*R2^2; %turbine inlet area
RPM = linspace(RPMbounds(1),RPMbounds(2),n); %turbine rotations per
minute
omega = RPM./60*2*pi; %angular velocity

%% fluid parameters
c = 2.5; %absolute water velocity
rho = 1000; %water density
Pavail = 1/2*rho*A*c^3; %total possible water power in given area

%% blade parameters
dr = 0.5/(n-1); %blade element section lengths
r = R1:dr:R2; %array of radii
chord = len/sind(stag); %chord length
solid = (N*chord)./(2*pi.*r); %solidity
TSRr = (omega.*r)./c; %local tip speed ratio
Cl = linspace(Clbounds(1),Clbounds(2),numel(r)); %lift coefficient
Cd = linspace(Cdbounds(1),Cdbounds(2),numel(r)); %drag coefficient

%% initializing variables and function
dtau = zeros(n,n,n,n); %incremental torque
dT = zeros(n,n,n,n); %incremental thrust
```

```
a = zeros(n,n,n,n); %axial induction factor
ap = zeros(n,n,n,n); %tangential induction factor
phi = zeros(n,n,n,n); %flow angle
F = zeros(n,n,n,n); %prandtl tip loss factor
AoA = zeros(n,n,n,n);
lift = zeros(n,n,n,n);
drag = zeros(n,n,n,n);

tau = zeros(n,n,n); %torque
T = zeros(n,n,n); %thrust
P = zeros(n,n,n); %power

fun = @bemtcalcrev;
guess = [0.5,0.5,40,0.8,5,1,0]; %initial guess [a,ap,phi,F]
options = optimoptions('fsolve','Display','none','Maxiterations',...
    2e5,'Algorithm','levenberg-marquardt'); %solver options

%% calculations
start = tic; %start timer

for i1 = 1:n %for rotational velocity
    for i2 = 1:n %for lift coefficients
        for i3 = 1:n %for drag coefficients
            for i4 = 1:n %for blade elements
                b = fsolve(fun,guess,options); %solve for parameters

                %if the turbine acts as a motor
                %i.e. if the turbine puts energy into the water
                %end that set of calculations
                if b(1) < 0 || b(1) > 1
                    break
                end


                %recording calculated values in appropriate variables
                a(i4,i2,i3,i1) = b(1);
                ap(i4,i2,i3,i1) = b(2);
                phi(i4,i2,i3,i1) = b(3);
                F(i4,i2,i3,i1) = b(4);
                AoA(i4,i2,i3,i1) = b(5);
                lift(i4,i2,i3,i1) = b(6);
                drag(i4,i2,i3,i1) = b(7);


                %incremental thrust from blade momentum theory
```

```
                dT(i4,i2,i3,i1) = 4*F(i4,i2,i3,i1)*a(i4,i2,i3,i1)*...
                    (1+a(i4,i2,i3,i1))*rho*c^2*pi*r(i4)*dr;

                %incremental torque from blade momentum theory
                dtau(i4,i2,i3,i1) = 4*F(i4,i2,i3,i1)*...
                    ap(i4,i2,i3,i1)*(1-a(i4,i2,i3,i1))*...
                    rho*c*omega(i1)*pi*r(i4)^3*dr;

            end
            tau(i1,i2,i3) = sum(dtau(:,i2,i3,i1)); %total torque
            T(i1,i2,i3) = sum(dT(:,i2,i3,i1)); %total torque
            P(i1,i2,i3) = tau(i1,i2,i3)*omega(i1); %total torque
            fprintf('%i/%i\n',(i1-1)*n^2+(i2-1)*n+i3,n^3) %tracker
        end


    end


end

stop = toc(start); %time for program to execute

%% outputs
[Pmax,ind] = max(P(:)); %getting value and location of greatest power
[i,j,k] = ind2sub(size(P),ind); %setting location of greatest power

%parameter values that give greatest power
fprintf('Max Power = %.2f W\n',Pmax)
fprintf('Cp = %.4f\n',Pmax/Pavail)
fprintf('Torque = %.2f Nm\n',tau(i,j,k))
fprintf('RPM = %f\n',RPM(i))
fprintf('Angular Velocity = %f rad/s\n',omega(i))
fprintf('Lift Coefficient = %f\n',Cl(j))
fprintf('Drag Coefficient = %f\n',Cd(k))
fprintf('Time to Complete = %d:%02d\n',floor(stop/60),...
                            round(rem(stop,60)))

%%%%%%%%%%%%%%%%%%%%%%%%bemtcalcrev.m%%%%%%%%%%%%%%%%%%%%%%%%
function b =  bemtcalcrev(x)

global i1 i2 i3 i4 solid TSRr N R1 r Cl Cd stag

b(1) = (solid(i4)*(Cl(i2)*cosd(x(3))+Cd(i3)*sind(x(3))))/...
    (4*x(4)*sind(x(3))^2)-x(1)/(1-x(1));
```

```
b(2) = (solid(i4)*(Cl(i2)*sind(x(3))-Cd(i3)*cosd(x(3))))/...
    (4*x(4)*sind(x(3))*cosd(x(3)))-x(2)/(1+x(2));
b(3) = atand((1-x(1))/((1+x(2))*TSRr(i1)))-x(3);
b(4) = (2/pi)*acos(exp(-(N*(r(i4)-R1))/(2*r(i4)*sind(x(3)))))-x(4);
b(5) = x(3)+stag-90-x(5);
b(6) = Cl(i2)+0.1*x(5)-5e-3*x(5)^2-x(6);
b(7) = Cd(i3)-1.61e-4*x(5)+3.13e-4*x(5)^2-x(7);
```

Appendix F - Tested Airfoils

AG19

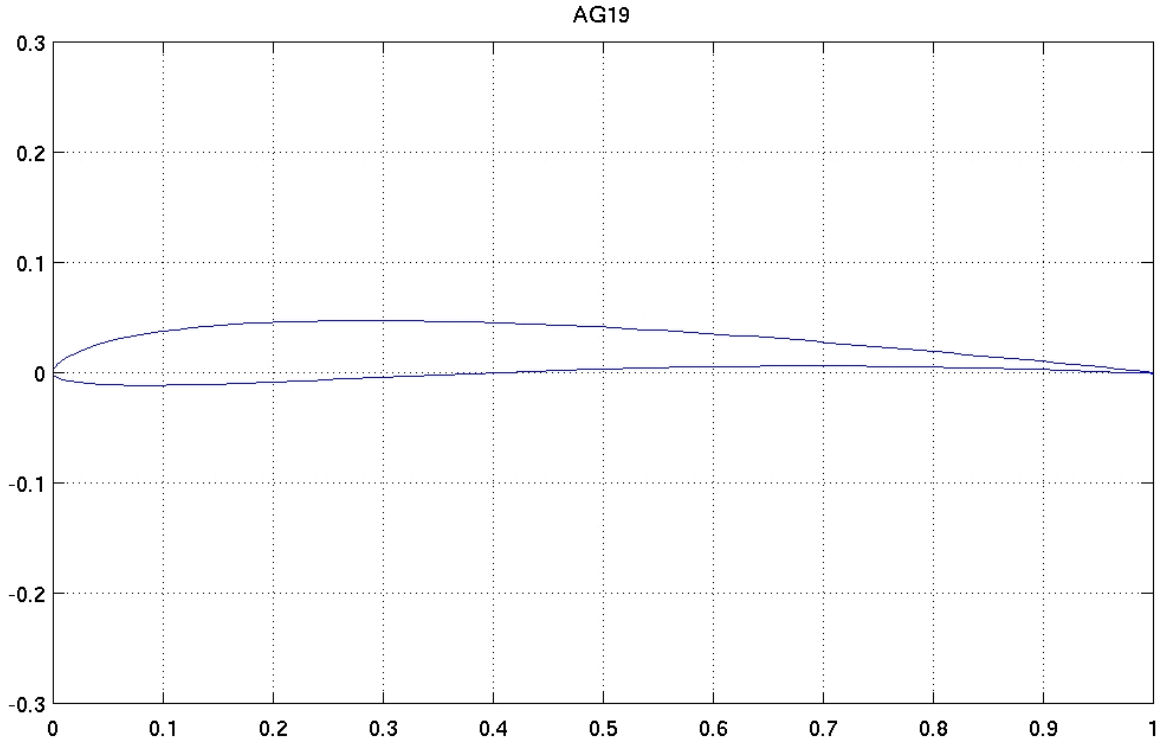

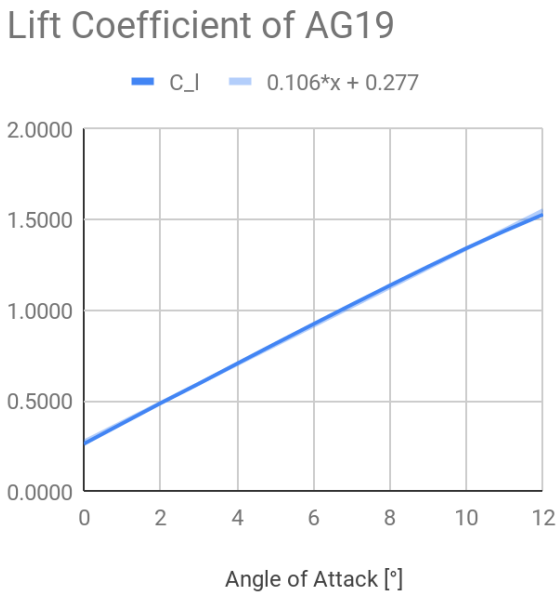

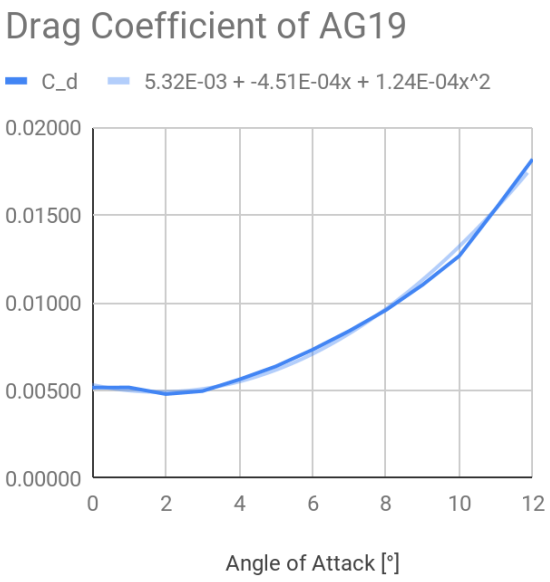

AH6407

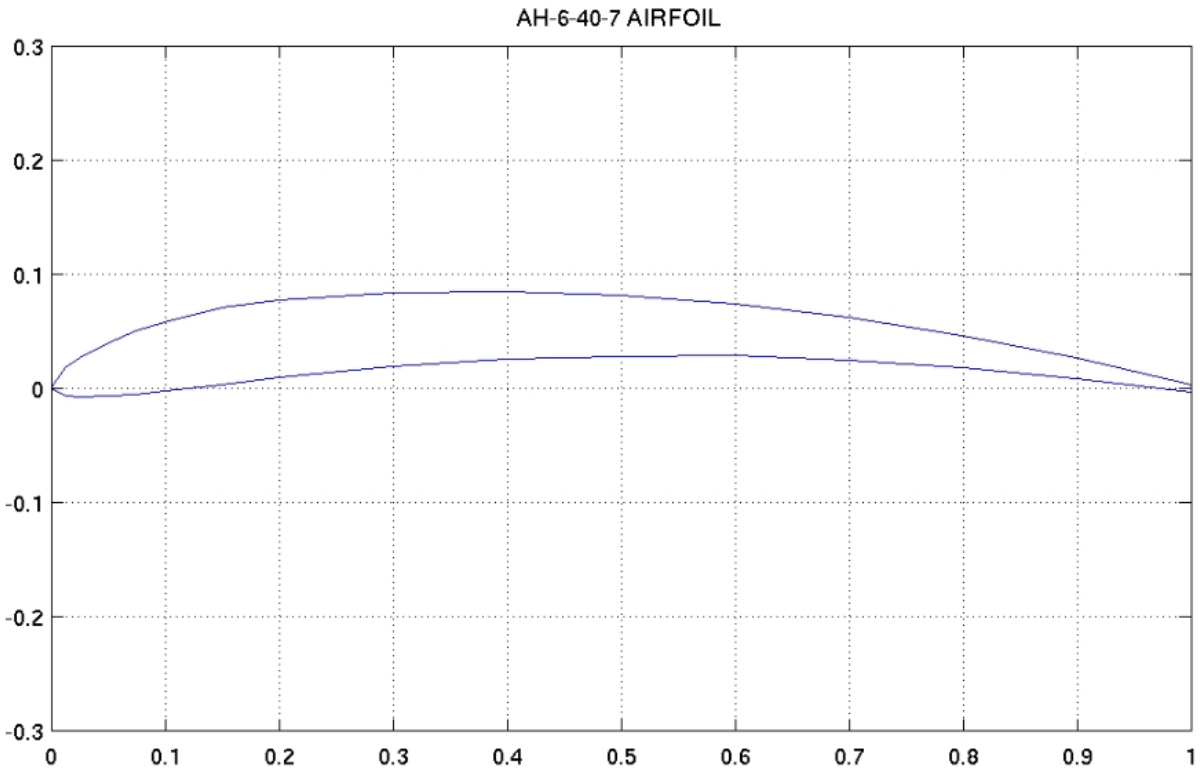
AH-6-40-7 AIRFOIL
0.3
0.2
0.1
0
-0.1
-0.2
-0.3
0
0.1
0.2
0.3
0.4
0.5
0.6
0.7
0.8
0.9
1

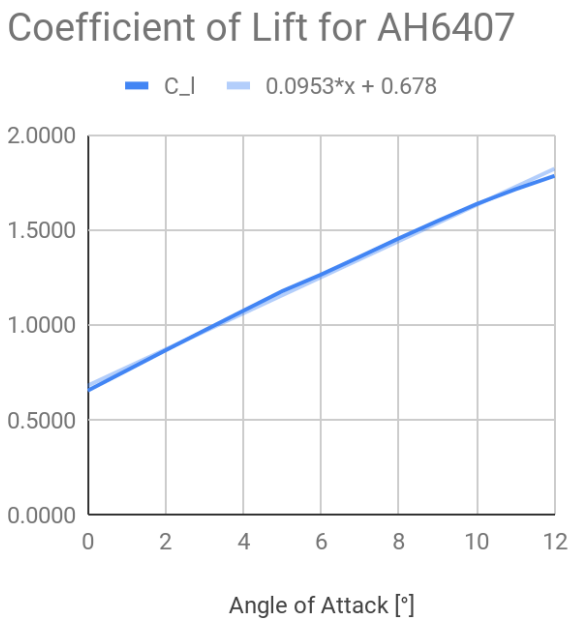
Coefficient of Lift for AH6407
C_l
0.0953*x + 0.678
2.0000
1.5000
1.0000
0.5000
0.0000
0
2
4
6
8
10
12
Angle of Attack [°]

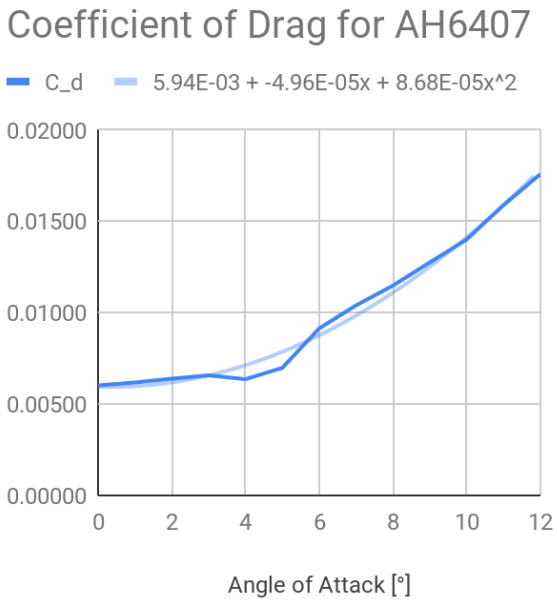
Coefficient of Drag for AH6407
C_d
5.94E-03 + -4.96E-05x + 8.68E-05x^2
0.02000
0.01500
0.01000
0.00500
0.00000
0
2
4
6
8
10
12
Angle of Attack [°]

HQ07 - The calculations for this airfoil did not converge beyond 6°

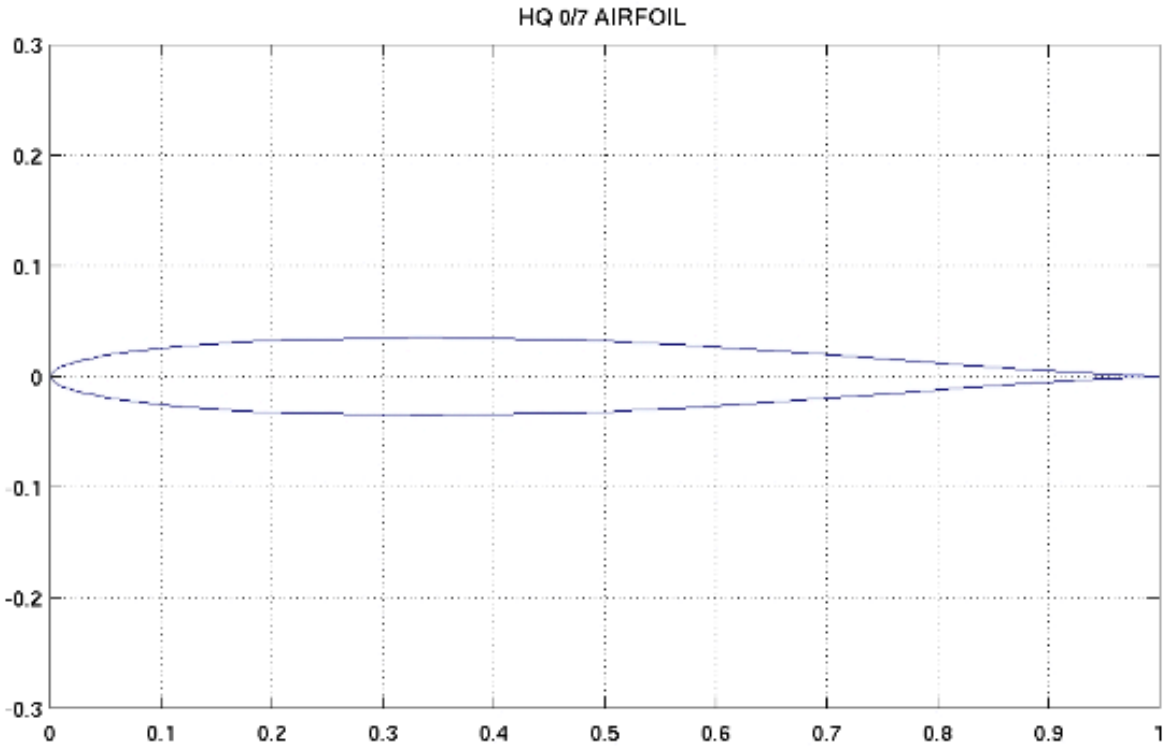

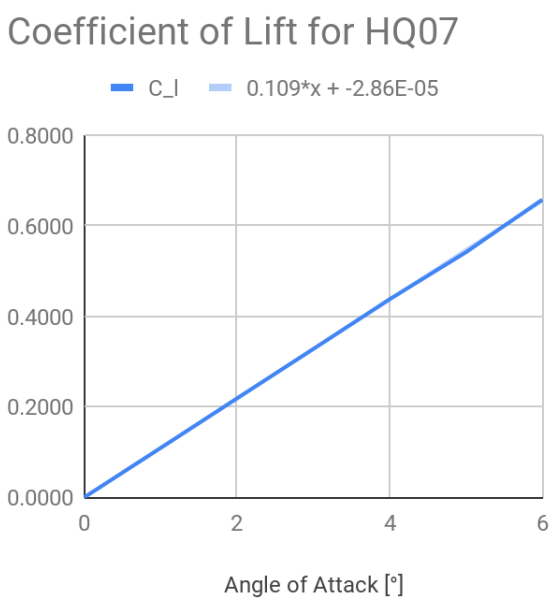

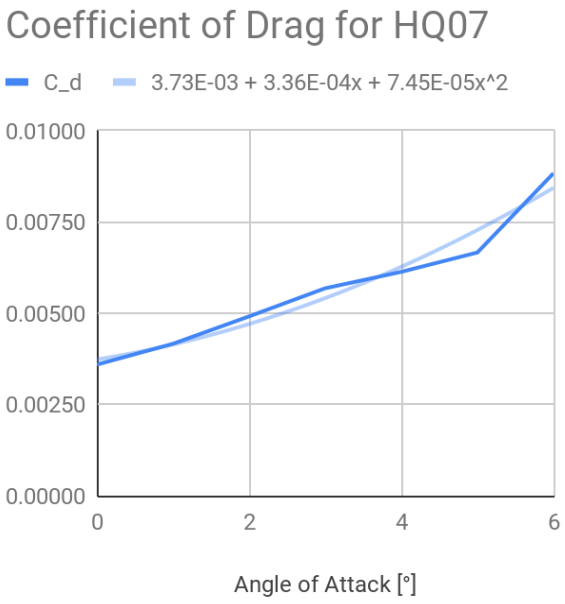

HT22

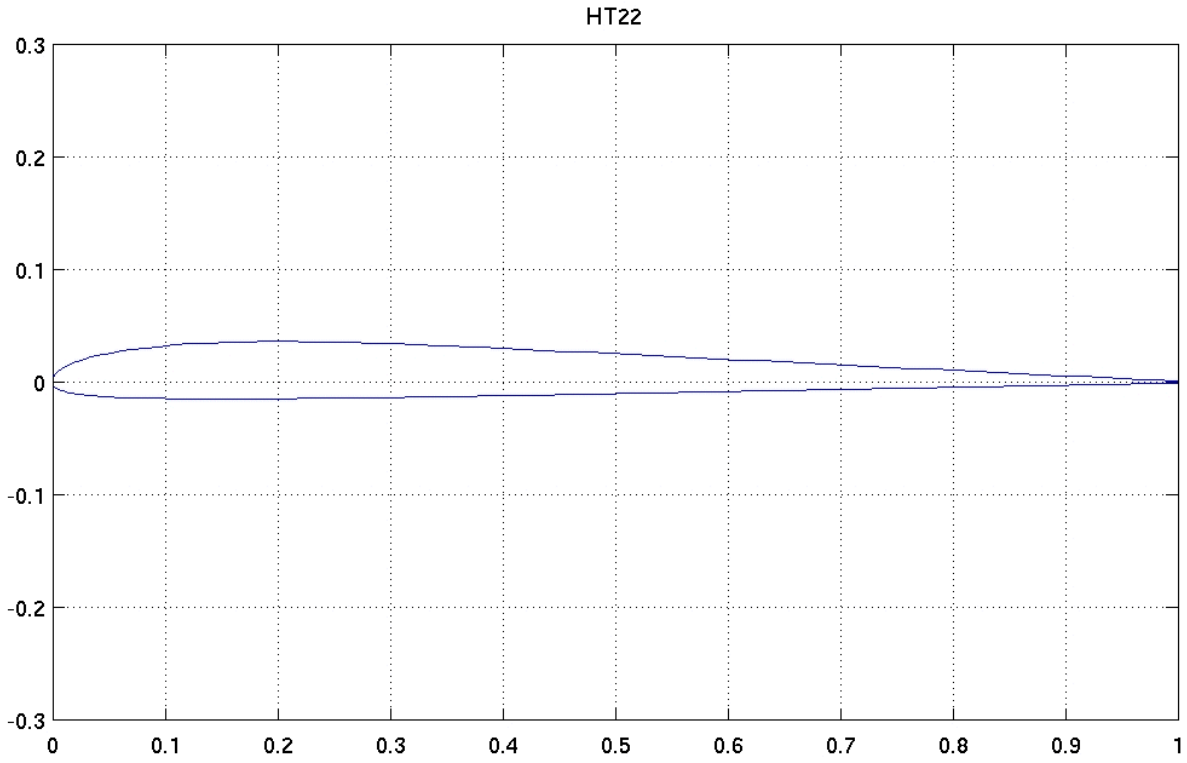
HT22
0.3
0.2
0.1
0
-0.1
-0.2
-0.3
0
0.1
0.2
0.3
0.4
0.5
0.6
0.7
0.8
0.9
1

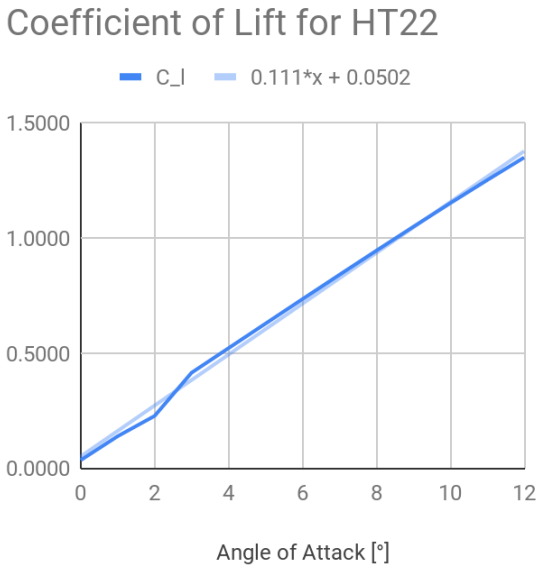
Coefficient of Lift for HT22
C_l
0.111*x + 0.0502
1.5000
1.0000
0.5000
0.0000
0
2
4
6
8
10
12
Angle of Attack [°]

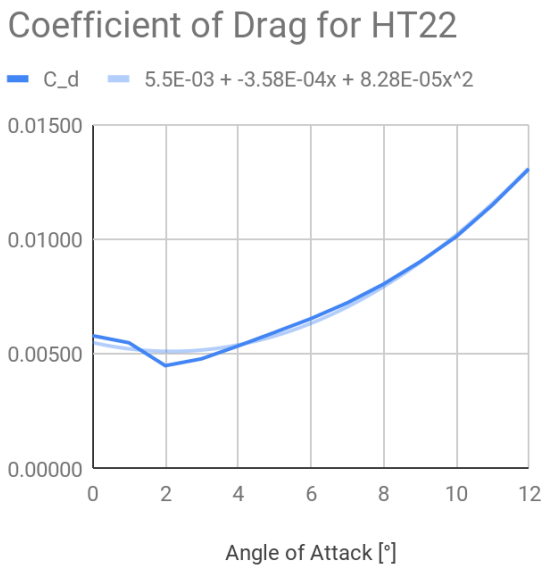
Coefficient of Drag for HT22
C_d
5.5E-03 + -3.58E-04x + 8.28E-05x^2
0.01500
0.01000
0.00500
0.00000
0
2
4
6
8
10
12
Angle of Attack [°]

OA206

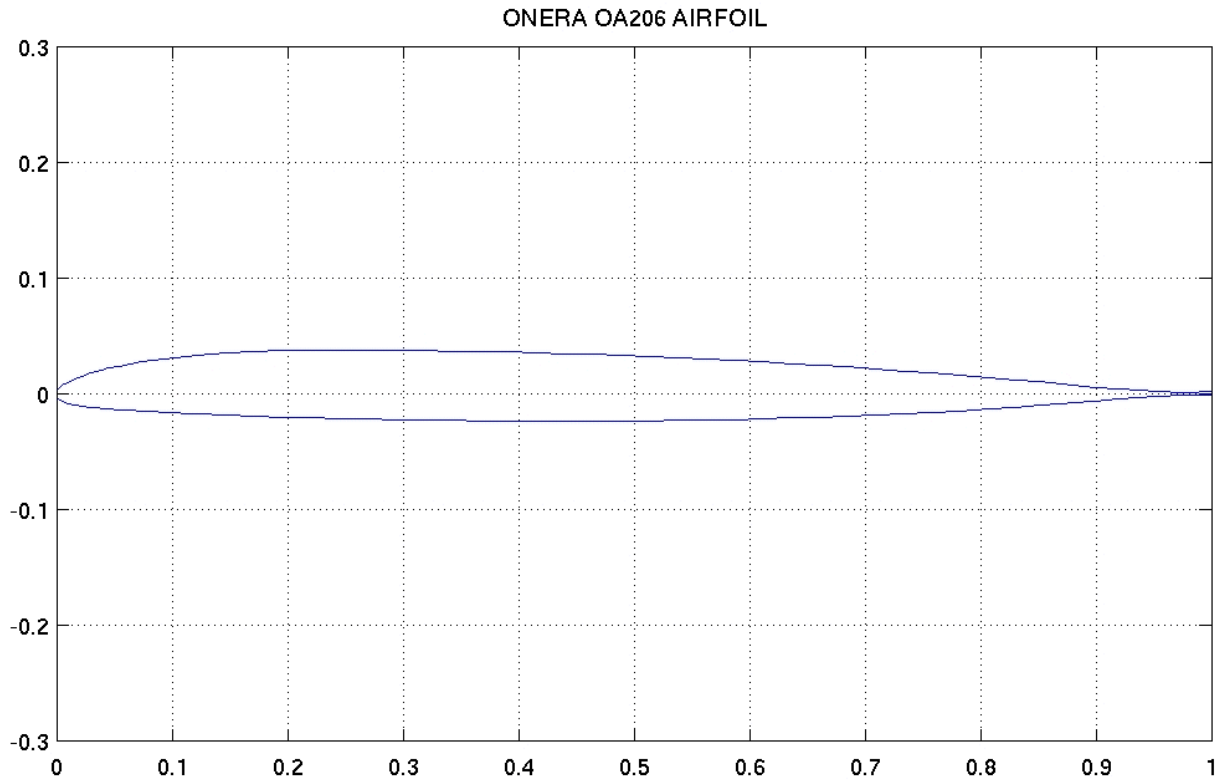
ONERA OA206 AIRFOIL
0.3
0.2
0.1
0
-0.1
-0.2
-0.3
0
0.1
0.2
0.3
0.4
0.5
0.6
0.7
0.8
0.9
1

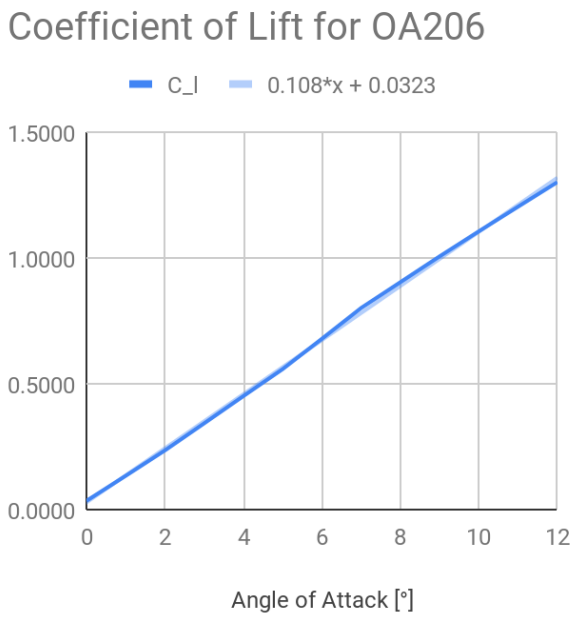
Coefficient of Lift for OA206
C_l
0.108*x + 0.0323
1.5000
1.0000
0.5000
0.0000
0
2
4
6
8
10
12
Angle of Attack [°]

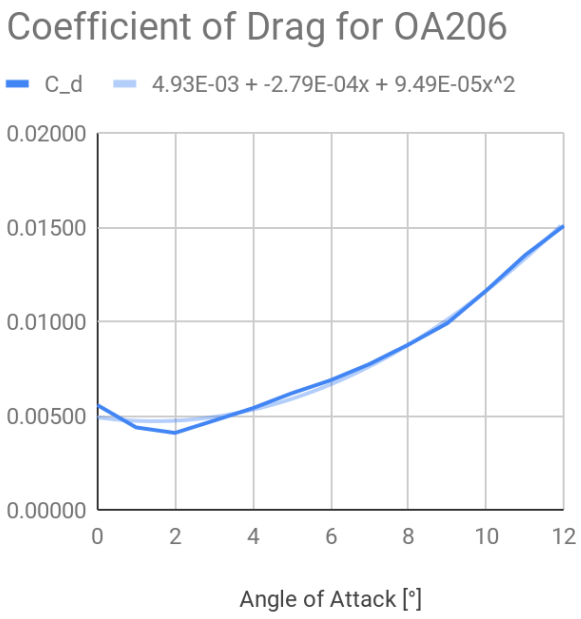
Coefficient of Drag for OA206
C_d
4.93E-03 + -2.79E-04x + 9.49E-05x^2
0.02000
0.01500
0.01000
0.00500
0.00000
0
2
4
6
8
10
12
Angle of Attack [°]

RAF26

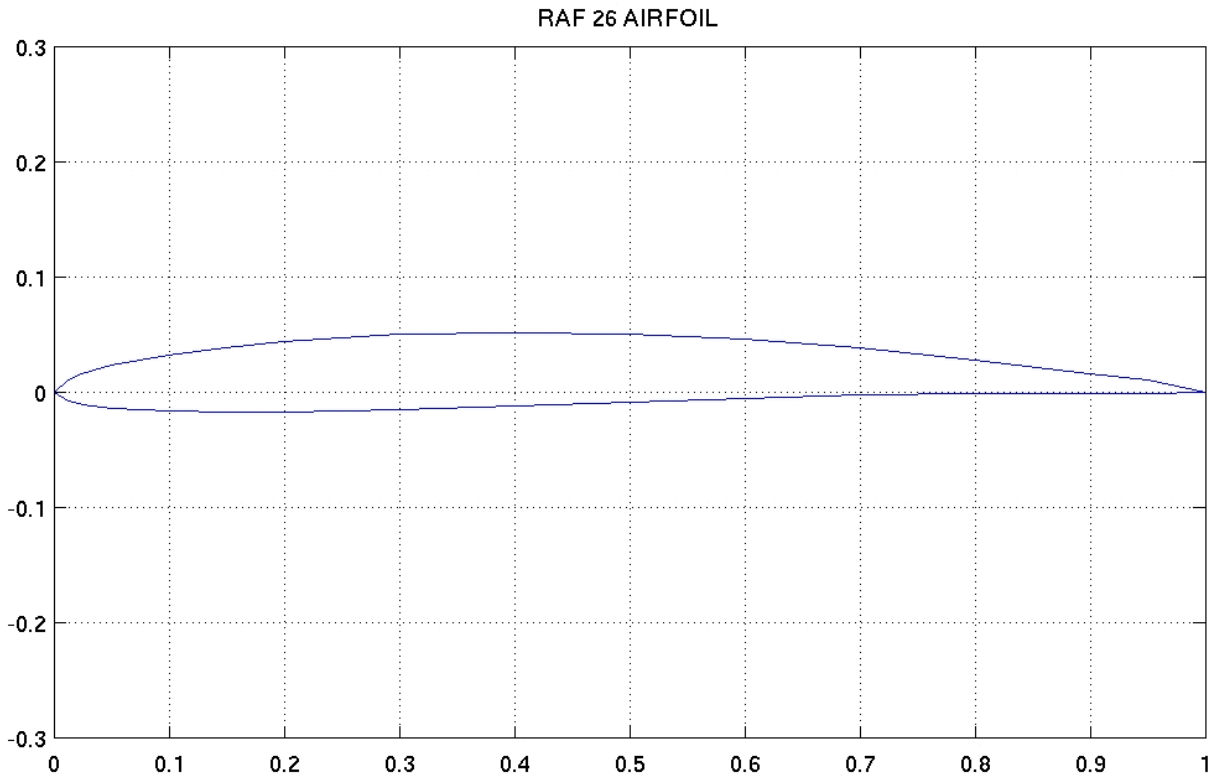
RAF 26 AIRFOIL
0.3
0.2
0.1
0
-0.1
-0.2
-0.3
0
0.1
0.2
0.3
0.4
0.5
0.6
0.7
0.8
0.9
1

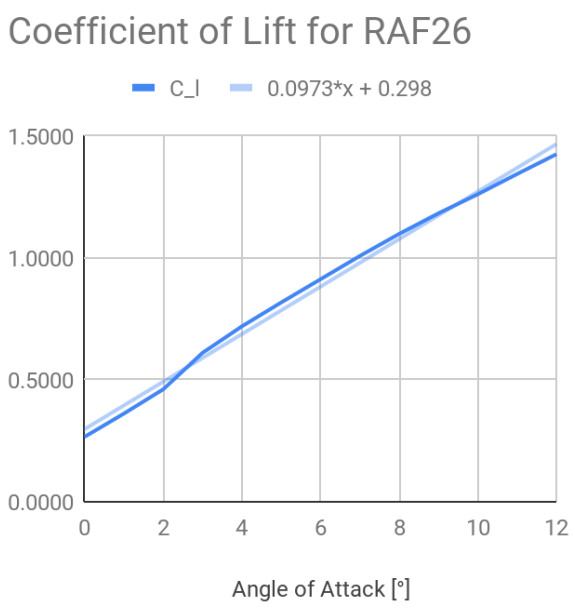
Coefficient of Lift for RAF26
C_l
0.0973*x + 0.298
1.5000
1.0000
0.5000
0.0000
0
2
4
6
8
10
12
Angle of Attack [°]

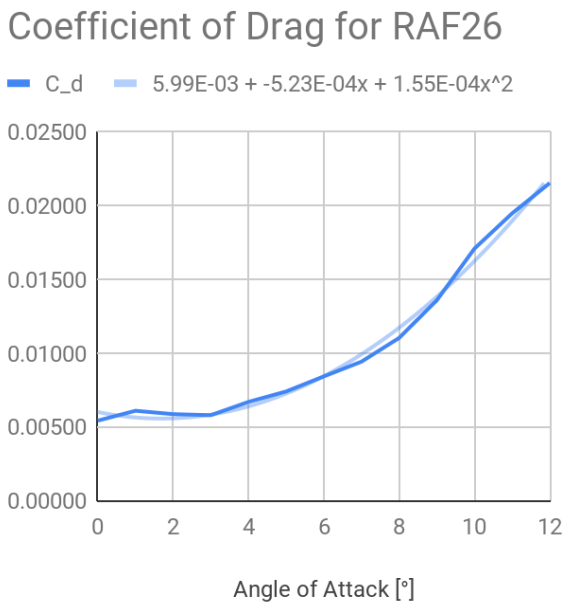
Coefficient of Drag for RAF26
C_d
5.99E-03 + -5.23E-04x + 1.55E-04x^2
0.02500
0.02000
0.01500
0.01000
0.00500
0.00000
0
2
4
6
8
10
12
Angle of Attack [°]

S1010

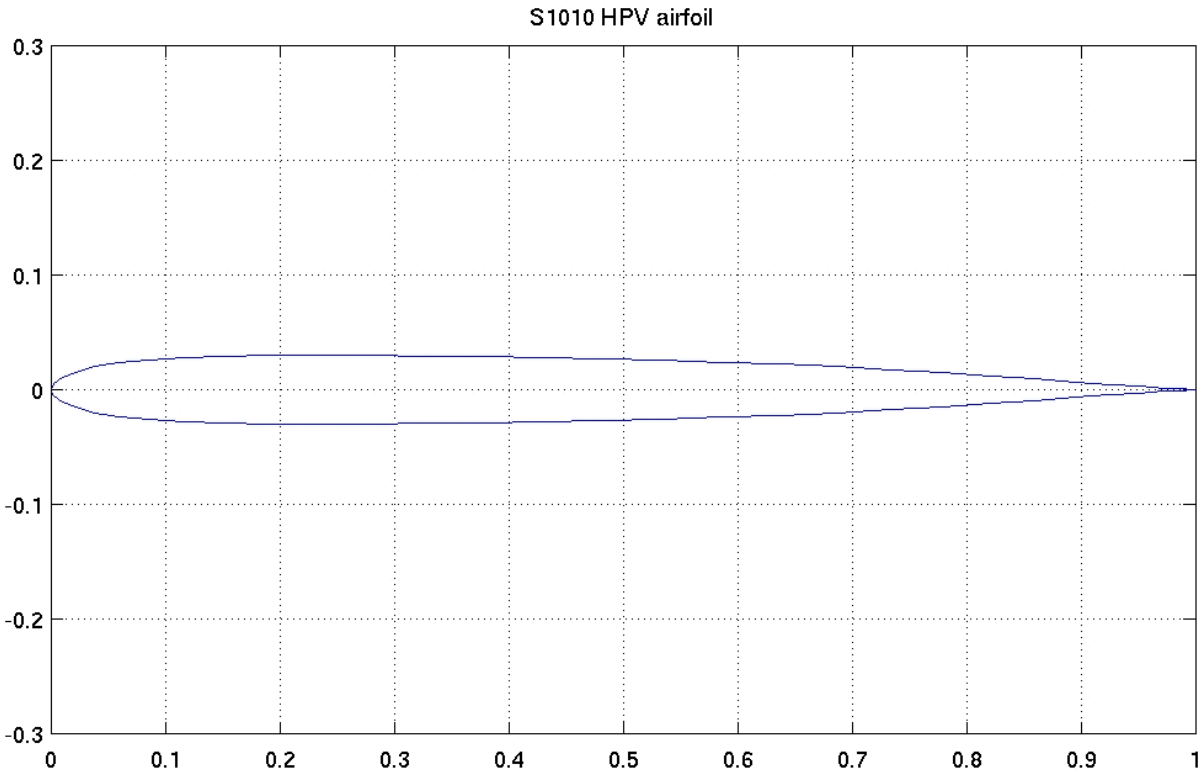
S1010 HPV airfoil
0.3
0.2
0.1
0
-0.1
-0.2
-0.3
0
0.1
0.2
0.3
0.4
0.5
0.6
0.7
0.8
0.9
1

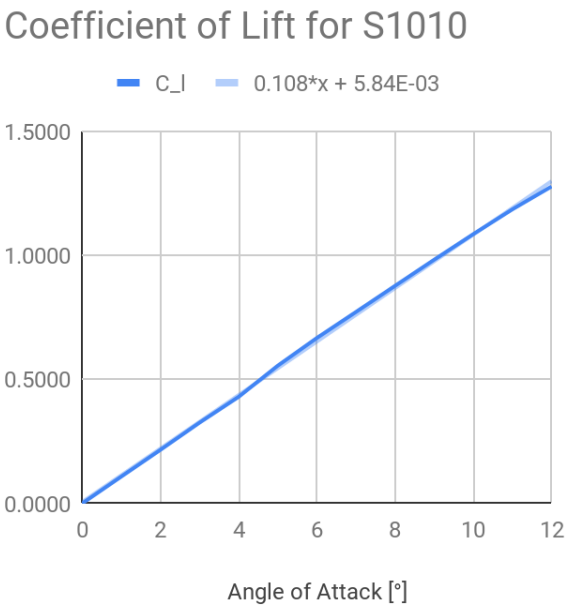
Coefficient of Lift for S1010
C_l
0.108*x + 5.84E-03
1.5000
1.0000
0.5000
0.0000
0
2
4
6
8
10
12
Angle of Attack [°]

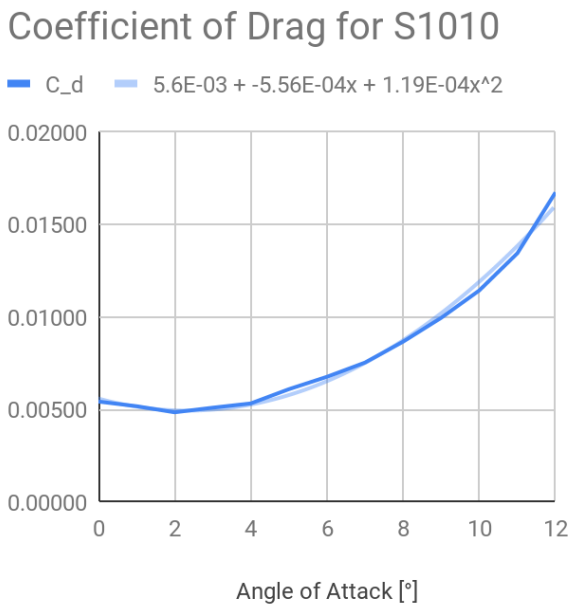
Coefficient of Drag for S1010
C_d
5.6E-03 + -5.56E-04x + 1.19E-04x^2
0.02000
0.01500
0.01000
0.00500
0.00000
0
2
4
6
8
10
12
Angle of Attack [°]

V13006

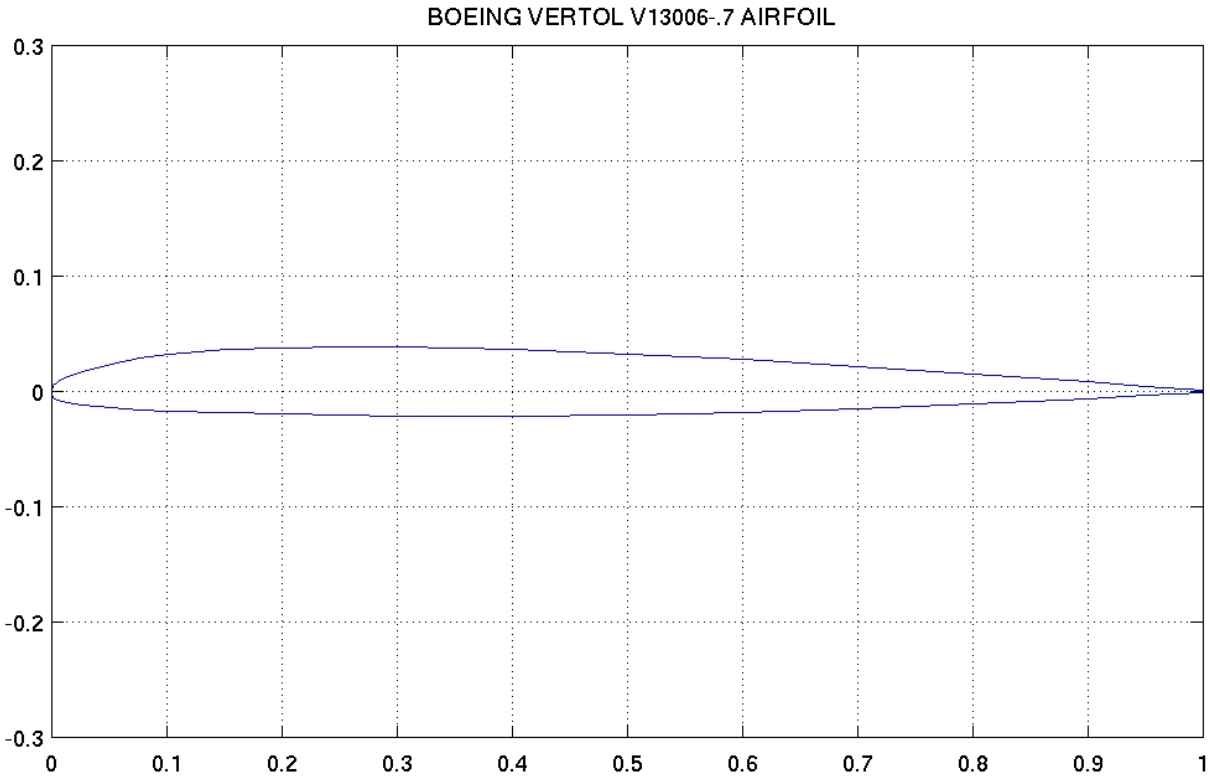
BOEING VERTOL V13006-.7 AIRFOIL
0.3
0.2
0.1
0
-0.1
-0.2
-0.3
0
0.1
0.2
0.3
0.4
0.5
0.6
0.7
0.8
0.9
1

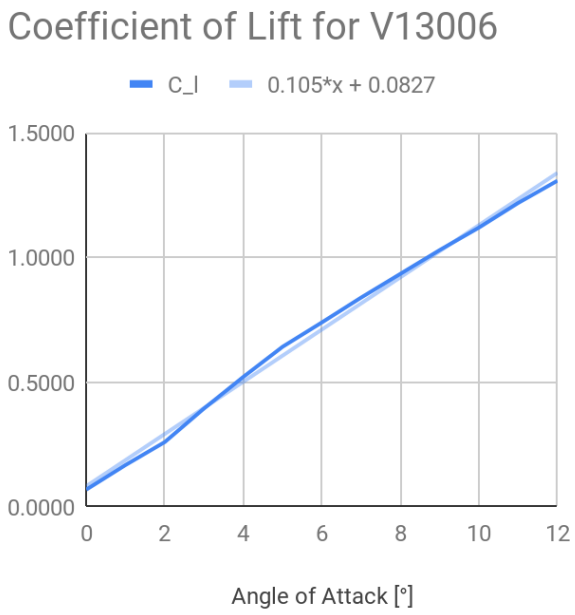
Coefficient of Lift for V13006
C_l
0.105*x + 0.0827
1.5000
1.0000
0.5000
0.0000
0
2
4
6
8
10
12
Angle of Attack [°]

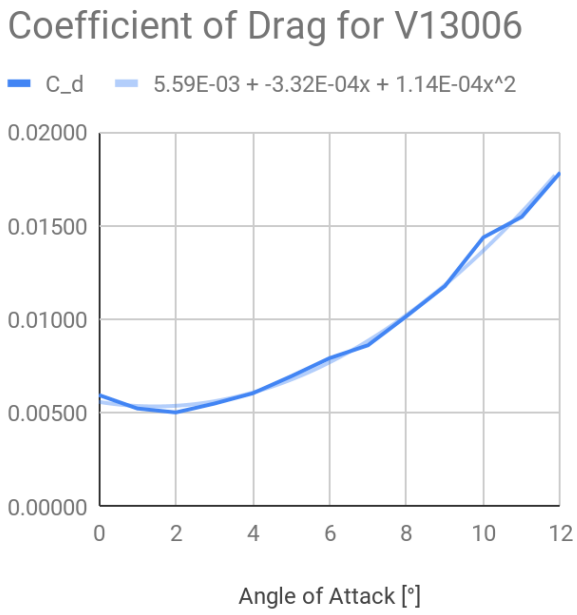
Coefficient of Drag for V13006
C_d
5.59E-03 + -3.32E-04x + 1.14E-04x^2
0.02000
0.01500
0.01000
0.00500
0.00000
0
2
4
6
8
10
12
Angle of Attack [°]